

**UNIVERSITÉ DU QUÉBEC EN ABITIBI-TÉMISCAMINGUE  
UNIVERSITÉ DE LORRAINE**

**DÉVELOPPEMENT D'OUTILS D'INTERPRÉTATION DE  
DONNÉES GÉOPHYSIQUES**

THÈSE PRÉSENTÉE EN COTUTELLE  
COMME EXIGENCE PARTIELLE DU DOCTORAT  
EN SCIENCES DE ENVIRONNEMENT  
ET EN GÉOSCIENCES

par

Nacim Foudil-Bey

Août 2012



**Cégep** de l'Abitibi-Témiscamingue  
**Université** du Québec en Abitibi-Témiscamingue

### **Mise en garde**

La bibliothèque du Cégep de l'Abitibi-Témiscamingue et de l'Université du Québec en Abitibi-Témiscamingue a obtenu l'autorisation de l'auteur de ce document afin de diffuser, dans un but non lucratif, une copie de son œuvre dans Depositum, site d'archives numériques, gratuit et accessible à tous.

L'auteur conserve néanmoins ses droits de propriété intellectuelle, dont son droit d'auteur, sur cette œuvre. Il est donc interdit de reproduire ou de publier en totalité ou en partie ce document sans l'autorisation de l'auteur.

*Je dédie ce modeste travail :*

*À toute ma famille pour leurs soutien sans faille durant toutes ces  
longues années d'études.*

*À mon petit Adam.*

*À la mémoire d'Albert TARANTOLA qui ma permis de voir le  
problème inverse sous d'autres angles.*

## REMERCIEMENTS

Tout d'abord je tiens à remercier mes deux directeurs de thèse Cheng et Royer.

Je remercie Li (la professeure Li Zhen Cheng) pour m'avoir proposé et convaincu d'effectuer ma thèse au Canada. Chère Li merci beaucoup pour tes conseils et tes corrections, j'ai beaucoup apprécié la grande liberté que tu m'as accordé pour la réalisation des mes travaux de thèse, notamment pour tester (presque) toutes les idées qui me sont passées par la tête et dont certaines restes en suspens. Bref, ce fut une expérience très riche de travailler avec toi.

Je tiens à remercier Jean-Jacques Royer pour avoir accepté de diriger mes travaux, pour ses remarques et conseils particulièrement pour ses contributions et sa relecture des articles de la présente thèse et des gOcad meeting.

Je remercie les membres du jury pour avoir accepté d'évaluer mes travaux de recherche, je suis très honoré par la présence dans mon jury de : Claude Jaupart Professeur à l'Université de Paris 7-Denis Diderot et directeur de l'Institut de Physique du Globe de Paris, Michel Diament Professeur, Directeur Scientifique Adjoint du Département Sciences de la Terre de l'INSU, Institut National des Sciences de l'Univers, directeur du laboratoire de gravimétrie et géodynamique de l'Institut de Physique du Globe de Paris, Alain Tabbagh Professeur à l'Université Pierre et Marie Curie, Paris 6, Colin Farquharson Assistant Professor in the Department of Earth Sciences at Memorial University, Jean Claude Mareschal Professeur au département des sciences de la Terre et de l'atmosphère, Fiona Ann Darbyshire Professeure au département des sciences de la Terre et de l'atmosphère et Fouad Erchiqui Professeur à l'unité d'enseignement et de recherche en sciences appliquées à l'université du Québec et directeur du Laboratoire de Nanotechnologie et Bioplasturgie.

Je remercie Jean Claude Mareschal (co-directeur de thèse) pour ses remarques et ses questions pertinentes particulièrement en théorie du potentiel. Je remercie également, Foued Erchiqui (co-directeur de thèse) pour ses conseils en particulier pour la partie qui concerne les réseaux de neurones.

Je tiens à remercier Guillaume (le professeur Guillaume Caumon) non seulement pour m'avoir initié à la programmation en C++ et au développement sous gOcad mais aussi pour toutes les discussions intéressantes et fructueuses "pourquoi faire compliqué quand on peut faire simple?" lors de mes passages au sein de l'équipe gOcad, ce fut un honneur et un immense plaisir ainsi qu'une chance de travailler avec toi.

Un grand merci à Denis (Denis Bois le directeur de l'URSTM) pour m'avoir accueilli à bras ouverts au sein de son équipe, pour ses encouragements et son enthousiasme pour allez toujours de l'avant "...proceed .. at PDAC, ça te rappelle quelque chose à Toronto ?".

Un grand merci aux organismes qui ont financé mes études et qui m'ont permis de payer **les onéreux frais d'inscriptions** ainsi que mes nombreux déplacements :

- l'association scientifique pour la géologie et ses applications (ASGA) et le consortium gOcad pour les subventions apportées à mes déplacements en particulier pour la prise en charge des billets d'avion et du matériel informatique, du salaire versé lors de ma présence en France ainsi que les licences de développement sous gOcad.
- le Fonds de recherche du Québec - Nature et technologies (FRQNT) ;
- la fondation UQAT (FUQAT) pour la bourse d'étude ;
- the KEGS Foundation ;
- UQAT et L'INPL pour m'avoir accordé certaines exemptions consternant les frais de scolarité.

Je remercie également Mahdi et Rafik (Yamate El A).

Je tiens à remercier particulièrement, Fatima Chtioui pour toutes les aides administratives en particulier pour mes réinscriptions à L'INPL. Christophe Aantoine pour ses conseils de programmation et d'optimisation d'algorithmes et surtout pour les solutions d'erreurs de compilations sous Linux. Pierre Jacquemin pour son aide pour les scripts de migration et génération de plug-in. Julien Clément qui ma aidé à régler les tracas liés à Linux et aux différents compilateurs **gcc**. Et à tout les gocadiens que j'ai eu l'occasion de rencontrer et avec qui je n'ai discuté bien sûr que de gOcad (Emmanuel, Pierre, Vincent, les deux Pauline, Luc, Anne-Laure, Marc-Olivier, Thomas, Sarah, Francois, Nicolas, Florent, Gautier, Romain, Jeanne, Fabrice).

Merci à labbé Louise pour toutes les aides administratives prodiguées.

Je remercie tout les professeurs du réseau université du Québec que j'ai eu l'occasion de côtoyer durant mes années de thèse, en particulier (Tikou et Pascal) résponsables du programme de doctorat à l'UQAT.

Je remercie toute la gang de l'Unité de recherche et de service en technologie minérale (Hassan, Thomas, Francine, Isabelle, Olivier, Jovette, Virginie, Mélanie, Yvan, Mélinda, Nil, Alain, Magalie, Karen, Yong Jun, Idrissa, Samuel).

Je remercie également Mahdi et Rafik (Yamate El A).

## TABLE DES MATIÈRES

<b>DÉDICACE</b>	<b>ii</b>
<b>REMERCIEMENTS</b>	<b>iii</b>
<b>LISTE DES FIGURES</b>	<b>ix</b>
<b>LISTE DES TABLEAUX</b>	<b>xv</b>
<b>LISTE DES SYMBOLES</b>	<b>xvii</b>
<b>RÉSUMÉ</b>	<b>xix</b>
<b>INTRODUCTION</b>	<b>1</b>
Problématiques . . . . .	2
Contributions . . . . .	4
Organisation du mémoire . . . . .	4
<b>CHAPITRE I</b>	
<b>CALCUL DIRECT DES CHAMPS DE POTENTIELS</b>	<b>7</b>
I.1 Introduction . . . . .	7
I.2 Modélisation géologique tridimensionnelle . . . . .	7
I.3 Calcul direct du champ de potentiel : état de l'art . . . . .	9
I.4 3D gravity and magnetic forward modelling using tetrahedra-based subdivision method . . . . .	11
I.4.1 Résumé . . . . .	11
I.4.2 Abstract . . . . .	12
I.4.3 Introduction . . . . .	13
I.4.4 Theory . . . . .	14
I.4.5 Comparing the responses with the analytical solutions . . . . .	17
I.4.6 Discussion . . . . .	20
I.4.7 Conclusions . . . . .	21
I.4.8 Acknowledgements . . . . .	22
I.4.9 References . . . . .	25
I.5 Applications de la modélisation directe . . . . .	35
I.6 Bilan . . . . .	37

**CHAPITRE II**

<b>INVERSION SEPARÉE DES DONNÉES DU CHAMP DE POTENTIEL</b>	<b>41</b>
II.1 Introduction . . . . .	41
II.2 Inversion au sens des moindres carrés . . . . .	42
II.3 Inversions stochastiques . . . . .	44
II.4 Gravity Inversion using stochastic methods . . . . .	47
II.4.1 Résumé . . . . .	47
II.4.2 Abstract . . . . .	47
II.4.3 Introduction . . . . .	48
II.4.4 Theory . . . . .	49
II.4.5 Inversion of the synthetic data set . . . . .	52
II.4.6 Inversion of a real data set . . . . .	54
II.4.7 Discussion . . . . .	56
II.4.8 Conclusions . . . . .	56
II.4.8 References . . . . .	61
II.5 Bilan . . . . .	75

**CHAPITRE III**

<b>INVERSION CONJOINTE</b>	<b>77</b>
III.1 Introduction . . . . .	77
III.2 Inversion conjointe : état de l'art . . . . .	78
III.3 Joint Gravity and Magnetic Inversion using Collocated Cokriging Simulation . . . . .	79
III.3.1 Résumé . . . . .	79
III.3.2 Abstract . . . . .	80
III.3.3 Introduction . . . . .	81
III.3.4 Theory . . . . .	82
III.3.5 Inversion on synthetic data . . . . .	85
III.3.6 Inverting real dataset data . . . . .	87
III.3.7 Discussion . . . . .	90
III.3.8 Conclusions . . . . .	91
III.3.9 References . . . . .	98
III.4 Bilan . . . . .	113

**CHAPITRE IV**

<b>RESEAUX DE NEURONES APPLIQUÉS POUR LA QUANTIFICATION DES INCERTITUDES</b>	<b>115</b>
IV.1 Neural Network Stochastic Simulation Applied for Quantifying Uncertainties . . . . .	115
IV.1.1 Abstract . . . . .	115
IV.1.2 Introduction . . . . .	116
IV.1.3 Neural networks . . . . .	117
IV.1.4 Application . . . . .	119
IV.1.5 Discussions and Conclusions . . . . .	121
IV.1.6 References . . . . .	124
<b>CONCLUSION GÉNÉRALE</b>	<b>131</b>
<b>BIBLIOGRAPHIE</b>	<b>132</b>
<b>ANNEXE A</b>	
<b>Gtetra Class</b>	<b>147</b>
A.1 Gtetra ::_Gtetra_gapi_decl Protocol Reference . . . . .	148
A.1.1 Detailed Description . . . . .	150
A.1.2 Member Function Documentation . . . . .	151
A.2 Gtetra ::_Gtetra_gravicompute_decl Protocol Reference . . . . .	158
A.2.1 Detailed Description . . . . .	160
A.2.2 Member Function Documentation . . . . .	160

# LISTE DES FIGURES

I.1	Représentation volumique d'un modèle structural par : une grille cartésienne (a), une grille stratigraphique (b), un modèle par frontières (c), ou un maillage tétraédrique (d). par (Caumon, 2010). . . . .	8
I.2	Corps géologique isolé (a) et son approximation tridimensionnelles (b) en tranche laminaire, (c) en surface polyédrale, pour le calcul du champ de potentiel . . . . .	11
I.3	rms errors (a) vertical component of gravity and (b) total magnetic fields for different number of tetrahedra in the prismatic body at various depths. . . . .	26
I.4	Dividing a coarse tetrahedral cell into smaller tetrahedra. (a) Using the corner subdivision algorithm and (b) using optimized corner subdivision algorithm. . . . .	27
I.5	Flow chart diagram describing (a) The subdivision algorithm and (b) the potential field contribution. (Step number refers to text comments). . . . .	28
I.6	Relative difference of the vertical component of gravity response between the analytical formula and the solution calculated by the subdivision method (a) ratio of 2, (b) ratio of 3 and (c) ratio of 4 for a rectangular prism ( $100m \times 100m \times 50m$ ) the top of the prism at 1m depth. The horizontal location of prism is given by dashed line. . . . .	28

I.7	Relative difference of the total magnetic-field between the analytical formula and the solution calculated by the subdivision method (a) ratio of 2, (b) ratio of 4 and (c) ratio of 6 for a rectangular prism ( $100m \times 100m \times 50m$ ) the top of the prism at 1m depth, $\chi = 0.01$ SI). the horizontal location of prism is given by dashed line. . . . .	29
I.8	difference of (a) vertical component of gravity field, (b) total magnetic-field between the analytical formula and the solution calculated by the subdivision method of a homogeneous sphere. (c) Vertical cross subsection of a sphere modeled by tetrahedra ( center at 45.1 m depth with a radius of 45 m). . . . .	30
I.9	Complex geological body modeled with (a) unstructured tetrahedral grid and (b) regular prismatic grid). . . . .	31
I.10	Density and magnetic susceptibility distribution on plan subsection of the tetrahedral model at depth of (a) 155 m, (b) 355 m and (c) 555 m. . . . .	32
I.11	forward modelling of a synthetic body (Figure I.10a) calculated using a subdivision tetrahedral mesh algorithm. (a) $B_x$ (b) $B_y$ and (c) $B_z$ components of magnetic field. (d) Vertical component of gravity field. Total magnetic-field e) without and f) with constant remanent magnetization. The inducing field has ( $I = 65^0$ , $D = -25^0$ ). . . . .	33
I.12	Résultat du calcul direct de la composante vertical du champ gravimétrique créé par un modèle complexe à base de tétraèdre. (a) Variations topographies au dessus du modèle, (b) composante verticale du champ gravimétrique, (c) coupe verticale suivant AA', (d) coupe verticale suivant BB'). (Modèle structural aimablement fourni par Harvard Univ./Chevron) . . . . .	36
I.13	Résultat d'inversion par la méthode des moindres carrés sur maillage cartésien qui permet de representer une géométrie de la faille de Cadillac	38

II.14	Calcul direct sur maillage tétraédrique. (a) Modification du pendage de la faille vers le Nord, (b) position initiale de la faille (a) et (c) modification du pendage de la faille vers le Sud. Construction du modèle tétraédrique (g),(h) et (i) sous la contrainte imposée respectivement par la position des failles (a), (b) et (c). Résultats du calcul direct de la composante verticale du champ gravimétrique créé respectivement par les modèles (d), (e) et (f).	39
II.1	Effet de l'incertitude du modèle sur le résultat du calcul direct, incertitude (a) négligée, (b) non négligée. Par (Tarantola, 2005)	42
II.2	Tetrahedral body. a) Reference model, b) initial model (prior information) and c) posterior model using least squares inversion.	62
II.3	The vertical component of the gravity field produced by the (a) reference model, contaminated by a random noise; (b) prediction from inversion model; and (c) the difference between reference model response and inverted model prediction.	63
II.4	Top view of density distribution between reference model (top) and inversion result (bottom) at (a) 150m, (b) 350m, (c) 650m of depth.	64
II.5	Accepted models (density distribution) using Monte Carlo simpling (likelihood > 0.75)	65
II.6	Vertical component of the gravity field for the accepted MTC models (Figure II.5 b., c. and d.)	66
II.7	Selected variograms (solid lines) of pilot points densities, Gaussian models are used for the variograms. a) Azimuth of $0^0$ dip of $0^0$ , b) azimuth of $90^0$ dip of $45^0$ and c) azimuth of $45^0$ dip of $85^0$ .	67
II.8	Simulated density distribution in the posterior model using conditional Gaussian simulations (a, b, c, d, e and f) from inverted model and (g, h, and i) from model in Figure II.5.b (likelihood > 0.7).	68
II.9	Simplified geological map of central Noranda mining camp showing selected volcanogenic massive sulphide and major lithological contact.	69

II.10 (a) Bouguer anomaly of the Blake River Group, solid blake line array inversion (array study in dashed line), (b) residual gravity anomaly of the Flavrian pluton and (c) surface density distribution. . . . .	70
II.11 Selected variograms (solid lines) of pilot points densities, Gaussian models are used for the variograms. a) Azimuth of $0^0$ dip of $0^0$ , b) azimuth of $90^0$ dip of $45^0$ and c) azimuth of $45^0$ dip of $85^0$ . . . . .	71
II.12 Inversion result using a) least squares inversion (b), (c), (d), and (e) conditional Gaussian simulation, (f) mean of 100 random Gaussian simulation . . . . .	72
II.13 Vertical component of the gravity field induced by (a)least squares model (b) and (c) Gaussian simulation. . . . .	73
II.14 Calculated probability from 100 realizations of the density of (a) 2.64 and (b) $2.8 \text{ g/cm}^3$ . . . . .	74
III.1 The vertical component of gravity field produced by the (a) reference model contaminated with random noise, (b) prior model , (c) inverted model and (d) the difference between the gravimetric inverted and reference field . . . . .	99
III.2 The first vertical derivative of the vertical component of the (a) gravity and (b) magnetic fields produced by the reference model. . . . .	100
III.3 Comparison between the reference model (in top), prior model (in medium) and inversion result (in bottom) along horizontal cross sections at depth of column (I) 150 m (II) 350 and (III) 650 m. . . . .	101
III.4 Magnetic susceptibility distributions in the a) Reference model and b), c), d), e) and f) accepted realizations. . . . .	102
III.5 Vertical component of the magnetic field for a) reference model and b), c), d), e) and f) accepted models (Figure III.4) . . . . .	103
III.6 Selected variograms (solid lines) of pilot points densities, Gaussian models are used for the variograms. a) Azimuth of $0^0$ dip of $0^0$ , b) azimuth of $90^0$ dip of $45^0$ and c) azimuth of $45^0$ dip of $85^0$ . . . . .	104

III.7 Simulated magnetic susceptibility distribution in the posterior model. a), Histogram of distribution b) semivariogram model , c)magnetic susceptibility-density cross plot, d), e), and f) collocated cokriged sim- ulations with correlation coefficient of -0.2, g) mean of mtc realizations, and collocated cokriged simulations with correlation coefficient 0f h) 0.8 and i) -0.8 . (likelihood values of models > 0.7). . . . .	105
III.8 Geologic setting of matagami from (Shamsipour et al., 2010a). The study area define with the solid line . . . . .	106
III.9 Potential field data. a) residual gravity anomaly, b) residual magnetic anomaly and vertical derivative of c) gravi and d) magnetic anomalies. . . . .	107
III.10Three-dimensional results using least square separate inversion. a) Density distribution , b) magnetic susceptibility distribution, and structural model given by gravity and structural model using c) density , d) magnetic susceptibility distributions. . . . .	108
III.11Result of zonation between the magnetic and gravimetric structural models	109
III.12Selected Cosimulation parameters. a) histogram of density contrast , b) selected variogram (Azimuth of 45 <sup>0</sup> dip of 45 <sup>0</sup> ) c) density and magnetic corss-correlation. . . . .	110
III.13Inversion result using a) Least squares , and b) c) d) Collocated Cokriging Simulation. . . . .	111
III.14Top view of density distribution in the inversion results. (a) Least squares (b) , (c) and (d) Collocated Cokriging Simulation . . . . .	112
IV.1 Neural network architecture. . . . .	125
IV.2 Geology of the Abitibi greenstone belt, Québec, Canada. From (Mueller et Mortensen, 2002) . . . . .	126
IV.3 Normalized (a) coded geological map (b) density contrast , (c) magnetic susceptibility, (e) interpolated density contrast using (ANN), training point and (f) interpolated magnetic susceptibility (ANN). . . . .	127

IV.4 Horizontal cross-sections showing three possible geological maps simulated by ANN at a depth of 930 m. . . . .	128
IV.5 3 selected realizations of simulated magnetization . . . . .	129

## LISTE DES TABLEAUX

- I.2 Results of root mean square (rms), absolute (abs) errors and computation time of prismatic approach with different resolutions and tetrahedral model 34



## LISTE DES SYMBOLES

$\gamma = 6.673 \times 10^{-8}$	constante universelle de gravitation ( $cm^3 g^{-1} s^{-2}$ )
$\rho$	masse volumique ( $g/cm^3$ )
$\mathbf{r}$	vecteur de distance ( $m$ )
$v$	volume du tétraèdre ( $m^3$ )
$\mathbf{g}$	vecteur du champ de potentiel (mGla)
$g_x$	composante du champ gravimétrique suivant la direction x (mGal)
$g_y$	composante du champ gravimétrique suivant la direction y (mGal)
$g_z$	composante du champ gravimétrique suivant la direction z (mGal)
$\mathbf{B}$	vecteur du champ magnétique (nT)
$B_x$	composante Nord du champ magnétique (nT)
$B_y$	composante Est du champ magnétique (nT)
$B_z$	composante verticale vers le bas du champ magnétique (nT)
$B_t$	composante du champ magnétique total (nT)
$\pi = 3,141592654$	rapport constant
$\mu_0 = 4\pi^{-7}$	perméabilité magnétique dans de vide ( $H/m$ )
$I$	angle d'inclinaison du champ magnétique par rapport à l'horizon (deg)
$D$	angle entre le Nord géographique et le vecteur horizontal du champ magnétique (deg)
$\rho(m)$	densité de probabilité <i>a priori</i>
$L(m)$	fonction de vraisemblance du modèle m
$\sigma(m)$	densité de probabilité <i>a posteriori</i>
$S(m)$	fonction objective
$C_i$	matrice de covariance des données $i$
$\nabla m_i$	gradient du modèle $m_i$
$\vec{t}(x, y, z)$	produit vectoriel croisé du gradient

$Sum_{t_n}$	somme du vecteur $\vec{t}$ normalisé
$X_i$	valeur d'entrée pour le neurone $i$
$Y_i$	valeur de sortie pour le neurone $j$
$b_i$	la valeur du biais pour le neurones $i$
$w_{ji}$	le poids de la connexion entre les neurones $i$ et $j$
$\varepsilon$	l'erreur à la sortie du réseau de neurones
$e_i$	la différence entre la prédition $Y_i$ et la sortie idéale $d_i$
$\mu$	facteur de pondération qui varie entre 0 et 1
$\Omega$	facteur de pondération qui varie entre 0 et 1

## RÉSUMÉ

Les méthodes géophysiques aéro-portées sont très utilisées pour la prospection du sous-sol à l'échelle régionale, permettant ainsi de couvrir de grandes surfaces en particulier les zones difficiles d'accès. Le sujet de thèse concerne le développement de techniques d'interprétation des données géophysiques pour le problème des ressources naturelles et de l'environnement. La première partie de cette thèse concerne le développement d'une méthode de calcul direct des composantes des champs gravimétrique et magnétique à partir d'une structure (corps) géologique modélisé(e) par une grille à base de tétraèdres, ce qui permet de représenter des modèles géologiques très complexes particulièrement en présence de zones faillees et hétérogènes avec un nombre d'éléments optimal. Plusieurs techniques d'inversions utilisent des contraintes mathématiques pour la résolution du problème inverse en modélisation. Ces contraintes permettent de réduire le nombre de modèles possibles. Cependant les solutions proposées appelées aussi « le modèle le plus probable » présentent des solutions lisses, ce qui est loin de représenter la réalité géologique. Pour éluder ce problème, la deuxième et troisième parties de la thèse proposent des améliorations majeures du processus d'inversion par l'utilisation des méthodes géostatistiques telle que la Simulation Gaussienne Séquentielle ou la Co-Simulation dans le cas d'une inversion conjointe afin d'estimer les probabilités *a posteriori* des modèles simulés. La quatrième partie de ce mémoire présente une alternative à la simulation de plusieurs variables. L'apprentissage du réseau de neurones supervisé par un certain nombre de points permet d'établir une relation entre les différentes variables.

**Mots clés :** Gravimétrie, Magnétique, Densité, Magnétisation, Tetraèdre, Modélisation, Simulation, Inversion, Stochastiques, Réseaux de Neurones.



## **INTRODUCTION**

Les travaux présentés dans cette thèse ont été réalisés dans le cadre d'une Cotutelle entre l'Université du Québec et en Abitibi-Témiscamingue (UQAT), Canada et l'Institut Polytechnique de Lorraine (INPL), France. Cette thèse a été financée et effectuée à 80 % au sein de l'Institut de Recherche en Mines et en Environnement de l'UQAT et à 20 % au sein du projet Gocad au niveau de l'École Supérieure de Géologie de Nancy (France).

L'acquisition des données géophysiques s'effectue soit par des levés pseudo-continus tels que levés aéroportés, des mesures au sol et par des enregistrements au niveau des puits de forages. Ces données constituent une information indispensable pour l'exploration et l'exploitation des ressources naturelles d'une part, ainsi que la compréhension des phénomènes géologiques mis en jeu d'autre part. Les variations observées (ou calculées) des champs de potentiels sont d'origine externe et interne à notre belle Terre. Les variations internes sont provoquées soit par des processus sédimentaires ou bien causées par des déformations induites par exemple, par le jeux de failles, par la présence d'hétérogénéités engendrées suite à la circulation de fluides hydrothermaux, la migration d'hydrocarbure et des intrusions magmatiques. Dans ce cas il est plus judicieux de parler d'anomalies observées au niveau des composantes des champs de potentiels. En général les petites sources proches de la surface produisent des anomalies de courtes longueurs d'ondes. Par contre, les larges et/ou profondes sources produisent des anomalies de grandes longueurs d'ondes au niveaux des champs de potentiels observés. Ainsi, les premières interprétations qualitatives des méthodes potentielles consistaient à représenter les variations des champs sur un plan horizontal et à localiser ces anomalies après traitement ([Evjen, 1936](#); [Henderson et Zietz, 1949](#)). Ensuite les techniques d'interprétations ont évolué vers des objectifs quantitatifs par la proposition de modèles en deux dimensions, sous forme de coupes verticales pour expliquer et/ou reproduire les anomalies observées ([Talwani et al., 1959](#); [Cady, 1980](#)). Avec l'avancement de l'informatique et l'apparition des techniques de conceptions assistées par ordinateur (CAO), la modélisation en trois dimensions devient alors plus accessible

([Li et Oldenburg, 1996, 1998](#)), permettant ainsi d'expliquer les phénomènes géologiques, la vérification de certaines hypothèse et l'estimation des réserves et ou des risques, ce qui peut constituer un outil très puissant d'aide à la décision.

L'interprétation des données géophysiques passe par la modélisation qui consiste à représenter la répartition en trois dimensions des propriétés physiques dans le sous-sol. Les principales étapes pour arriver au modèle final sont les suivantes :

1. Acquisition des données,
2. traitement des données (filtrage, corrections, séparation du champ régional),
3. discrétisation en grille de l'espace d'étude,
4. introduction du contexte géologique et l'information *a priori*,
5. calcul de la répartition spatiale des propriétés physiques par les méthodes directes ou inverses,
6. validation et interprétation des résultats.

La plupart des techniques de modélisation utilisent un maillage cartésien ce qui a pour effet de biaiser la représentation géométrique des structures dans le cas d'un nombre insuffisant d'éléments, ou bien dans le cas contraire, d'augmenter considérablement l'espace mémoire et le temps de calcul. En plus, la majorité des méthodes d'inversions converge vers un modèle unique et lisse. Le travail effectué dans cette thèse a trait particulièrement à l'étape 5, à savoir, développer une méthode de calcul directe des composantes des champs gravimétrique et magnétique par un corps géologique complexe en trois dimensions avec des propriétés physiques variables. Il est également proposer plusieurs solutions possibles qui peuvent expliquer les données observées.

## Problématiques

Il existe deux moyens de modéliser les données géophysiques : soit par calcul direct basé sur un modèle géologique, ou bien par inversion (automatique) des données. Par conséquent, la modélisation géologique constitue une étape clé de l'interprétation, elle représente un outil précieux contribuant à la prise de décisions d'une part et à la compréhension des phénomènes géologiques mis en cause d'autre part. Les nouvelles techniques de représentation géométrique assistées par ordinateur intègrent de plus en plus de détails et d'information. Elle sont même considérées comme de plus en plus réalistes ([Caumon, 2009](#)).

La première partie de ce mémoire s'intéresse au calcul des composantes des champs de potentiels (gravimétrique et magnétique) créés par des structures géologiques complexes et hétérogènes. Le modèle géologique est représenté par un maillage à base de tétraèdre, ce qui permet une bonne représentation géométrique des marqueurs géologiques (faille, horizon, plissement, etc.) avec un nombre optimal d'éléments.

Le deuxième aspect a trait au problème de la non-unicité de la modélisation inverse. Contrairement aux méthodes d'inversions classiques qui tentent de représenter au mieux les données observées sur le terrain par la proposition d'une distribution unique et lisse de propriétés physiques, la méthode proposée pour contourner ce problème, combine les résultats obtenue par l'inversion classiques au sens des moindres carrés avec les techniques de simulations géostatistiques par une formulation bayésienne pour ne garder que les modèles ayant une forte probabilité *a posteriori*.

Chaque méthode géophysique est sensible à une variation de propriétés physique dans le sous-sol. Ainsi l'information obtenue par inversion individuelle de chaque variable physique pourrait suggérer des interprétations structurales différentes en fonction de la méthode utilisée. Dans le souci d'améliorer le résultat d'inversion, le troisième aspect de ce mémoire vise à combiner la géostatistique avec l'approche bayésienne pour une inversion conjointe. En effet, l'information structurale peut être extraite à partir des résultats d'inversions individuelles de chaque propriété physique, cela peut être imposé sous forme de contrainte géométrique. Ainsi la co-simulation entre deux propriétés physiques permet la génération de plusieurs réalisations de modèles possibles. A la fin seuls les modèles produisant une bonne valeur de vraisemblance avec le champ de référence seront sélectionnés.

Les différentes propriétés physiques sont spatialement complémentaires, leur lien étant la géologie. En présence de plusieurs données telles que la densité, la susceptibilité magnétique et les unités géologiques, il est difficile de trouver une relation systématique ou empirique qui relie toutes les variables. Pour contrer ce problème, le dernier volet de cette thèse propose une utilisation supervisée des réseaux de neurones afin de faire un lien entre différentes variables. La supervision sera conditionnée au niveau de quelques points de l'espace préalablement sélectionné. Ce qui permettra de simuler plusieurs distributions possibles d'une variable donnée en tenant compte de plusieurs variables.

## Contributions

La majorité de cette thèse est présentée sous forme d'articles. L'apport des co-auteurs a été très fructifiant, notamment pour : l'optimisation des algorithmes, les réflexions théoriques et la relecture des articles. De l'avis de l'auteur les contributions majeures de cette thèse sont :

1. Le développement d'une nouvelle technique de calcul des composantes des champs magnétiques et gravimétriques provoquées par des structures (ou objets) complexes et hétérogènes modélisés par maillage tétraédrique.
2. Le développement d'une méthode d'inversion stochastique exploitant les techniques de simulation géostatistique pour la génération de plusieurs modèles probables.
3. Le développement d'une approche d'inversion conjointe utilisant la co-simulation entre les variables et par l'introduction d'information *a priori*.
4. Le développement d'une méthode de simulation basée sur l'apprentissage des réseaux de neurones artificiels.
5. Les différentes classes et fonctions ont été programmées avec le langage C++, et incorporées sous forme de module additionnel nommé Gtetra sous le logiciel gOcad.

## Organisation du mémoire

Le Chapitre I est consacré au développement d'algorithme de calcul des composantes des champs de potentiels (gravimétrique et magnétique) créés par des structures géologiques complexes. Pour cela, le modèle géologique est représenté par un maillage non structuré à base de tétraèdres, ce qui a l'avantage de reproduire les corps ou structures géologiques complexes avec un nombre optimal d'éléments et par conséquent réduire l'espace mémoire et le temps de calcul. Le calcul des composantes des champs de potentiels est basé sur une approximation par une masse ponctuelle dans le cas de la gravimétrie ou un dipôle magnétique dans le cas du magnétisme. Un algorithme de subdivision est implémenté pour subdiviser de manière récursive chaque tétraèdre afin que l'approximation énoncée soit valide.

Le Chapitre II intervient dans un cadre d'inversions stochastiques. La méthode proposée est une combinaison des techniques de simulations utilisées en géostatistiques et les résultats trouvés par les méthodes d'inversions aux sens des moindres carrés. Sous une formulation bayésienne, la méthode d'inversion débute par la génération de l'information *a priori*, celle-ci est obtenue à partir des données géologiques et géophysiques.

Ainsi, plusieurs distributions spatiales et équiprobables des propriétés physiques dans le sous-sol sont simulées. A la fin la méthode sélectionne les modèles dont les réponses gravimétriques et/ou magnétiques offrent une bonne valeur de vraisemblance avec les données de référence. Le deuxième article présenté dans ce mémoire propose une inversion stochastique par l'utilisation de la Simulation Gaussienne Séquentielle. La méthode a été testée d'abords sur un exemple synthétique puis sur un cas réel qui constitue le Pluton du Flavrian situé au Nord du Québec (Canada).

Le Chapitre III présenté sous forme d'article présente une méthode d'inversion stochastique semblable à celle présentée au Chapitre II, avec l'introduction d'une variable secondaire. Ceci permet d'effectuer une inversion conjointe. Une contrainte sur la géologie structurale est obtenue à partir des résultats d'inversions de chaque variable séparément, puis cette contrainte géométrique est imposée. Ensuite, une co-simulation entre les variable primaire et secondaire est utilisée pour générer plusieurs réalisations. A la fin seules les réalisations ayant une propriété physique de probabilité *a posteriori* satisfaisantes seront gardées. La méthode a été appliquée sur un exemple synthétique et sur un cas réel localisé au dessus du Pluton McIvor dans le camp minier de Matagami au Québec (Canada).

Le Chapitre IV est présenté aussi sous forme d'article. Ce papier propose d'utiliser une méthode de simulation stochastique basée sur un apprentissage de réseau de neurones. Cette méthode a l'avantage d'intégrer plusieurs variables, aucune étude géostatistique telle que l'analyse du variogramme, la cosimulation, le coefficient de corrélation ou bien les relations empiriques entre les différentes variables n'est nécessaire. L'analyse des propriétés physiques est conditionnée par un certains nombre de données existantes soit au niveau des forages soit par les résultats d'inversion des méthodes géophysiques. Cette approche a été testée dans le camp minier de Val d'Or dans la province du Québec (Canada) pour démontrer la capacité des réseaux de neurones à intégrer plusieurs variables.

Enfin une conclusion générale dresse un bilan des travaux.



# CHAPITRE I

## CALCUL DIRECT DES CHAMPS DE POTENTIELS

### I.1 Introduction

L'existence d'un champ physique se traduit par l'action d'une force (gravitationnelle, magnétique, etc.) créée par une source qui agit sur tout corps présent dans l'espace. L'intensité du champ est directement proportionnelle aux paramètres intrinsèques de la source et inversement proportionnelle au carré (pour le champ gravimétrique) et au cube (pour le champ magnétique) de la distance qui sépare le point d'observation de la source. Sachant que les champs étudiés (gravitationnel et magnétique) sont conservatifs, il existe alors des niveaux d'équilibres appelés équipotentiels qui correspondent à des surfaces où les grandeurs du champ mesurées prennent la même valeur numérique.

### I.2 Modélisation géologique tridimensionnelle

Par définition la modélisation géologique est une représentation géométrique d'un objet présent dans le sous-sol. Un modèle géologique peut être représenté numériquement par une forme géométrique à l'aide de l'outil informatique ([Mallet, 2002](#)), mais il est difficile de trouver une définition du mot modèle géologique car sa définition varie d'une spécialité à une autre ([Massot, 2002](#)). En effet, le géophysicien a tendance à représenter le sous-sol par une répartition de propriétés physiques (densité, vitesse, magnétisation, etc.) dans une grille plus ou moins régulière en 2 ou 3 dimensions. En revanche pour un géologue (structuraliste par exemple), il va représenter le sous-sol par un ensemble de géométries (fille, horizon, anticinal, etc.). Néanmoins, le but de la modélisation est une représentation simplifiée du sous-sol qui pourrait aider à la compréhension et à l'interprétation géologique, voire la mise en évidence de ressources naturelles (pétrole, minéraux, eau), la détection de zones à risque (tectonique, écoulement, faille), etc.

Dans le but de se rapprocher de la réalité géologique, la modélisation géophysique doit être impérativement dans un espace 3D, car les structures (ou objets) géologiques possèdent trois dimensions. Le modèle géologique peut être représenté par une approche surfacique ou volumique. [Caumon \(2010\)](#) montre un bel exemple de modélisation où le même modèle structural est représenté selon des approches différentes Figure I.1.

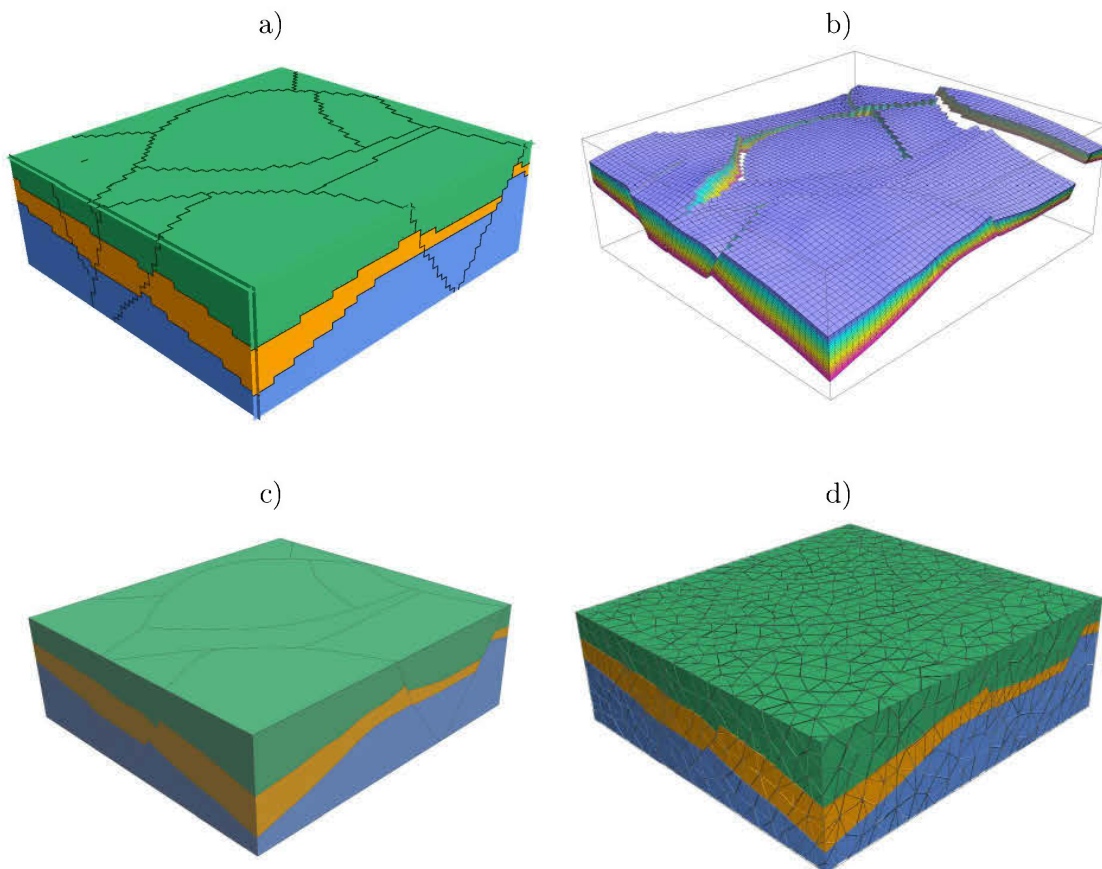


FIGURE I.1: Représentation volumique d'un modèle structural par : une grille cartésienne (a), une grille stratigraphique (b), un modèle par frontières (c), ou un maillage tétraédrique (d). par ([Caumon, 2010](#)).

Dans le cas d'une approche surfacique, comme son nom l'indique, la méthode utilise une combinaison de surfaces pour une représentation 3D du modèle géologique. Chaque surface représente une interface géologique qui correspond à la présence de faille, limite de couche ou une intrusion. Cette méthode a l'avantage d'être facile à manipuler au niveau du géomodelleur, elle requiert moins d'espace mémoire par rapport à l'approche volumétrique et offre une grande malléabilité pour la représentation des limites

géologiques avec des niveaux de résolutions variables en particulier lors de l'utilisation de surface à facettes triangulaires. Cependant certains règles concernant la chronologie, la résolution, doivent être respectées lors de la conception du modèle 3D ([Caumon et al., 2009](#)).

Dans le cas d'une approche volumétrique, le modèle peut être construit de deux façons :

1. Le découpage de l'espace suivant un maillage structuré, dans ce cas l'espace est découpé en grilles qui peuvent être séparés à leurs tours en deux groupes :
  - Les grilles aux géométries régulières : Cette méthode de modélisation consiste à effectuer un remplissage de l'espace par des volumes élémentaires de forme cubique ou rhomboédrique (voxels) ([Gjøystdal et al., 1985](#)). Cette méthode a l'avantage d'être simple à modéliser, mais son plus grand inconvénient réside dans l'augmentation de la résolution pour la modélisation des interfaces géologiques ou des modèles complexes, ce qui a pour effet d'augmenter l'espace mémoire. La modélisation par des éléments cubiques de différents volumes (Octree) permet de réduire le nombre d'éléments et par conséquent l'espace mémoire en effectuant un raffinement local au voisinage des zones complexes tel que les interfaces géologiques par exemple.
  - Les grilles stratigraphiques : le remplissage de l'espace s'effectue par des cellules hexaédriques déformées de manière à suivre la géométrie de l'objet. Par exemple la grille pourrait être déformée suivant un horizon pour s'aligner avec la stratigraphie ([Swanson, 1988](#)) ou bien pour s'ajuster aux failles ([Mallet, 2002](#)).
2. Le découpage de l'espace suivant un maillage non structuré : Une des techniques consiste à remplir l'espace par des polyèdres élémentaires. La méthode la plus utilisée est le remplissage de l'espace par des tétraèdres (cas particulier et simple du polyèdre) élémentaires où la limite de chaque volume est définie par une surface triangulée. La résolution varie dans l'espace pour respecter les données ([Caumon et al., 2004; Tertois et Mallet, 2007; Frank et al., 2007](#)).

### I.3 Calcul direct du champ de potentiel : état de l'art

En théorie du potentiel, le calcul (ou problème) direct revient à calculer, en un point donné  $P(x, y, z)$ , la ou les composante(s) du champ de potentiel (gravimétrique ou magnétique) d'un modèle synthétique défini par une géométrie et une distribution de

propriété physique. Par conséquent l'expression mathématique pour le calcul direct est directement liée à la méthode de modélisation géologique. La difficulté majeure dans le problème direct est l'approximation due à la modélisation numérique d'une part et au calcul de l'intégrale volumique définie par la géométrie du corps d'autre part. En présence de corps simples, par exemple sphère, parallélépipède ou cylindre vertical, le problème ne se pose pas sur le choix de la méthode de calcul, mais la nature est loin d'être aussi simple (sauf dans le cas d'une cavité ou de tunnel).

Dans le cas d'une modélisation par Voxel ou Octree, le calcul direct est souvent basé sur l'expression analytique d'un prisme rectangulaire droit avec une propriété physique constante (Bhattacharyya, 1964; Nagy, 1966; Vallabh Sharma, 1966; Mufti, 1973; Plouff, 1976), tandis que Chai et Hinze (1988); García-Abdeslem (1992); Jessell (2001); Zhou (2009) améliorent la méthode précédente par la prise en compte de la variation de la propriété physique au niveau du prisme.

Pour un corps isolé, les premières méthodes proposées par Talwani (1976) et Plouff (1976) consistait à approcher la forme du corps géologique (ou les variations topographique) par un empilement de polygones laminaires plus ou moins fins (Figure I.2.b). Le champ de potentiel est alors calculé par sommation des effets de chaque polygone.

Une autre stratégie formulée par Bott (1963); Barnett (1976); Okabe (1979); Hansen et Wang (1988); Holstein et al. (1999) permet de passer d'une intégrale tridimensionnelle à une bidimensionnelle par assimilation de la géométrie du corps géologique en une surface polygonale fermée (Figure I.2.c). Ces méthodes de calculs pourraient être utilisées dans le cas d'une modélisation surfacique ou par frontière dans l'hypothèse d'une propriété physique constante par région ou dans le cas d'une variation linéaire (Holstein et al., 1999).

Dans le cas d'une modélisation par grille stratigraphique, la géométrie d'une cellule en forme d'hexaèdre complique le calcul. Néanmoins, il est possible de calculer le champ de potentiel en considérant chaque cellule du maillage comme un cas particulier d'un polyèdre, ce qui a pour effet d'augmenter considérablement le temps de calcul.

Dans le souci de se rapprocher plus de la réalité géologique, nous avons développé une

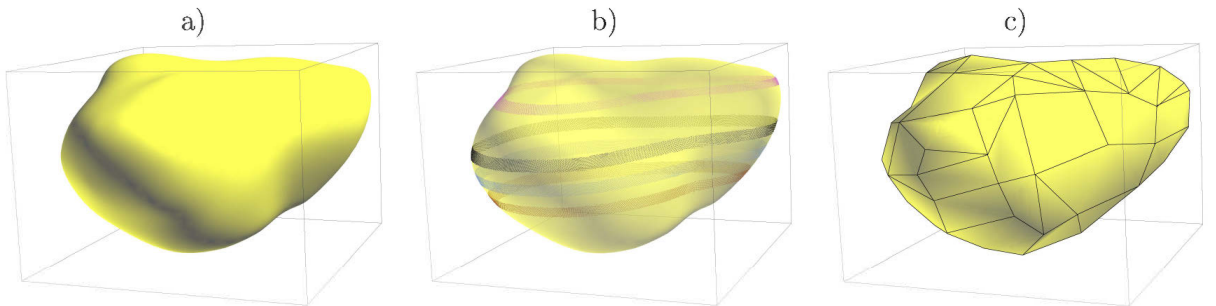


FIGURE I.2: Corps géologique isolé (a) et son approximation tridimensionnelles (b) en tranche laminaire, (c) en surface polyédrale, pour le calcul du champ de potentiel

nouvelle méthode qui permet de calculer les composantes des champs de potentiels (gravimétrique et magnétique) et qui a fait l'objet du premier article de cette thèse. Dans ce cas le modèle géologique est représenté par un maillage tétraédrique, ce qui offre une bonne acuité lors des modélisations, particulièrement, en présence de structures géologiques hétérogènes et complexes (plissement, présence de failles, intrusion, etc).

#### I.4 3D gravity and magnetic forward modelling using tetrahedra-based subdivision method

Nacim Foudil-Bey<sup>\*†</sup>, Jean-Jacques Royer\*, Guillaume Caumon\*, Li Zhen Cheng<sup>†</sup> and Christophe Antoine\*

##### I.4.1 Résumé

Le maillage tétraédrique est une méthode très efficace pour modéliser les structures géologiques complexes faillées et avec des propriétés physiques hétérogènes, offrant ainsi une meilleure précision, car cette approche utilise moins d'éléments que la modélisation par approche prismatiques conventionnelles ou par grille cartésienne. L'article suivant présente une nouvelle méthode de modélisation directe des champs gravimétrique et magnétique produit par une source géologique complexe en 3D avec une distribution de propriétés physiques connues (pour le cas gravimétrique c'est la densité, pour le cas magnétique c'est la l'inclinaison la déclinaison de l'aimantation et du champ géomagnétique) par l'utilisation de maillage tétraédrique. Les composants du champ de gravimétrique sont calculés par l'approximation de chaque tétraèdre élémentaire à une masse ponctuelle, tandis que les composantes du champ magnétique et l'anomalie magnétique totale sont calculées dans l'hypothèse où chaque cellule élémentaire est réduite à un

dipôle magnétique. Ces approximations sont valables pour tétraèdres profonde où la distance du tétraèdre au point observation est beaucoup plus grandes que la dimension de la cellule. Près de la surface l'algorithme subdivise récursivement chaque tétraèdre qui ne respecte pas l'hypothèse de départ en huit nouveaux tétraèdres afin de subdiviser les tétraèdres grossiers en plus petits avec un ratio de 4 entre la distance et la taille de la cellule. Ce processus appelé méthode de subdivision tétraédrique est effectué de manière récursive sur chaque tétraèdre jusqu'à ce que la condition du ratio soit respectée. La réponse du champ de potentiel est alors calculée par la sommation des effets de chaque tétraèdre à chaque emplacement des données. L'algorithme a été testé sur des modèles théoriques simples (telles que la sphère et le prisme) avec des paramètres homogènes. Les résultats numériques montrent une très bonne corrélation avec les solutions théoriques comportant des erreurs relatives allant généralement de 0,1% à 1% pour le champ de gravité, mais avec une plus grande erreur relative dans le cas du champ magnétique. La méthode est ensuite appliquée au corps synthétique avec une distribution hétérogène de la densité et la susceptibilité magnétique.

#### I.4.2 Abstract

Tetrahedral grids are efficient to describe heterogeneous complex faulted geological structures and petro-physical properties, providing novel accuracy because they require less elements than conventional prismatic or Cartesian regular grids. We have developed a gravity and magnetic forward modelling produced by 3D complex geologic sources with a known physical property distribution (for the gravity case the density and for the magnetic case, the susceptibility, the inclination and azimuth of the magnetization and geomagnetic field vectors) using tetrahedral unstructured grids. The components of gravity field are calculated assuming that each elementary cell of mass can be reduced to a single point at the center of an elementary tetrahedron cell, while the components of magnetic field and the total magnetic anomaly are computed under the assumption that the elementary cell is reduced to a magnetic dipole. These approximations are valid for deep tetrahedra where distances to the observed point at the surface are much larger than the cell dimensions. It fails near the surface where a recursive meshing based on 8 tetrahedra is performed in order to split coarse tetrahedra into smaller ones with a distance to cell size ratio close to 4. This process named tetrahedra-based subdivision method is performed recursively on each tetrahedron until the size ratio condition is respected. The potential-field response is then approximated by summing the effects of

every tetrahedron at each data location. The algorithm has been tested on simple theoretical models (such as sphere and prism) with homogeneous parameters. The numerical results show a very good fit to the theoretical solutions with relative errors typically ranging from 0.1% to 1% for gravity field, but with a greater relative error in the case of the magnetic field. The method is then applied to synthetic body with heterogeneous distribution of the density and the magnetic susceptibility.

### I.4.3 Introduction

3D tetrahedra model with an optimal number of elements is an efficient technique commonly used for representing complex faulted structures in a number of geological and geomechanical applications. Considering that a complex geological body can be discretized into a set of tetrahedra. This approach can be more accurate and faster than the classical discretization of the body into a grid of 3D vertical, juxtaposed prisms in the horizontal and vertical directions. In addition, the prismatic approach requires more elements for a comparable resolution, especially for isolated sources in presence of faults, like those encountered in mineral exploration. Historically, fast forward potential methods were developed for complex geometry by (Hubbert, 1948); (Murthy and Rao, 1979); (Zhang et al., 2001) and (Zhou, 2008). These methods were applied in 2D with constant density contrast or depth variations. (Ruotoistenmätki, 1992) and then, (Martín-Atienza and García-Abdeslem, 1999) extended the theory for calculating the gravity response of a 2D shape body and surface density distribution represented by polynomial functions. Recently, (Zhou, 2009a) applied a *General Line Integral* method for computing the gravity anomalies of irregular 2D masses with density contrast varying both in the horizontal and vertical directions, but which can be expressed as a separable function of the coordinate system. The most popular pioneer numerical methods applied to gravity and magnetic forward modelling were developed by (Talwani and Ewing, 1960) and (Plouff, 1976). Their methods consisted in approximating the underground body shape by a stack of laminar horizontal solid polygons assuming a constant property value per polygon, highly variable parameter (density or magnetic susceptibility) zones being refined using smaller polygons. The potential field is then estimated by integrating the contribution of each elementary polygon in the *space domain*. These methods are particularly well adapted to estimate anomalies induced by the topography or the bathymetry (Plouff, 1977). Other approaches have also been developed in the *spectral domain*, such as the early work by (Bhattacharyya, 1964) who estimated the total magnetic field or gravity responses induced by a 3D model made of a set

of prisms, while (Chai and Hinze, 1988), (García-Abdeslem, 1992), (Jessell, 2001) and (Zhou, 2009b) extended this method to vertical prisms with density contrast varying according to depth. Other works by (Bott, 1963), (Barnett, 1976), (Okabe, 1979), (Hansen and Wang, 1988) and (Götze and Lahmeyer, 1988) suggested simplified techniques that approximate the complex body by shape surfaces modeled with polygonal facets. The variants between these methods (surface, line and vertex) aim at increasing the precision imposed by the calculation terms which can be arbitrarily large after summation as noticed by (Holstein and Ketteridge, 1996). For uniform polyhedra, (Holstein et al., 1999) presented a comparison study of different algorithms published on gravity studies by (Strakhov and Yefimov, 1986b), (Strakhov and Yefimov, 1986a), (Pohánka, 1988), (Pohánka, 1990) and (Holstein and Ketteridge, 1996). (Holstein, 2003) concluded that the recent algorithms produce smaller errors but are more complex to be implemented and that they are limited to polyhedra with constant parameters (density, magnetization) or with linear spatial variation for those parameters. This paper presents a more general 3D approach in which the geometry and physical properties are modeled using elementary tetrahedra in which parameters (density and magnetization) are constant or vary linearly. Complex faulted structures are refined using smaller tetrahedra takes into account complex geometrical structures, or to reproduce the high spatial variability of the parameters. Our proposed tetrahedra approach is compared with theoretical responses calculated on simple reference shapes and is then applied to synthetic complex body with heterogeneous properties distribution.

#### I.4.4 Theory

##### I.4.4.1 Components of the gravity field

Let's assume that a 3D source can be modelled by using a tetrahedral unstructured grid. Under the assumption that each tetrahedron can be approximated to a point mass, the gravitational attraction produced by the point mass is given by (Blakely, 1996, p.44) :

$$\mathbf{g}(P) = -\gamma \frac{m}{r^2} \hat{\mathbf{r}} \quad (\text{I.1})$$

where  $r = (r_x^2 + r_y^2 + r_z^2)^{\frac{1}{2}}$  and  $\hat{\mathbf{r}}$  are the Euclidean distance and a unit vector from the point mass  $m$  to the observed point  $P$ , respectively ;  $\gamma$  is the universal gravitational constant.

The components of gravitational field at the observed point  $P$  are given by the following

equation :

$$\mathbf{g}(P) = \begin{bmatrix} g_x \\ g_y \\ g_z \end{bmatrix} = \begin{cases} -\gamma \frac{m r_x}{r^3} \\ -\gamma \frac{m r_y}{r^3} \\ -\gamma \frac{m r_z}{r^3} \end{cases} \quad (\text{I.2})$$

#### I.4.4.2 Components of the magnetic field

In 3D magnetic forward modelling the following fundamental simplification is assumed : *the magnetic field components are calculated approximating each tetrahedron to an elementary magnetic dipole*. The components of the dipole field are then given by the following classical formula ([Blakely, 1996, p.75](#)) :

$$\mathbf{B} = \frac{m}{r^3} [3(\hat{\mathbf{m}} \cdot \hat{\mathbf{r}})\hat{\mathbf{r}} - \hat{\mathbf{m}}] \quad (\text{I.3})$$

The components of magnetic field are given by :

$$\mathbf{B}(P) = \begin{bmatrix} B_x \\ B_y \\ B_z \end{bmatrix} = \begin{cases} \frac{\mu_0}{4\pi} \frac{m (3 r_m r_x - r^2 m_x)}{r^5} \\ \frac{\mu_0}{4\pi} \frac{m (3 r_m r_y - r^2 m_y)}{r^5} \\ \frac{\mu_0}{4\pi} \frac{m (3 r_m r_z - r^2 m_z)}{r^5} \end{cases} \quad (\text{I.4})$$

the the total magnetic is given by :

$$B_t = \sin(I) B_z + \cos(I) \{ \cos(D) B_y + \sin(D) B_x \} \quad (\text{I.5})$$

where  $r = \|\mathbf{r}\|$  is the distance between the observed point ( $P$ ) and the dipole center;  $r_m = \hat{\mathbf{r}} \cdot \hat{\mathbf{m}}$  is the scalar product of the distance vector  $\mathbf{r} = (r_x, r_y, r_z)$  and  $(m_x, m_y, m_z)$  are the three direction cosines of the unit vector  $\hat{\mathbf{m}}$  oriented along the magnetic dipole; the dipole moment  $m$  is given by the product of the volume of the tetrahedron and its magnetization\* ;  $\mu_0$  is the magnetic permeability of the free space;  $I$  and  $D$  are the inclination and the declination of geomagnetic field, respectively.

---

\*. the magnetization vector is the sum of induced and remanent magnetizations

#### I.4.4.3 Sensitivity to the tetrahedral grid

The approximations (point source in the case of gravity data or point dipole in the case of magnetic data) are valid when the size of the elementary tetrahedron is not too big, when the distance  $d$  from the observation  $P$  to the source  $S$  is much greater than the maximum distance  $l$  of the barycenter to the tetrahedral cell vertices ( $d \gg l$ ), otherwise a mesh refinement must be applied or an exact analytical formula is required. In order to quantify how the computed solution fits adequately to the true analytical one, a root mean square (rms) error criterion has been used. It is defined as the square root of the average of the squared differences between the *analytical* and *calculated* fields on each surface cell. Figure I.3.a and I.3.b shows the variation of the rms error versus the number of tetrahedra in the prism for various depth configurations respectively for gravity and magnetic<sup>†</sup> case. Evidently, it can be noticed that : (i) the rms error decreases as the number of tetrahedra increases ; (ii) the deeper the prism, the smaller the rms error ; (iii) in the gravity case, the rms error decreases more rapidly than the magnetic case, because the gravity field is varying inverse of distance square, the magnetic field is varying inverse distance cube, therefore for the same tetrahedron the induced error via approximation (mass point, magnetic dipole) is greater for magnetic field rather than for the gravity field.

#### I.4.4.4 Mesh subdivision algorithm

Equations I.1 and I.5 are valid for cells far from the earth surface when the distance  $d$  to the source  $S$  is much greater than the maximum distance  $l$  of the barycenter to the tetrahedral cell vertices ( $d \gg l$ ). In this work, this criteria is referred to as the *distance to cell size ratio*. Near the surface, when the distance ratio  $d/l$  is less than 4 (a value chosen experimentally after several numerical trials in the gravity case), the elementary tetrahedral cells are refined into smaller tetrahedral cells. Several strategies can be used to subdivide a tetrahedral cell (Conreaux, 2001; Frank et al., 2007). For splitting the tetrahedral cells, the eight tetrahedra corner decomposition algorithm has been chosen for this work because it keeps a similar aspect ratio for each new generated cell (Figure I.4.a), then the splitting strategy has been optimized for the shallow tetrahedra (Figure I.4.b.) A source code has been written in C++ and implemented using two algorithms. The first one described in (Figure I.5.a) is the *subdivision algorithm* : it requires as input a 3D model composed by a set of tetrahedra (*step 1*) ; for each tetrahedron

---

<sup>†</sup>. the total magnetic field was normalized by the magnetization intensity

(*step 2*) the algorithm finds the smallest distance ( $d$ ) (*step 3*) between the surface point and the barycenter of the current tetrahedron ; if the distance ratio ( $d/l$ ) is less than the threshold ratio (fixed to 4 by default) (*step 4*), the current tetrahedron is subdivided in 8 new tetrahedra (*step 5*) and then stored in a temporary list. This algorithm is repeated recursively as long as all tetrahedra satisfy the distance ratio condition (*step 6*) (Figure I.4.b).

The second algorithm (Figure I.5.b) computes the *potential field* of each tetrahedron in the list. First, it reads the locations of the measurement point on the ground surface on which the total-field response is calculated (*step 1*), the field value is then initialized to zero (*step 2*), for each tetrahedron, the potential field contribution is computed using equations I.1, I.4 and I.5 respectively for the components of gravity data, components of magnetic data and total magnetic anomaly, (*step 3*) and summed (*step 4*), then the algorithm is performed on the next measurement point (*step 5*).

## I.4.5 Comparing the responses with the analytical solutions

### I.4.5.1 Validation on a prism of uniform density

The analytical response of the vertical component of the gravity field at the observation point  $P(x_p, y_p, z_p)$  produced by a homogeneous prism immersed in a uniform medium can be derived from the Green theorem as following (Plouff, 1976) :

$$g_z = \gamma \rho \sum_{i=1}^2 \sum_{j=1}^2 \sum_{k=1}^2 \mu_{ijk} z_k \arctan \left( \frac{d_{x_i} d_{y_j}}{d_{z_k} d} \right) - d_{x_i} \ln(d + d_{y_j}) - d_{y_j} \ln(d + d_{x_i}) \quad (\text{I.6})$$

where  $d_{x_i} = (x_p - x_i)$ ,  $d_{y_i} = (y_p - y_i)$  and  $d_{z_i} = (z_p - z_i)$  are the distances to the point source at the coordinates  $(x_i, y_j, z_k)$  to the observation point  $P$  along the coordinate axes,  $d = \sqrt{d_{x_i}^2 + d_{y_j}^2 + d_{z_k}^2}$ ,  $\mu_{ijk} = (-1)^i(-1)^j(-1)^k$  a signed coefficient,  $\gamma$  the gravitational constant and  $\rho$  is the density of the prism.

Figure I.6 compares the vertical component of the gravity field produced by a rectangular prism using the analytical formula (equation I.6) with vertical component of the gravity calculated using our subdivision method with different values ratio. The prism is meshed assuming that each tetrahedron is sufficiently small to be assimilated to an infinitesimal point mass (Equation I.1). Figure I.6 shows that the relative error decreases with increasing the *ratio* factor. For the small value *ratio* of 2 (Figure I.6.a) the relative error is less than 0.7%, for *ratio* of 3 the relative error is less than 0.3% (Figure I.6.b).

In this case it is assumed that aspect *ratio* of 3 is adequate end enough for gravity computation (Figure I.6.b).

#### I.4.5.2 Validation on prism with uniform magnetic susceptibility

We discuss the validity of our approach for computing the total magnetic field. To validate our method we compare the analytical response of the total magnetic field produced by a buried prism with the one calculated by our division algorithm. The total magnetic anomaly at the observation point  $P(x_p, y_p, z_p)$  produced by a prism with top located at  $z_t$  and the bottom at infinity is given by (Bhattacharyya, 1964) :

$$\begin{aligned} B_t(P) = & M \sum_{i=1}^2 \sum_{j=1}^2 \mu_{ij} \frac{\alpha_{23}}{2} \ln \left( \frac{d - d_{x_i}}{d + d_{x_i}} \right) + \frac{\alpha_{13}}{2} \log \left( \frac{d - d_{y_j}}{d + d_{y_j}} \right) \\ & \cdots - \alpha_{12} \ln(d + z_t) - M_x F_x \tan^{-1} \left( \frac{d_{x_i} d_{y_j}}{d_{x_i}^2 + d z_t + z_t^2} \right) \\ & \cdots - M_y F_y \tan^{-1} \left( \frac{d_{x_i} d_{y_j}}{d^2 + d z_t - d_{x_i}^2} \right) \\ & \cdots + M_z F_z \tan^{-1} \left( \frac{d_{x_i} d_{y_j}}{d d_{z_t}} \right). \end{aligned} \quad (\text{I.7})$$

where  $d_{x_i} = (x_p - x_i)$ ,  $d_{y_j} = (y_p - y_j)$ , are the distances to the point source at the coordinates ( $x = x_i$ ,  $y = y_j$  and  $z = z_t$ ) to the observation point  $P(x_p, y_p, z_p)$  along the coordinate axes and  $d_{z_t} = (z_p - z_t)$  the distance from the top of the prism to the vertical coordinate of the point source,  $d = \sqrt{d_{x_i}^2 + d_{y_j}^2 + d_{z_t}^2}$ ,  $M$  the intensity of magnetization,  $\mu_{ij} = (-1)^i(-1)^j$  a signed coefficient,  $\alpha_{12} = M_x F_y + M_y F_x$ ,  $\alpha_{13} = M_x F_z + M_z F_x$  and  $\alpha_{13}(M_y F_z + M_z F_y)$ , the utits vectors of the magnetic earth field and magnetization vectors are defined respectively by the direction cosine  $(F_x, F_y, F_z)$  and  $(M_x, M_y, M_z)$ .

Figure I.7 compares the total magnetic field of the rectangular prism with constant magnetic susceptibility ( $\chi = 0.01 \text{ SI}$ , *earth field* = 50000 nT) using analytical formula (equation I.7) with the magnetic response computed using the subdivision algorithm proposed in this paper (equation I.5). As we could expect, the relative errors decrease as values for ratio increase. However a *ratio* of 6 is required to get a relative error less than 3%.

#### I.4.5.3 Validation on a sphere with uniform parameter (density / magnetic susceptibility)

We evaluate the performance of our method by applying it to sphere with uniform density and magnetic susceptibility. First, we computed the analytical responses of the vertical component of gravity field and total magnetic field yielded by uniform sphere is known ([Blakely, 1996](#)). Then, we compared these analytical responses with those computed by the subdivision method proposed in this paper. The reference model is a sphere composed by 16681 tetrahedra of radius 45 m (Figure I.8.c), the center is located at a depth of 45.1 m below the surface with a constant parameters of  $\rho = 1 \text{ g/cm}^3$  and  $\chi = 0.01SI$ . The inducing earth field has an inclination of  $90^\circ$ , a declination of  $0^\circ$  and a strength of 50000 nT.

The vertical component of gravity response computed at a planar surface was calculated on 2401 points, separated by 4m over an area of 200 m  $\times$  200 m.

Figure I.8.a shows the absolute differences between the analytical and the subdivision algorithm computed for the vertical component of gravity fields produced by a sphere; the latter is produced by the proposed tetrahedral approach with subdividing algorithm with *ratio* of 3. The maximum absolute error is less than 0.004 mGals over value of 1.2 mGals (i.e less than 0.3%). Figure I.8.b shows the absolute differences between the analytical and the subdivision algorithm computed for total magnetic fields produced by a sphere; the latter is produced by the proposed tetrahedral approach with subdividing algorithm with *ratio* of 4. For most of the area, this difference is smaller than 3nT corresponding to about 1% of the maximum value of the total field anomaly (300nT).

#### I.4.5.4 Application to synthetic complex geological body

For testing the performance of the tetrahedral approach using the subdivision algorithm, we generate synthetic [complex geometry](#) model using tetrahedral grid(Figure I.9.a) and prismatic grid (Figure I.9.b). The body is confined in the interior of a subsurface region with a dimension of 1457 m  $\times$  1560 m  $\times$  885 m with a density and magnetic susceptibility variations, however the properties are constant for each tetrhedron (Figure I.10). The inducing earth field has an inclination of  $65^\circ$ , a declination of  $-25^\circ$  and a strength of 50000 nT. The magnetization with remanence has an inclination of  $45^\circ$ , a declination of  $75^\circ$  and a strength of 1 A/m.

For the tetrahedra approach the number of elements composing the body is equal to 76,003. However, for the prismatic approach, the body is represented into the regular Cartesian grid which is divided into  $127 \times 127 \times 63 = 1,016,127$  elementary cells.

The components of the gravity and the magnetic fields are computed above the center of the model at an altitude of 20 m on a surface of dimensions 2700 m × 2500 m, sampled regularly by 2805 points. In this paper, we used an Intel Core 2 Duo Processor 64-bit, by applying the equations [I.6](#) and [I.7](#) for different grid resolutions consisting of (30×30×15), (50×50×30), (127×127×63), (200×200×150) and (300×300×200) grid of 3D prisms, the computation time for a vertical component of gravity field and total magnetic anomaly are represented in ([Table I.1](#)), the computation times for the total magnetic-field takes 4, 17, 60, 80 minutes and 8 hours respectively. For the vertical component of gravity field, the computation times takes 3, 13, 35, 60 minutes and 4 hours respectively. Finally using the tetrahedra-based subdivision algorithm on the tetrahedron model which leads to a computation time of less than 2 minute for total magnetic field and 1 minute for vertical component of gravity field.

Figures [I.11.a](#) , [I.11.b](#) and [I.11.c](#) shows respectively the  $B_x$ ,  $B_y$  and  $B_z$  components of the magnetic fields, Figure [I.11.d](#) [I.11.e](#) and [I.11.f](#) shows respectively the vertical component of the gravity field, total magnetic-field without remanent magnetization and total magnetic-field with remanent magnetization using subdivision algorithm for the synthetic body ([Figure I.9.a](#)). However we notice some small differences induced by the effect of prismatic approach with (300 × 300 × 200) resolution. For the gravity case, the rms and abs errors are respectively 0.1% and 0.02%. For the magnetic case, the rms and abs errors are respectively 11% and 1.5%. This difference is mainly caused by the rough approximation of the complex geometry made in the prismatic model compared to the tetrahedral model which is more accurate. As the geometry is simplified in the grided model, the error is larger. we notice that the rms error of total magnetic field is 90 times greater than rms error of vertical component of gravity field

#### I.4.6 Discussion

By comparing the analytical gravity and magnetic responses with both forward gravity and magnetic responses computed by our tetrahedra approach using subdivision algorithm, we assure the performance of our method. The rms errors are estimated to less than 1% 0.3% for *ratio* of 3 for the vertical component of the gravity field yielded respectively by a prism and a sphere. However, the rms errors for the total magnetic field yielded by the prism and sphere are respectively around 5% for *ratio* of 6. In case of homogeneous rectangular prism, in order to have the same relative average error, the aspect ratio used for magnetic computation must be greater than the aspect ratio used for gravity calculation. These numerical errors can be considered as admissible and falling

within the numerical errors due to the meshing algorithm. Preliminary tests show that a greater precision is obtained with additional refinement of the tetrahedral mesh, but this of course implies slower computing time. For a reasonable precision, the computing time requested by the tetrahedra-based subdivision algorithm is on average ten times faster than those requested by the classical methods, because the size of the tetrahedra can be adapted to the complexity of both the geometry and spatial variability of parameters.

#### I.4.7 Conclusions

We have developed gravity and magnetic forward modelling for calculating the components of gravity and magnetic fields produced by 3D geological sources using an unstructured tetrahedral grid. The physical properties are defined at the four vertices of the elementary tetrahedral cells or at the center of the tetrahedron. The algorithms used in this work are based on an approximations (point mass or magnetic dipole) of the elementary tetrahedral cells, provided the distance from the tetrahedron to the measurement points is sufficiently large (usually, four times the average size of the cell) such that the proposed approximations remains valid. Elsewhere, if the elementary cell is too large, or located near the surface, we applied an iterative refinement technique which consists in dividing each tetrahedron into 8 new smaller tetrahedral, setting up a new set of tetrahedral. The algorithm is applied recursively until the above distance criterion is satisfied. The major advantages of the suggested subdivision tetrahedra algorithm are : (i) it can be implemented easily; (ii) it is fast as the meshing is adaptable to the complexity; (iii) applicable to any complex faulted geological body with any property spatial distribution; (iv) It can compute the potential field responses at any location and it does not require a regular meshed surface with imposed number of cells. The main drawbacks of the proposed tetrahedra-based subdivision algorithm are : (i) the ratio criterion that controls the subdivision procedure that automatically divides each tetrahedron into eight new tetrahedra depends on the nature of the problem to be solved; a smaller ratio is required for gravity compared to magnetic or micro gravimetric methods; (ii) the dividing methods requires as an input a tetrahedral mesh for representing the complex faulted 3D body, together with a data model to store physical properties; (iii) for models with constant parameters (density, susceptibility and magnetization) and simple geometry, indeed not a realistic case in practice, the subdivision is sometimes applied when it might be not necessary and consequently may imply slower computing time compared to direct analytical solutions. In conclusion, the tetrahedra-based formulation is faster than the traditional prismatic meshing. There is no need to make

complex coordinate transformations, as it is the case with some previously published schemes. This new approach, used in conjunction with an efficient meshing algorithm will considerably improved the numerical modelling of gravity and magnetic anomalies from complex bodies. It is hoped that our contribution will help in improving gravity and magnetic methods, especially in the case of complex faulted geological models with heterogeneous physical properties.

#### I.4.8 Acknowledgements

The authors would like to express their thanks to the gOcad consortium, ASGA and to the French National Scientific Research Center CNRS-CRPG for their support. This work was made within a Cotutelle cooperative program between the Nancy University, France and the UQAT, Université du Québec en Abitibi - Témiscamingue, Québec, Canada.

## References

- Barnett, C. T., 1976, Theoretical modelling of the magnetic and gravitational fields of an arbitrarily shaped Three-Dimensional body : *Geophysics*, **41**, 1353–1364.
- Bhattacharyya, B. K., 1964, Magnetic anomalies due to prism-shaped bodies with arbitrary polarization : *Geophysical Prospecting*, **24**, 633–649.
- Bhattacharyya, B. K., and M. E. Navolio, 1976, A Fast Fourier Transform method for rapid computation of gravity and magnetic anomalies due to arbitrary bodies : *Geophysical Prospecting*, **24**, 633–649.
- Blakely, J. R., 1996, Potential theory in gravity & magnetic applications : Cambridge University Press.
- Bott, M. H. P., 1963, Two methods applicable to computers for evaluating magnetic anomalies due to finite three dimensional bodies : *Geophysical Prospecting*, **11**, 292–299.
- Chai, Y., and J. Hinze, W., 1988, Gravity inversion of an interface above which the density contrast varies exponentially with depth : *Geophysics*, **53**, 837–845.
- Conreaux, S., 2001, Modélisation de 3-variétés à base topologique : application à la géologie : PhD thesis, Institut National Polytechnique de Lorrain.
- Frank, T., A.-L. Tertois, and J.-L. Mallet, 2007, 3D-reconstruction of complex geological interfaces from irregularly distributed and noisy point data : *Computers and Geosciences*, **33**, no. 7, 932–943.
- García-Abdeslem, J., 1992, Gravitational attraction of a rectangular prism with depth-dependent density : *Geophysics*, **57**, 470–473.
- Götze, H.-J., and B. Lahmeyer, 1988, Application of three-dimensional interactive modeling in gravity and magnetics : *Geophysics*, **53**, 1096–1108.
- Hansen, R. O., and X. Wang, 1988, Simplified frequency-domain expressions for potential fields of arbitrary three-dimensional bodies : *Geophysics*, **53**, 365–374.
- Holstein, H., 2003, Gravimagnetic anomaly formulas for polyhedra of spatially linear media : *Geophysics*, **68**, 157–167.

- Holstein, H., and B. Ketteridge, 1996, Gravimetric analysis of uniform polyhedra : Geophysics, **61**, 357–364.
- Holstein, H., P. Schurholz, J. Starr A., and M. Chakraborty, 1999, Comparison of gravimetric formulas for uniform polyhedra : Geophysics, **64**, 1438–1446.
- Hubbert, M. K., 1948, A line-integral method of computing the gravimetric effects of two-dimensional masses : Geophysics, **13**, 215–225.
- Jessell, M., 2001, Three-dimensional geological modelling of potential-field data : Computers & Geosciences, **27**, 455 – 465.
- Martin-Atienza, B., and J. García-Abdeslem, 1999, 2-D gravity modeling with analytically defined geometry and quadratic polynomial density functions : Geophysics, **64**, 1730–1734.
- Murthy, I. V. R., and D. B. Rao, 1979, Gravity anomalies of two dimensional bodies of irregular cross-section with density contrast varying with depth : Geophysics, **44**, 1525–1530.
- Okabe, M., 1979, Analytical expressions for gravity anomalies due to homogeneous polyhedral bodies and translations into magnetic anomalies : Geophysics, **44**, 730–741.
- Parker, R. L., 1972, The rapid calculation of potential anomalies : Geophys. J. Roy Astr. Soc., **31**, 447–455.
- Plouff, D., 1976, Gravity and magnetic fields of polygonal prisms and application to magnetic terrain corrections : Geophysics, **41**, 727–741.
- , 1977, Preliminary documentation for a fortran program to compute gravity terrain corrections based on topography digitized on a geographic grid : U. S. Geological Survey Open-File Report, **45**, 77–535.
- Pohánka, V., 1988, Optimum expression for computation of the gravity field of a homogeneous polyhedral body : Geophysical Prospecting, **36**, 733–751.
- , 1990, Reply to comment by M. Ivan : Geophysical Prospecting, **38**, 333–335.
- Ruotoistenmätki, T., 1992, The gravity anomaly of two-dimensional sources with continuous density distribution and bounded by continuous surfaces : Geophysics, **57**, 623–628.
- Strakhov, V. N., L. M. I., and A. B. Yefimov, 1986a, Solution of direct gravity and magnetic problems with new analytical expressions of the field of typical approximating bodies II : Izvestiya : Earth Sciences, **22**, 566–575.
- , 1986b, A solution to forward problems in gravity and magnetism with new analytical expressions for the field elements of standard approximating bodies I : Izvestiya : Earth Sciences, **22**, 471–482.

- Talwani, M., and M. Ewing, 1960, Rapid Computation of Gravitational Attraction of Three-Dimensional Bodies of Arbitrary Shape : Geophysics, **25**, 203–225.
- Zhang, J., B. Zhong, X. Zhou, and Y. Dai, 2001, Gravity anomalies of 2-D bodies with variable density contrast : Geophysics, **66**, 809–813.
- Zhou, X., 2008, 2D vector gravity potential and line integrals for the gravity anomaly caused by a 2D mass of depth-dependent density contrast : Geophysics, **73**, I43–I50.
- \_\_\_\_\_, 2009a, 3d vector gravity potential and line integrals for the gravity anomaly of a rectangular prism with 3d variable density contrast : Geophysics, **74**, I43–I53.
- \_\_\_\_\_, 2009b, General line integrals for gravity anomalies of irregular 2D masses with horizontally and vertically dependent density contrast : Geophysics, **74**, I1–I7.

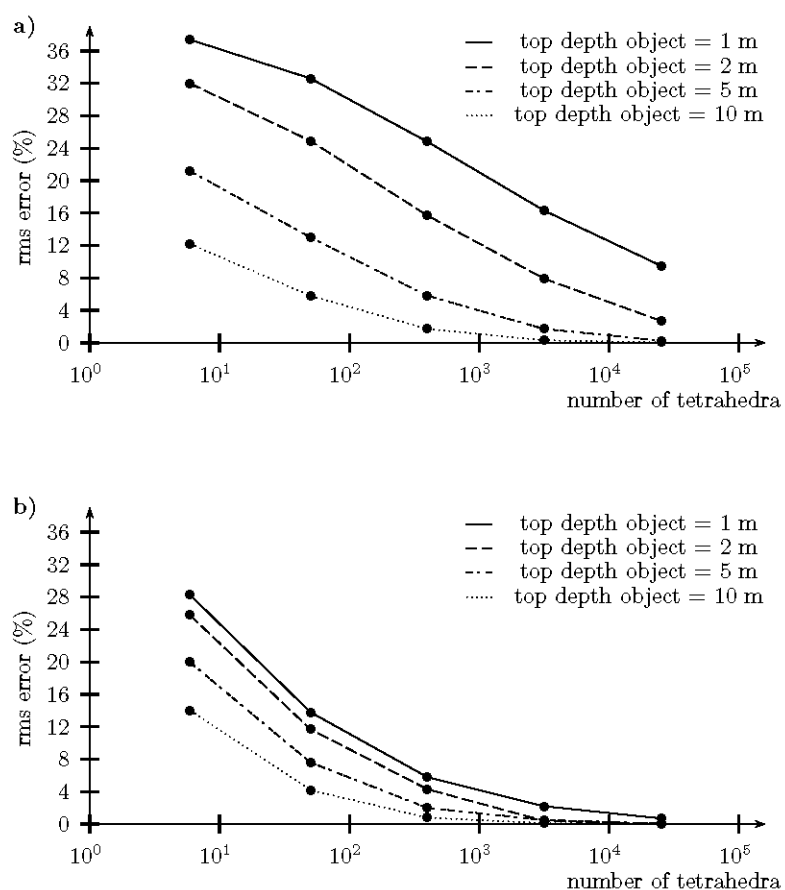


FIGURE I.3: rms errors (a) vertical component of gravity and (b) total magnetic fields for different number of tetrahedra in the prismatic body at various depths.

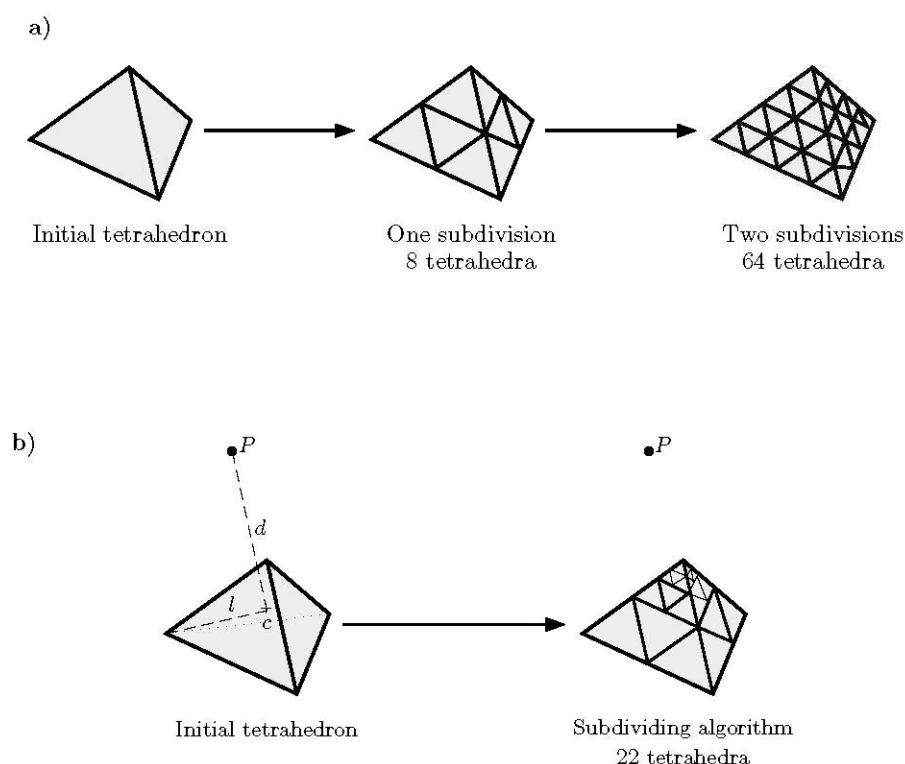


FIGURE I.4: Dividing a coarse tetrahedral cell into smaller tetrahedra. (a) Using the corner subdivision algorithm and (b) using optimized corner subdivision algorithm.

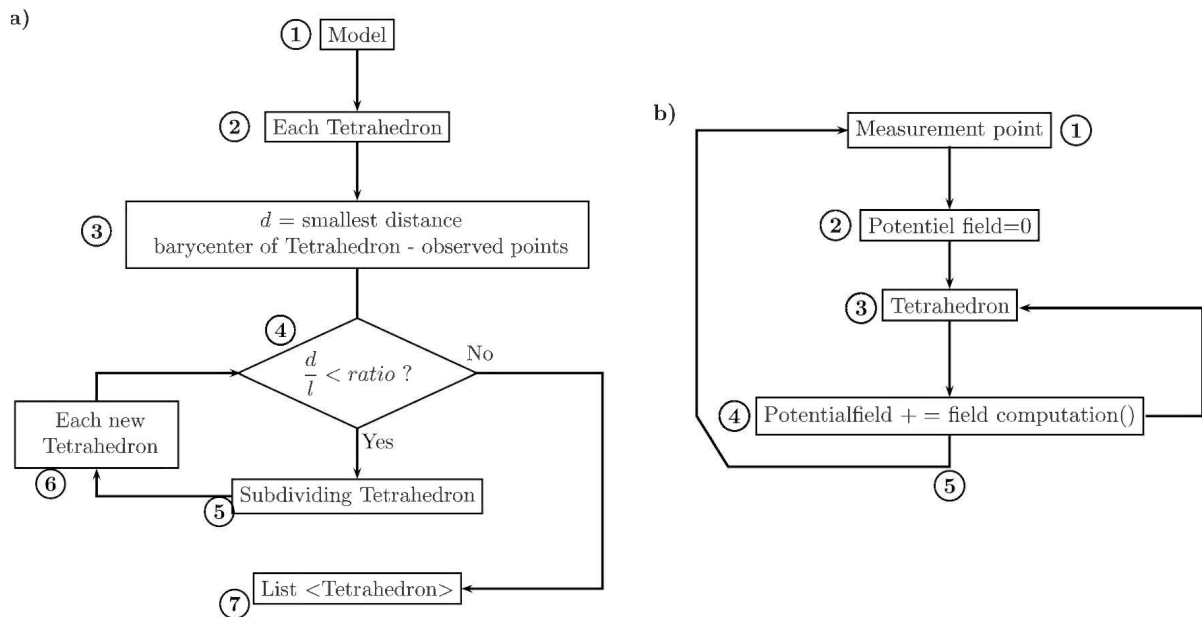


FIGURE I.5: Flow chart diagram describing.(a) The subdivision algorithm and (b) the potential field contribution. (Step number refers to text comments).

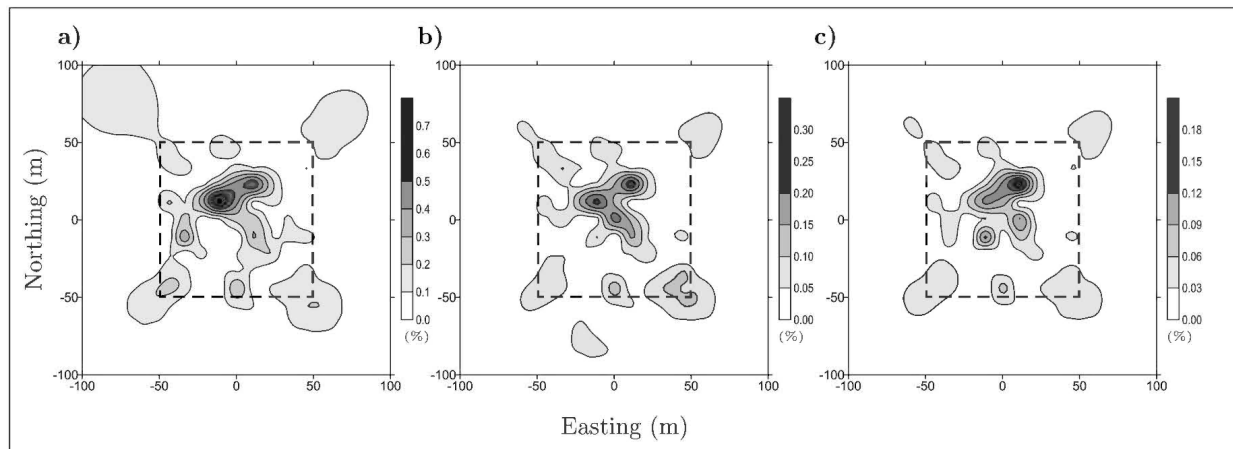


FIGURE I.6: Relative difference of the vertical component of gravity response between the analytical formula and the solution calculated by the subdivision method (a) ratio of 2, (b) ratio of 3 and (c) ratio of 4 for a rectangular prism ( $100m \times 100m \times 50m$ ) the top of the prism at 1m depth. The horizontal location of prism is given by dashed line.

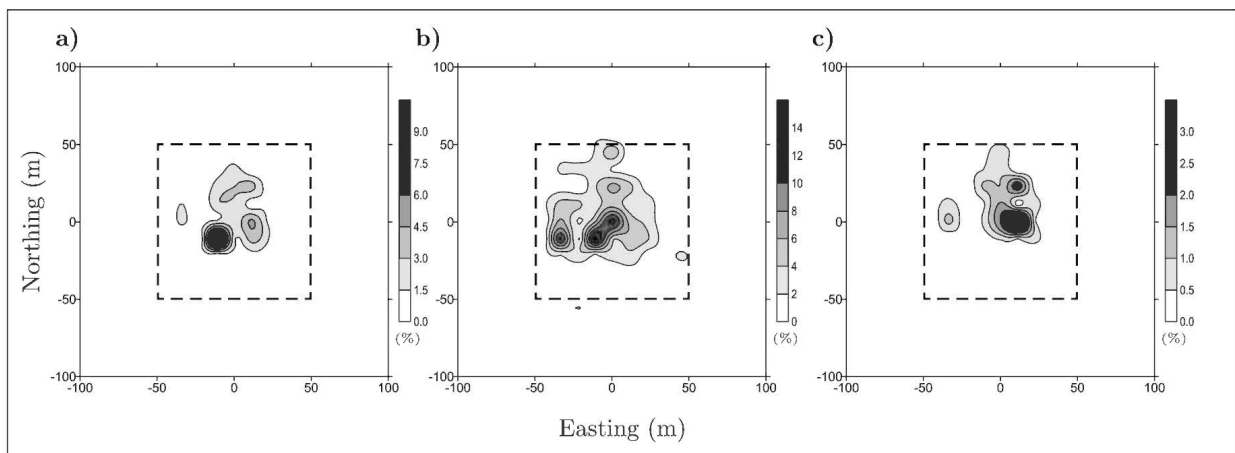


FIGURE I.7: Relative difference of the total magnetic-field between the analytical formula and the solution calculated by the subdivision method (a) ratio of 2, (b) ratio of 4 and (c) ratio of 6 for a rectangular prism ( $100\text{m} \times 100\text{m} \times 50\text{m}$ ) the top of the prism at 1m depth,  $\chi = 0.01 \text{ SI}$ . the horizontal location of prism is given by dashed line.

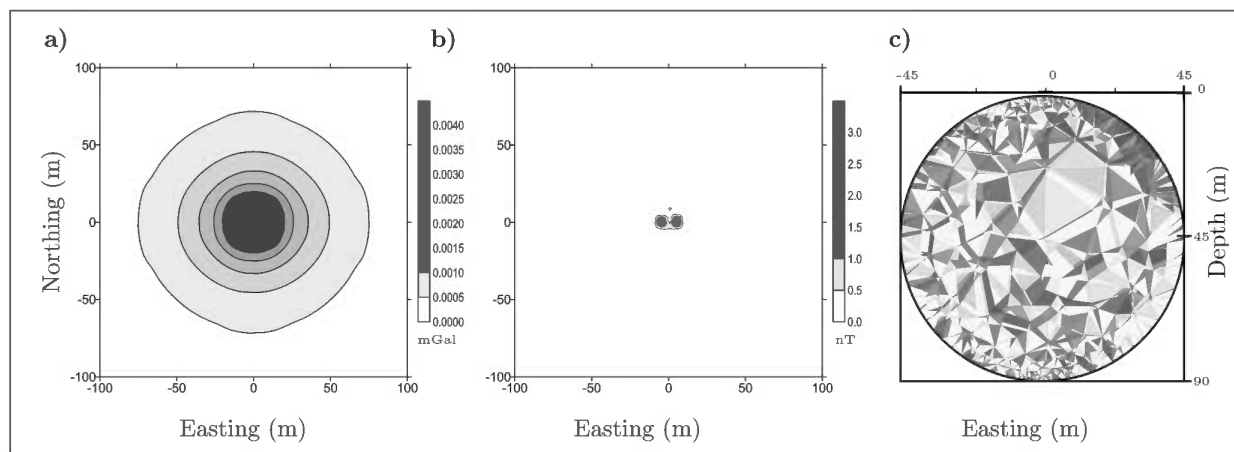


FIGURE I.8: difference of (a) vertical component of gravity field, (b) total magnetic-field between the analytical formula and the solution calculated by the subdivision method of a homogeneous sphere. (c) Vertical cross subsection of a sphere modeled by tetrahedra ( center at 45.1 m depth with a radius of 45 m).

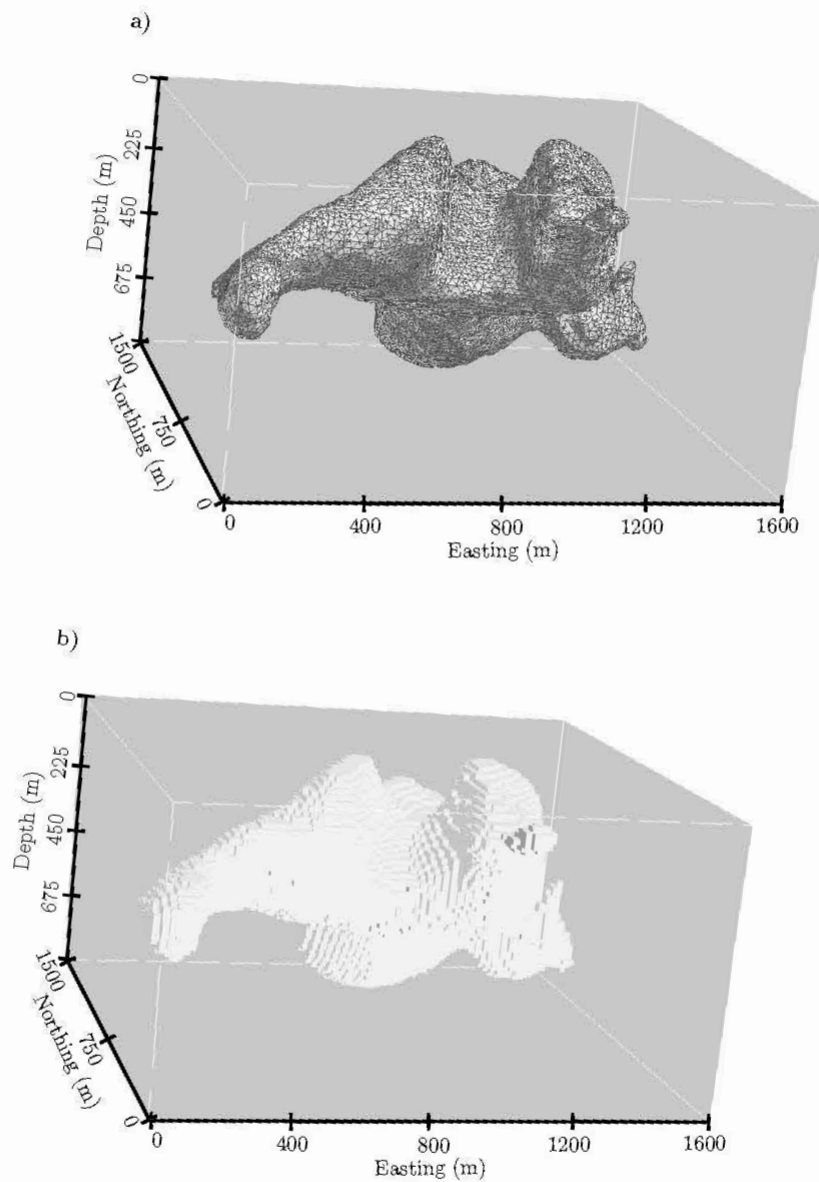


FIGURE I.9: Complex geological body modeled with (a) unstructured tetrahedral grid and (b) regular prismatic grid.

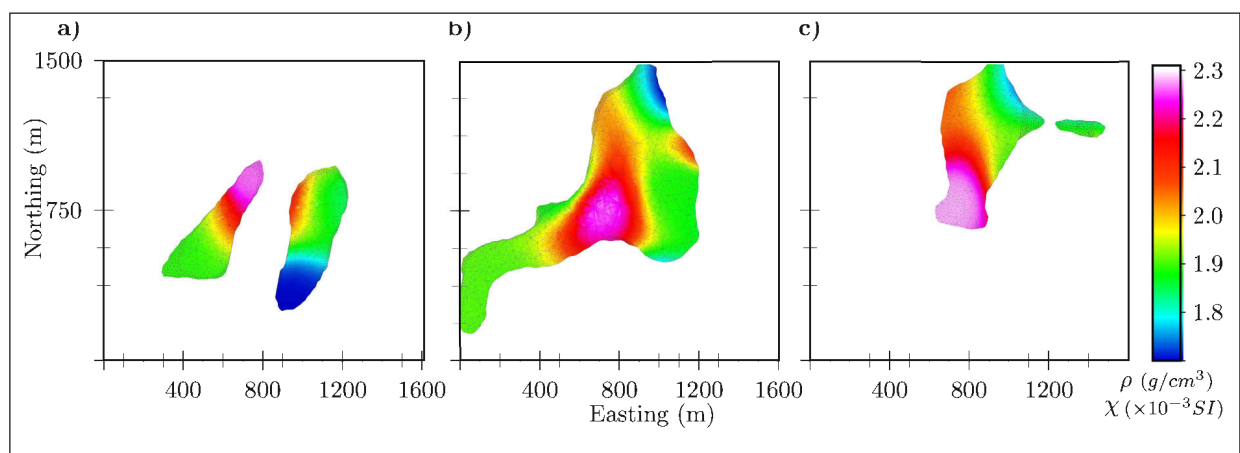


FIGURE I.10: Density and magnetic susceptibility distribution on plan subsection of the tetrahedral model at depth of (a) 155 m, (b) 355 m and (c) 555 m.

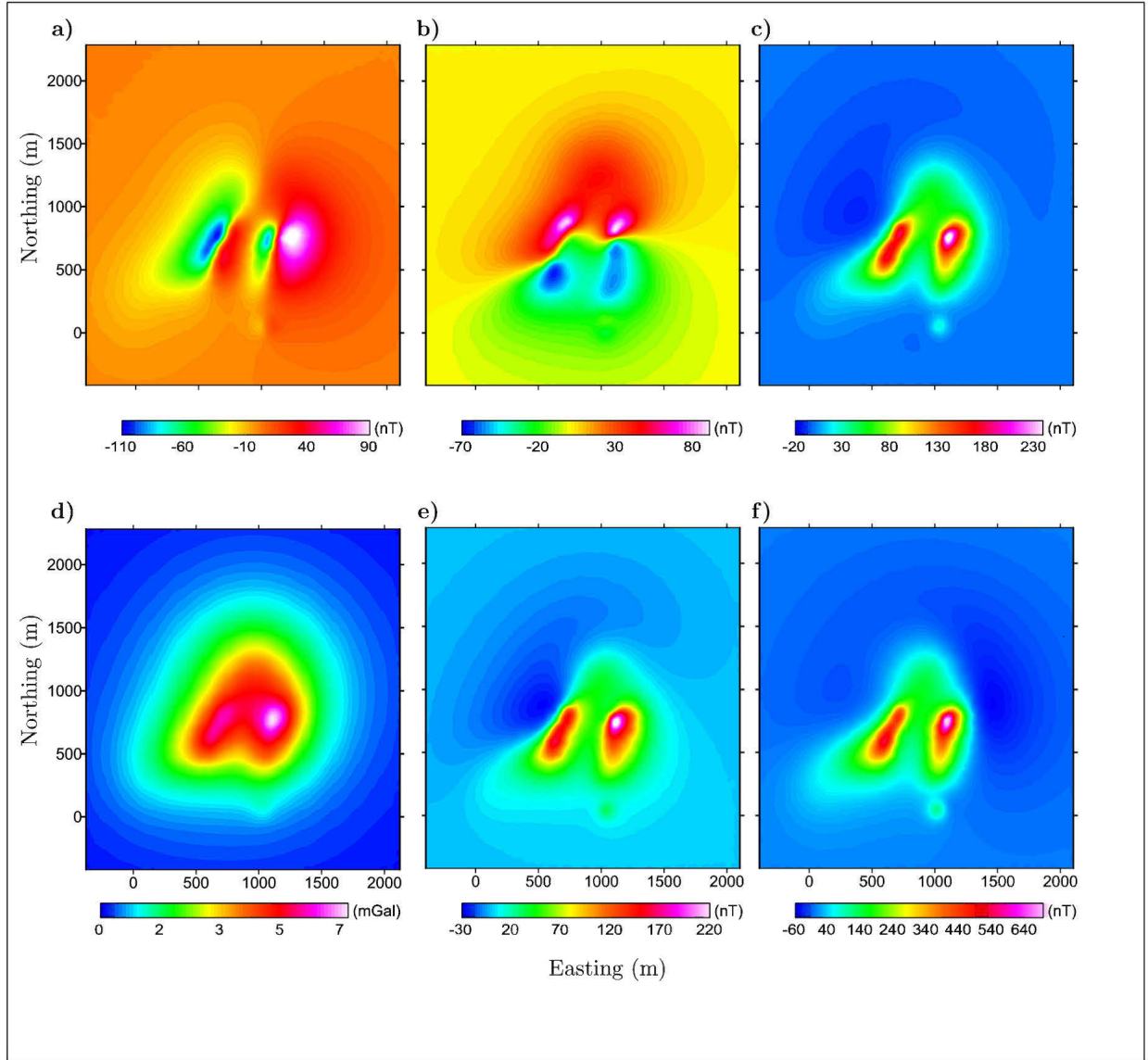


FIGURE I.11: forward modelling of a synthetic body (Figure I.10a) calculated using a subdivision tetrahedral mesh algorithm. (a)  $B_x$  (b) $B_y$  and (c) $B_z$  components of magnetic field. (d) Vertical component of gravity field. Total magnetic-field e) without and f) with constant remanent magnetization. The inducing field has ( $I = 65^0$ ,  $D = -25^0$ ).

TABLE I.2: Results of root mean square (rms), absolute (abs) errors and computation time of prismatic approach with different resolutions and tetrahedral model

Resolution	rms error(%)	abs error (%)	time	rms error(%)	abs error(%)	time
	magnetic	magnetic	magnetic	gravity	gravity	gravity
$30 \times 30 \times 15$	169	37	4 minutes	2	1	3 minutes
$50 \times 50 \times 30$	75	16	17 minutes	0.8	0.4	13 minutes
$127 \times 127 \times 63$	26	4	60 minutes	0.4	0.2	35 minutes
$200 \times 200 \times 100$	18	2.5	80 minutes	0.2	0.1	60 minutes
$300 \times 300 \times 200$	11	1.5	8 hours	0.1	0.02	4 hours

## I.5 Applications de la modélisation directe

La modélisation directe (MD) est utilisée dans trois cas :

1. la MD est une étape de la procédure d'inversion (voir CHAPITRE II).
2. la MD permet de calculer la réponse théorique d'un modèle synthétique au niveau des points d'observations, ce qui va aider à choisir les paramètres d'acquisitions et par conséquent de définir le pouvoir de résolution lié à la zone d'étude, c'est à dire de pouvoir séparer (horizontalement ou verticalement) deux sources proches l'une de l'autre en profondeur ;
3. la MD permet la vérification et la validation de certaines hypothèses géologiques. Dans ce cas, l'ajustement du modèle de départ est effectué de manière manuelle ou semi-automatique successive par la modification de la géométrie voire des propriétés physiques des structures afin de réduire l'écart entre les données observées et calculées. Généralement celle-là est utilisée en 2D dans l'hypothèse où la structure géologique est suffisamment grande (ou épaisseur constante dans le cas de la modélisation 2.5D) dans la direction perpendiculaire à la direction de modélisation, ce qui est loin d'être le cas.

Finalement, le calcul direct des composante du champ de potentiel à partir d'un modèle à base de tétraèdres est une approche robuste et souple à la fois :

- Robuste car il est facile de générer un modèle complexe en présence d'informations *a priori*, la Figure I.12.a montre le résultat du calcul direct effectué sur un modèle géologique (modèle Chevron/Harvard) construit par l'intégration des informations issues de la sismique. Au départ les surfaces triangulées sont créées pour représenter les horizons stratigraphiques et les failles formant ainsi un squelette géologiquement cohérent. Ensuite un remplissage par tétraèdres des régions qui sont définies par les limites des surfaces et des failles est appliqué. Puis un remplissage de propriétés physiques est attribué à chaque région tétraédrique (Figure I.12.c et .d). Dans ce type de modélisation la topographie est incluse dans le modèle géologique pour éviter de faire les corrections de topographies proches des points de mesures.
- Souple car une fois la géométrie du modèle modifiée, il suffit de retrancher le champ de potentiel causé par un tétraèdre requis pour un déplacement ou pour une destruction dans le modèle initial. Ensuite de rajouter l'effet du champ de potentiel engendré par les tétraèdres rajoutés ou bien déplacés dans le modèle final (principe de superposition). Donc toute la difficulté demeure dans la modification du modèle géologique. En effet, [Euler \(1999\)](#) présente la méthodologie à suivre pour la modification de modèle défini par frontières, par exemple [Caumon \(2003\)](#) proposent

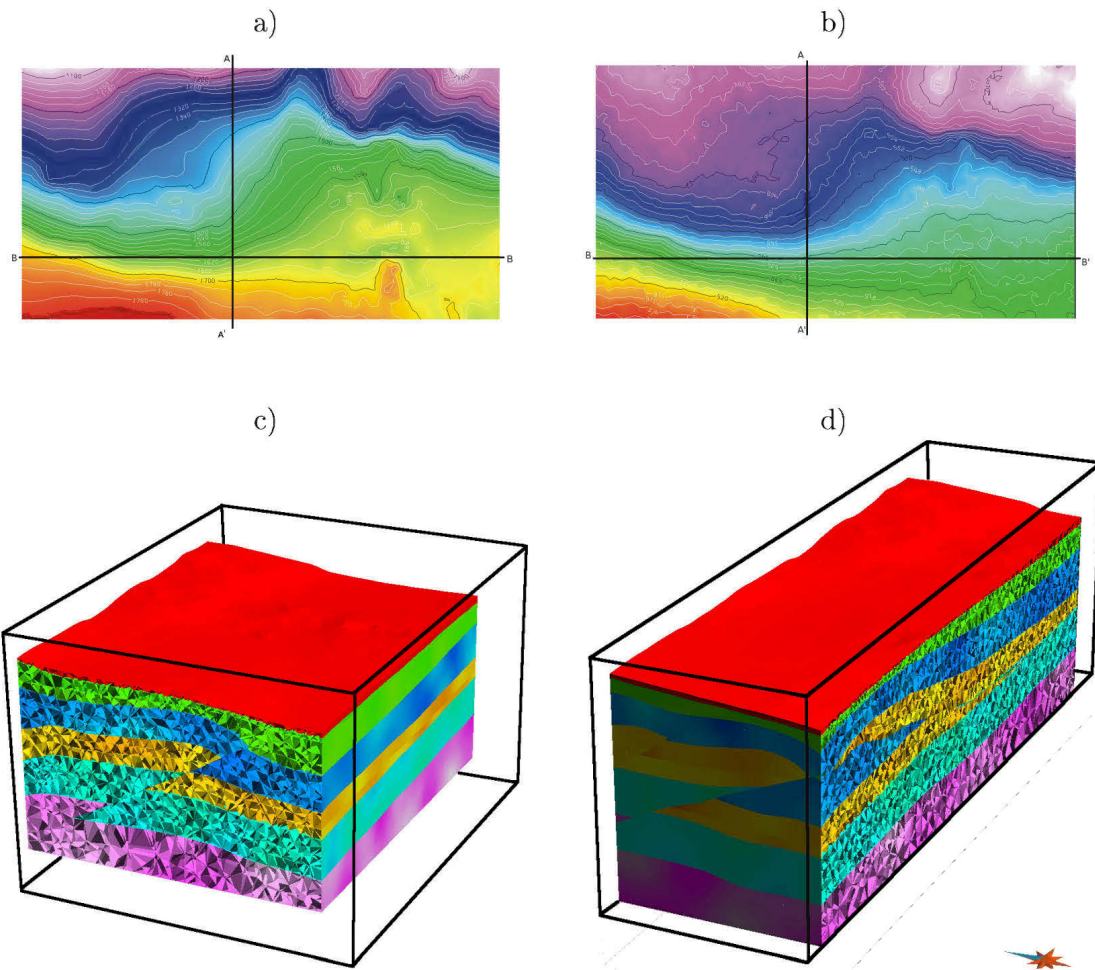


FIGURE I.12: Résultat du calcul direct de la composante verticale du champ gravimétrique créé par un modèle complexe à base de tétraèdre. (a) Variations topographiques au dessus du modèle, (b) composante verticale du champ gravimétrique, (c) coupe verticale suivant AA', (d) coupe verticale suivant BB'). (Modèle structural aimablement fourni par Harvard Univ./ Chevron)

une paramétrisation locale de la surface à déplacer afin de modifier interactivement le modèle géologique tout en gardant les contraintes géologiques imposées au modèle. Tertois (2007) offre la possibilité d'ajuster interactivement la géométrie des failles sans avoir à reconstruire le maillage tétraédrique.

La localisation de la faille de Cadillac présente exemple d'application de la modélisation directe. En effet, la faille présente un grand intérêt d'un point de vu économique car elle représente l'un des métallotectes les plus importants pour l'or dans la sous-province de l'Abitibi, Canada (Rabeau, 2010). Selon une étude précédente

(Cheng et al., 2010), la géométrie de la faille trouvée par une inversion au sens des moindres carrés (voir SECTION II.2) présente une plan quasi-vertical le long de la direction Est-Ouest (Figure I.13). Afin d'évaluer les inclinaisons du plan de faille possibles, une série de modélisations directes a été effectuée sur un modèle géologique caractérisé par un maillage tétraédrique en trois dimensions. Pour ce faire, les frontières du modèle tétraédrique sont définies à partir de la cage géométrique du modèle cartésien et par l'iso-surface ayant la valeur de contraste de densité de  $0g/cm^3$  et qui correspond à la faille recherchée. Ainsi le modèle est décomposé en deux blocs : un petit bloc au Sud de la faille avec un contraste de densité négative (sédiments) et un plus grand bloc au Nord avec une variation de contraste de densité correspondant aux formations du Groupe du Blake River. Puis, le changement du pendage de la faille (Figure I.14.a, .b et .c) permet de définir la nouvelle géométrie des blocs. Ensuite, la propriété physique (contraste de densité) est initialisée pour les nouveaux tétraèdres au voisinage de la faille (Figure I.14.c, .e et .f). A la fin, le champ de gravité créé par chaque nouveau modèle est comparé au champ de référence (Figure I.14.g, .h et .i). Dans cet exemple il est difficile de connaître la position exacte de la faille. Néanmoins il est possible d'évaluer les positions extrêmes de la faille d'une part, de définir une zone d'incertitude au voisinage de la faille d'autre part. Dans ce cas la zone d'incertitude est mince près de la surface mais augmente considérablement en profondeur. Par modélisation directe nous estimons que le pendage de la faille de Cadillac varie de 70 degré à 105 degré.

## I.6 Bilan

Nous avons développé un algorithme simple et efficace pour le calcul des composantes des champs gravimétrique et magnétique produits par des structures géologiques complexes modélisées par un maillage tétraédrique. La méthode est basée sur une approximation de masse ponctuelle pour le calcul des composantes du champ gravimétrique et d'un dipôle magnétique pour le calcul des composantes du champ magnétique. Pour que cette approximation soit valable nous avons appliqué une technique de raffinement récursif qui consiste à subdiviser chaque tétraèdre en 8 nouveaux petits tétraèdres sous une condition géométrique liée à la profondeur des sources. Cette condition revient à calculer la valeur du ratio qui est défini par le rapport entre (la distance barycentre-sommé du tétraèdre) et (la distance barycentre du tétraèdre-point d'observation le plus proche). Ainsi l'opérateur peut imposer un seuil à la valeur ratio à partir duquel les tétraèdres sont

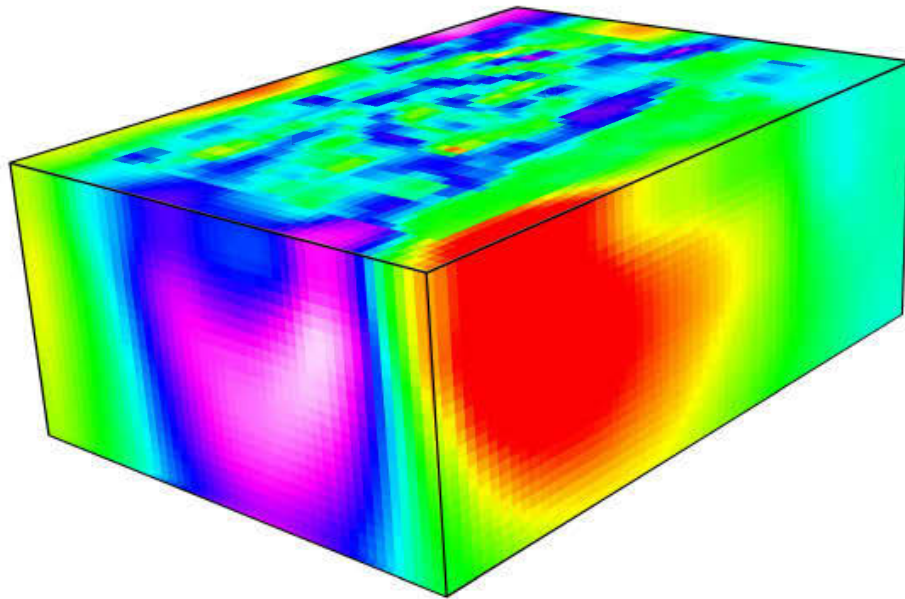
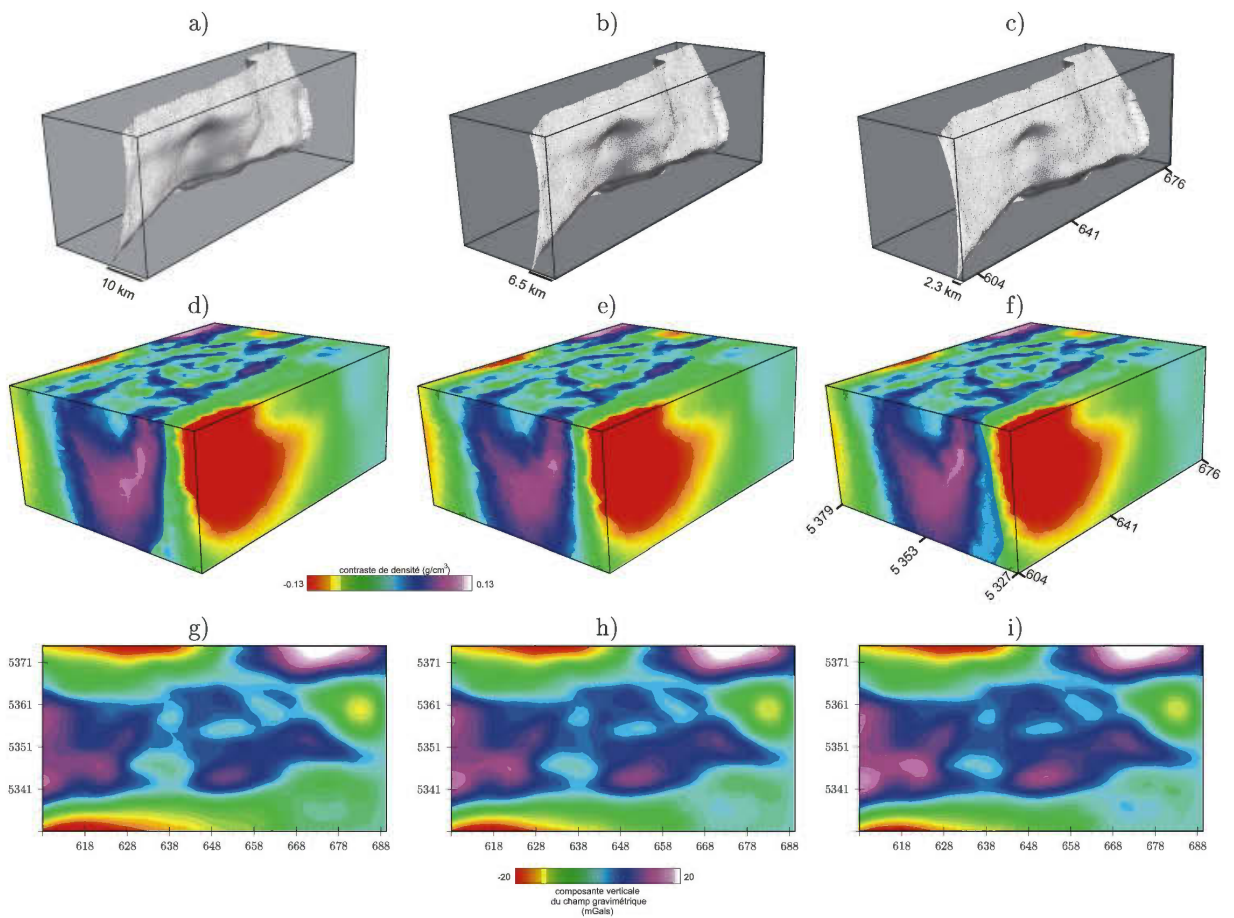


FIGURE I.13: Résultat d'inversion par la méthode des moindres carrés sur maillage cartésien qui permet de représenter une géométrie de la faille de Cadillac

subdivisés en fonction de la précision de calcul voulue. Cette approche est utilisée dans une modélisation directe comme elle peut être intégrée dans un code de modélisation inverse.



**FIGURE I.14:** Calcul direct sur maillage tétraédrique. (a) Modification du pendage de la faille vers le Nord, (b) position initiale de la faille (a) et (c) modification du pendage de la faille vers le Sud. Construction du modèle tétraédrique (g),(h) et (i) sous la contrainte imposée respectivement par la position des failles (a), (b) et (c). Résultats du calcul direct de la composante verticale du champ gravimétrique créé respectivement par les modèles (d), (e) et (f).



## CHAPITRE II

### INVERSION SEPARÉE DES DONNÉES DU CHAMP DE POTENTIEL

#### II.1 Introduction

La géophysique a pour but de procurer des informations concernant la partie invisible voire inaccessible du sous-sol. Comme nous l'avons présenté dans le chapitre précédent le calcul direct est défini comme étant le résultat du calcul analytique des composantes du champ de potentiel en un point donné et qui est provoqué par une répartition spatiale de propriétés physiques bornées par une géométrie donnée. Les données calculées (ou prédites)  $\mathbf{d}_{cal}$  sont liées aux paramètres du modèle  $\mathbf{m}$  par la relation :

$$\mathbf{d}_{cal} = \mathbf{g}(\mathbf{m}) \quad (\text{II.1})$$

où  $\mathbf{g}(.)$  est l'opérateur (linéaire ou non) du calcul direct.

Résoudre le problème inverse revient à trouver les paramètres du modèle ( $\mathbf{m}$ ) de telle sorte à réduire l'erreur entre les données observées et calculées d'une part, et l'écart entre les modèles *a priori* ( $\mathbf{m}_{prior}$ ) et calculé ( $\mathbf{m}$ ) d'autre part.

Cependant, trouver une solution unique au problème inverse est quasi-impossible, ceci est dû principalement aux raisons suivantes : (i) les erreurs et les incertitudes qui affectent les données observées ; (ii) le problème à résoudre est sur-dimensionné, c'est à dire que le nombre de paramètres du modèle est supérieur au nombre de données observées ; (iii) l'existence des problèmes d'équivalence entre les sources et (iv) les imperfections liées à la modélisation. Dans ces conditions il est plus judicieux de parler de probabilité *a posteriori* du modèle trouvé. Tarantola (2005) montre l'effet de l'incertitude du modèle sur le résultat de la prédiction. Dans le cas où l'incertitude liée au modèle est négligée alors le résultat du calcul direct est unique (Figure II.1.a). Dans le cas contraire le

résultat du calcul direct est associé à une densité de probabilité (Figure II.1.b).

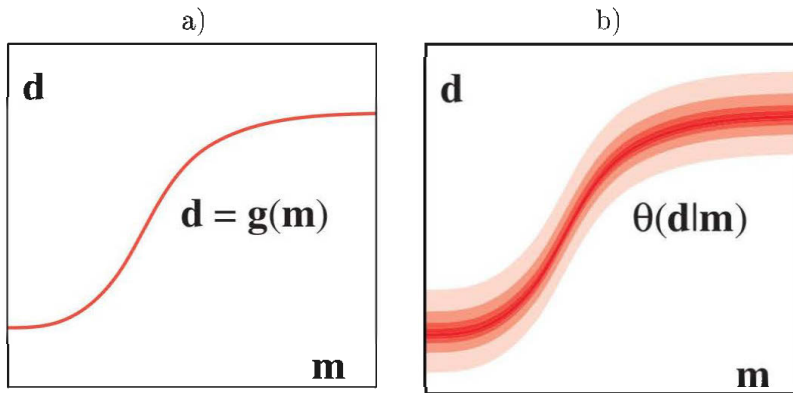


FIGURE II.1: Effet de l'incertitude du modèle sur le résultat du calcul direct, incertitude (a) négligée, (b) non négligée. Par ([Tarantola, 2005](#))

Selon la théorie Bayésienne la probabilité *a posteriori* d'un modèle  $m$  est une fonction de la probabilité du modèle *a priori* et de la probabilité des données calculées conditionnées par un modèle  $m$ . La densité de probabilité *a posteriori* (normalisée) de l'espace des modèles  $\sigma(m)$  est donnée par [Tarantola \(2005\)](#) :

$$\sigma(m) = \rho_M(m)L(m) \quad (\text{II.2})$$

où  $\rho_M(m)$  représente l'information *a priori* des paramètres du modèle et  $L(m)$  est la fonction de vraisemblance qui est l'indicateur du bon ou du mauvais ajustement entre les données calculées et observées.

## II.2 Inversion au sens des moindres carrés

Cette méthode suppose une distribution Gaussienne de la probabilité *a priori* du modèle  $m_{\text{prior}}$  et des données observées  $d_{\text{obs}}$ . Dans ce cas la probabilité *a posteriori* de l'espace des modèles (équation II.2) s'écrit sous la forme ([Tarantola, 2005](#)) :

$$\sigma(m) = k \exp(-S(m)) \quad (\text{II.3})$$

où  $k$  est une constante et  $S(\mathbf{m})$  est la fonction écart (ou fonction objective) donnée par la formule :

$$S(\mathbf{m}) = \underbrace{\frac{1}{2}(\mathbf{g}(\mathbf{m}) - \mathbf{d}_{\text{obs}})^t \mathbf{C}_d^{-1} (\mathbf{g}(\mathbf{m}) - \mathbf{d}_{\text{obs}})}_{\begin{array}{l} \text{Information liée à la} \\ \text{densité de probabilité } a \text{ posteriori} \\ \text{des données calculées conditionnées} \\ \text{par un modèle} \end{array}} + \underbrace{\frac{1}{2}(\mathbf{m} - \mathbf{m}_{\text{prior}})^t \mathbf{C}_m^{-1} (\mathbf{m} - \mathbf{m}_{\text{prior}})}_{\begin{array}{l} \text{Information liée à la} \\ \text{densité de probabilité } a \text{ priori} \\ \text{de l'espace des modèles} \end{array}}$$

(II.4)

où  $\mathbf{C}_d$  et  $\mathbf{C}_m$  sont les matrices de covariances des données observées  $\mathbf{d}_{\text{obs}}$  et du modèle  $\mathbf{m}$  respectivement.

Finalement, résoudre le problème inverse au sens des moindres carrés revient à maximiser la probabilité *a posteriori* de l'espace des modèles  $\sigma(\mathbf{m})$ . Autrement dit, il s'agit de minimiser la fonction écart  $S(\mathbf{m})$ . L'inversion aux sens des moindres carrés est une méthode qui réduit progressivement l'écart entre les données observées et calculées en ajustant les paramètres du modèle à chaque itération. La solution généralisée du problème inverse sous la formulation des moindres carrés proposée par Tarantola et Valette (1982) permet de déterminer de manière itérative la correction  $\Delta\mathbf{m}$  à apporter au modèle  $\mathbf{m}_n$ . Pour déterminer le modèle suivant  $\mathbf{m}_{n+1}$ , la correction peut s'écrire de la façon suivante :

$$\Delta\mathbf{m} = -[\mathbf{G}_n^t \mathbf{C}_d^{-1} \mathbf{G}_n + \mathbf{C}_m^{-1}]^{-1} [\mathbf{G}_n^t \mathbf{C}_d^{-1} (\mathbf{g}(\mathbf{m}_n) - \mathbf{d}_{\text{obs}}) + \mathbf{C}_m^{-1} (\mathbf{m}_n - \mathbf{m}_{\text{prior}})] \quad (\text{II.5})$$

Dans le cas gravimétrique le problème direct est linéaire, donc l'équation (II.1) s'écrit sous la forme ( $\mathbf{d}_{\text{cal}} = \mathbf{G} \mathbf{m}_{n+1}$ ) et la matrice ( $\mathbf{G}_n = \mathbf{G}$ ) est constante. En revanche, dans le cas d'une inversion magnétique le calcul direct est linéarisé au premier ordre par conséquence l'équation (II.1) est approximée à ( $\mathbf{d}_{\text{cal}} \simeq \mathbf{g}(\mathbf{m}_n) + \mathbf{G}_n(\mathbf{m}_{n+1} - \mathbf{m}_n)$  et ( $(\mathbf{G}_n^i)_\alpha = \partial g^i / \partial m_n^\alpha$ ) est la matrice de dérivée partielle qu'il faudrait recalculer à chaque itération et la matrice de covariance du modèle *a posteriori* est donnée par :

$$\tilde{\mathbf{C}}_m = \mathbf{C}_m - \mathbf{C}_m \mathbf{G}^t (\mathbf{G} \mathbf{C}_m \mathbf{G}^t + \mathbf{C}_d)^{-1} \mathbf{G} \mathbf{C} \quad (\text{II.6})$$

La matrice  $\tilde{\mathbf{C}}_m$  du modèle *a posteriori* dépend des matrices de covariance *a priori* du modèle et des données observées. Ainsi l'analyse de ces matrices permet de déterminer

le poids des données observées par rapport à l'information *a priori* dans la résolution du problème inverse, autrement dit plus l'incertitude augmente au niveau d'une donnée, moindre est la contribution de celles-ci sur le résultat final de l'inversion. [Backus et Gilbert \(1968\)](#) introduisent le concept de l'opérateur de résolution qui compare la covariance *a posteriori* à la covariance *a priori* du modèle résultat de l'inversion. Le nombre total des paramètres du modèle final est égal au nombre de paramètres résolus par les données observées plus la contribution du nombre des paramètres résolus par l'information *a priori* ([Tarantola, 2005](#)).

Finalement, résoudre le problème inverse au sens des moindres carrés revient à modifier les paramètres du modèle pour que les données calculées convergent vers les données observée sans que le modèle final ne diverge trop de l'information *a priori*. Le plus souvent l'information *a priori* est imposée comme contrainte pour augmenter la convergence de l'algorithme.

Il existe plusieurs stratégies pour optimiser la résolution du problème d'inversion aux sens des moindres carrés. Le plus souvent une pondération est introduite comme le proposent les auteurs [Last et Kubik \(1983\)](#); [Guillen et Menichetti \(1984\)](#); [Li et Oldenburg \(1996, 1998\)](#); [Barbosa et al. \(1999\)](#); [Boulanger et Chouteau \(2001\)](#), ou bien par la méthode du gradient conjugué comme le propose [Pilkington \(1997\)](#); [Li et Oldenburg \(2003\)](#), soit par l'introduction d'information *a priori* sous forme de matrice de covariance calculée à partir de données de forages, de cartes géologiques et d'autres informations provenant des résultats des autres méthodes géophysiques ([Richard et al., 1984](#); [Van de Meulebrouck et al., 1988](#); [Lee et Biehler, 1991](#))

### II.3 Inversions stochastiques

Le but de l'inversion stochastique est de générer plusieurs modèles qui respectent les informations *a priori* et les données observées. Cette méthode est bien adaptée pour traiter le problème de la non unicité de la solution et pourrait être utilisée comme un outil d'aide à la prise de décisions par le calcul de la probabilité *a posteriori* des modèles et/ou des paramètres des modèles. Historiquement ce type de méthode a été utilisée pour les études de la réaction nucléaire, dans les années cinquante où [Metropolis et Ulam \(1949\)](#) présentent pour la première fois la méthode de Monte Carlo. En géophysique, cette méthode a été utilisée initialement par [Keilis-Borok et Yanovskaja \(1967\)](#) et [Press \(1968\)](#) pour résoudre le problème inverse.

Le principe de l'inversion par la méthode Monte Carlo (IMC) est d'échantillonner des modèles (variation de géométrie et\ou de la distribution de propriétés physiques dans le cas de la géophysique) d'une manière aléatoire puis de calculer leurs réponses, ainsi les modèles dont la probabilité *a posteriori* est satisfaisante seront acceptés dans le cas contraire ils seront rejettés. Dans ce cas, dans l'équation (II.3) la probabilité *a posteriori* s'écrit sous la forme :

$$\sigma(m) = \rho_M(m)L(m) \quad (\text{II.7})$$

Les raisons qui favorisent l'utilisation de la méthode (IMC) sont nombreuses parmi lesquelles :

1. La méthode n'est pas affectée par la non linéarité du problème direct (approximation par dérivée partielle).
2. L'absence de coefficients de pondération et ou d'amortissement qui peuvent affecter le résultat final.
3. La méthode non itérative (le modèle suivant ne dépend pas du précédent), ce qui permet d'éviter les problèmes de convergences locales engendrés par les algorithmes itératifs.
4. L'absence d'instabilité numérique produite par l'inversion de matrices mal conditionnées ou par l'échec de la convergence.
5. La procédure d'inversion n'est pas affectée par la complexité de la fonction écart.
6. Ce type d'algorithme est aisément parallélisable sur plusieurs processeurs.

Parmi les inconvénients de la méthode (IMC) :

1. Le temps de calcul peut être considérablement long. Il dépend de la machine de calcul, de l'expression analytique du problème direct, de la manière dont les modèles *a priori* sont générés aléatoirement et de la résolution spatiale des modèles ;
2. il est difficile de connaître le nombre minimal de modèles à tester ;
3. en présence de faible (ou en l'absence) information *a priori* il est possible de trouver des modèles acceptables mais qui contiennent des résultats erronés.

La puissance de calcul des ordinateurs a tendance à augmenter avec le temps et l'expression analytique étant ce qu'elle est, la plus grande difficulté demeure dans la génération des modèles par des géométrie différentes ou par simulation de la répartition de propriétés physiques de manière aléatoire. [Sambridge et Mosegaard \(2002\)](#) proposent d'introduire l'échantillonnage pseudo-aléatoire de l'espace des modèles dans la définition de la méthode (MC).

Le but étant d'échantillonner un maximum de modèles dont la densité de probabilité *a posteriori* sera acceptable. En d'autres termes, il s'agit d'éviter dans la mesure du possible, de sélectionner un modèle qui sera rejeté après calcul de la fonction de vraisemblance. Il existe plusieurs algorithmes qui permettent l'optimisation de recherche de modèles *a posteriori* :

- **La méthode de Metropolis** ([Metropolis et Ulam, 1949](#)) appelée aussi Monte Carlo chaîne de Markov (MCMC), cette méthode permet de sélectionner des modèles de proche en proche en rajoutant des petites perturbations successives aux modèles déjà trouvés. Ainsi le modèle trouvé à la simulation  $m_{i+1}$  dépend des quelques modèles précédents  $m_i$ ,  $m_{i-1}$  etc. En fonction de la fenêtre de perturbation  $\delta m$ , mais ne dépend pas de tous les modèles précédents ([Mosegaard et Tarantola, 2002](#)) .
- **La méthode du recuit simulé** ([Kirkpatrick et al., 1983; Geman et Geman, 1984](#)) est une méthode similaire à la précédente mais exploite une analogie mécanique qui est le refroidissement pour la recherche du minimum global d'une fonction objectif possédant un grand nombre de minima secondaires. Cette méthode a été utilisée avec succès pour résoudre le problème inverse en présence de la non linéarité de la fonction objective ([Rothman, 1985](#))
- **La méthode utilisant les algorithmes génétiques** est une méthode fondée sur les mécanismes de la sélection naturelles. Elle exploite l'information sur les modèles trouvés précédemment pour générer de nouveaux modèles, avec l'espoir d'améliorer la probabilité *a posteriori* à chaque fois ([Goldberg, 1989](#)).
- **Les méthodes de simulation stochastiques** permettent de fournir un grand nombre de réalisations (ou modèles) équiprobables en respectant les informations préalablement disponibles. Les méthodes les plus utilisées sont : la simulation gaussienne séquentielle ([Journal et Alabert, 1989; Deutsch et Journel, 1998](#)) et la simulation par indicatrices ([Journel et Isaaks, 1984; Goovaerts, 1997](#)). Dans le deuxième article de cette thèse nous proposons une approche qui permet d'intégrer les méthodes de simulations géostatistique dans la formulations bayésienne, ce qui a pour effet de tayloriser la recherche de modèle *a posteriori*.

## II.4 Gravity Inversion using stochastic methods

Nacim Foudil-Bey<sup>\*†</sup>, Li Zhen Cheng<sup>†</sup> Jean-Jacques Royer<sup>\*</sup> and Guillaume Caumon<sup>\*</sup>

### II.4.1 Résumé

Lors de la modélisation gravimétrique plusieurs modèles différents peuvent reproduire les données observées. Ceux-ci en effet sont dus principalement au phénomène d'équivalence des sources et au sur-dimensionnement du problème inverse. Exprimée sous forme de contrainte, l'information *a priori* obtenue à partir des données géologiques \ ou géophysiques réduit le nombre de modèles possibles. Généralement l'intégration d'une pondération lors de la résolution du problème inverse force la solution à converger vers une solution unique avec une répartition lisse de propriété physique dans l'espace de modélisation. Néanmoins les méthodes stochastiques telles que la technique de Monte-Carlo permet la génération d'un ensemble de modèles avec des distributions diverses et possibles de la propriété physique recherchées. Cependant, fournir des solutions possibles de manière aléatoire peut engendrer un temps de calcul important, en particulier dans le cas d'un grand nombre de paramètres inconnus. Afin de contourner ce dernier inconvénient, la méthode proposée dans cet article, procède tout d'abord, à une estimation du modèle de covariance et de la distribution de la densité d'une solution donnée. Ensuite une simulation Séquentielle Gaussienne au niveau d'une grille sous-jacente est réalisée pour générer des distributions de densité possibles. Enfin, les réalisations de la propriété sont transférées vers le modèle tétraédrique afin de calculer les réponses des modèles *a posteriori*. La méthode a été testée sur un modèle synthétique et sur des données réelles du pluton Flavrian situé dans la ceinture verte d'Abitibi au Québec, Canada.

### II.4.2 Abstract

The inverse problem in gravity is an oversized problem. Expressed as a constraint, the *a priori* information like geological and/or geophysical information reduces the number of possible models. Nevertheless the Stochastic methods such as Monte Carlo technique allows generation of a set of models with different density distribution, but the inconvenient remains the required time to find out a solution randomly, especially in case of a large number of unknown parameters. In this work, the proposed method firstly estimates the covariance model and the density distribution of a given solution, then uses the Sequential Simulation method on an underlying grid to generate distributions

of possible density. Finally, the realizations of the properties are transferred to a tetrahedral model in order to calculate the response of *a posteriori* model. The method was performed on synthetic model and real data from the Blake River Group in the Flavrian pluton (Québec, Canada).

**key word :** Gravity, Stochastic Inversion, Gaussian Sequential Simulation.

### II.4.3 Introduction

Our knowledge of the Earth interior depends on observations made on or the near surface. Inversion techniques in geophysics had been developed and continue to be improved in order to extract the geological information of the Earth from observations. The most popular approach is based on the least squares principle via iteration for both analytic and statistic methods (Tarantola et Valette, 1982; Last et Kubik, 1983; Guillen et Menichetti, 1984; Barbosa et Silva, 1994; Fregoso et Gallardo, 2009).

Due to the non unicity in the inversion solution, some known prior information is always useful to constrain the solution. Silva et al. (2002) and Barbosa et al. (2002) integrated the constrain by translating the prior geological information (structural and/or density distribution) to mathematical conditions to ensure an unique and stable solution of gravity data inversion. Last et Kubik (1983) constrained the gravity inversion by imposing the anomalous source density and determined their geometry around axes which concentrate most of the anomalous masses. Gallardo-Delgado et al. (2003) proposed a joint gravity and magnetic data inversion, assuming that both fields share in common similar sources caused by a sedimentary basin. In their study, the depth of the bottom of basin is determined from the joint inversion by imposing upper and lower limits on the variation of density contrast and of the magnetic susceptibility. Li et Oldenburg (1998) and Pilkington (1997) proposed a smoother solution by varying the cell sensitivity along a given direction. In contrary to the above mentioned works, Portniaguine et Zhdanov (1999, 2002); Bertete-Aguirre et al. (2002) proposed a non smooth solution. Boulanger et Chouteau (2001) combined some constraints (flatness, smoothness and compactness) using the Lagrangian formulation and the application of multi-grid technique to resolve separately large and short gravity wavelengths. Chasserau et Chouteau (2003) performs gravity inversion by incorporating constraints like misfit data weighted by the data errors covariance and a model norm weighted by covariance parameters. While other works use simulation annealing techniques during the inversion for estimating the incertitudes of the model (Roy et al., 2005) .

The non-uniqueness of the inverse problem means that many different geological models can reproduce similar observed surface anomaly. Analytical methods limit the resulting model space when searching the optimal solution by introducing specific constraints, and propose a unique solution (within certain tolerance) generally called ‘the best model’. However, stochastic process investigate a large model space and often produce many possible solutions Tarantola (2006). One example of statistic methods is the Monte Carlo technique. It was used firstly by Franklin (1970) and then popularized by Tarantola et Valette (1982). Bosch et al. (2006) applied the Monte Carlo approach to estimate 3D density and magnetic susceptibility distributions in a sedimentary basin using seismic prior information. Recently Hansen et al. (2006); Hansen et Mosegaard (2008); Gloaguen et al. (2005, 2007) used the posterior probability density function of any Gaussian linear inverse problem for ground-penetrating-radar tomography. The advantage of the Monte Carlo inversion method is that number of models with different geometries or parameters are randomly created, and then calculated their responses keeping only the meaningful solutions with high posterior probability (Metropolis et Ulam, 1949; Metropolis et al., 1953; Mosegaard et Tarantola, 1995; Bosch, 1999; Bosch et al., 2007; Mosegaard et Sambridge, 2002; Sambridge et Mosegaard, 2002).

This procedure reduces the computer time requested at the inversion step. The distribution of geological features and natural resources are sufficiently complicated that they can be considered as random. Thus, we integrate the Sequential Gaussian Simulation (SGS) for 3D stochastic inversion of gravity data in order to generate many realizations that *a posteriori* model with a high probability to be accepted. The spatial analysis is performed on a temporary structured grid then the results of the simulation (property) are transferred to a tetrahedral grid to validate the model by calculating the gravity response. The utility of tetrahedral gridding technique is for saving the computation time with higher model resolution. The proposed method was tested on synthetic data. It is also applied to model the heterogeneity of the Flavrian pluton using data collected from the Black River Group in the Abitibi greenstone belt of Canada.

#### II.4.4 Theory

Monte Carlo sampling methods have been suggested to explore efficiently a large number of possible models in the solution space, and therefore, helping geologists to select the models deemed to be the most realistic. However, the Monte Carlo (MC) simulation method is characterized by low performances in terms of computer time efficiency. It is due to the algorithm itself, but also because empty space problems arise very quickly

in the MC sampling, making convergence an issue. To overcome these limitations, we propose to use a compact model parameterization based on random sampling of a reference model obtained by deterministic or stochastic inversions. The arguments to use the stochastic method are : (i)stochastic procedures sample the multitude of possible equivalent models ; (ii)usually, there are not enough observed data to determine a unique solution compared to the model parameters, stochastic methods simulate missing values in a statistical and special homogeneous way, (iii)stochastic techniques introduce spatial sampling of the field data, filter observed data (choice of regional / residual) and separate noise from significant information the data contamination by noise.

The sampling technique consists of generating random models by varying the geometry or the model parameters (density), then, calculating the response (gravity fields) of the simulated models, finally in keeping only the meaningful solutions (with hight posterior probability) by rejecting the models with low probability. The computation time of this method depends on the method used to calculate the forward potential field, on the dimension space in which solutions are searched as possible models, on the size of the study area and the model resolution, on the technique used in the modeling, and the power of the computer used for modeling.

The *posterior* model probability  $\sigma(m)$  is a function of the prior model density probability  $\rho_M(m)$ , and the likelihood function  $L(m)$  of the randomly sampled model, the *posterior* probability density defined by Tarantola (2005) as follows :

$$\sigma(m) = \rho_M(m)L(m) \quad (\text{II.8})$$

where  $m$  is the parameter defined by the density or magnetic susceptibility distribution in the space of possible models and the likelihood probability density function (pdf) is given either by :

- A *Gaussian model* (assuming the same uncertainty  $\sigma_0$  for all measurement data)

$$L(m) = \exp \left( -\frac{1}{2\sigma_0^2} \sum_{i=1}^n (F_{cal}^i(x, y, z) - F_{obs}^i)^2 \right) \quad (\text{II.9})$$

- A *Laplacian model*

$$L(m) = \exp \left( - \sum_{i=1}^n \left| \frac{1}{\sigma_i} (F_{cal}^i(x, y, z) - F_{obs}^i) \right| \right) \quad (\text{II.10})$$

For instance,  $F_{cal}^i$  represent the gravity data in the likelihoods function  $L(m)$  associated with the gravity data. Monte Carlo method accept or reject models after computing the posterior probability density of the models. However when the model space has a large number of dimensions, the probability to find an acceptable model is very small or sub-null (Tarantola, 2005), because the number of rejected models is larger than the number of accepted models. Tarantola (2005) demonstrates that the model found by resolving the inverse problem using a classical least square methods correspond to averaging all possible random models solutions. In this paper, we consider a generalized solution of the inverse problem that can be formulated by the following equation (Tarantola et Valette, 1982) :

$$\tilde{m} = m_{prior} + C_m G^t (G C_m G^t + C_d)^{-1} (d_{obs} - G m_{prior}) \quad (\text{II.11})$$

with a covariance given by :

$$\tilde{C} = C_m - C_m G^t (G C_m G^t + C_d)^{-1} G C_m \quad (\text{II.12})$$

Where  $\tilde{m}$  is the posterior model with the maximum likelihood value;  $\tilde{C}$  is the covariance of posterior model;  $m_{prior}$  is the prior model;  $C_m$  is the covariance of the subsurface model;  $G$  is the linear (or non linear<sup>†</sup>) operator relating the model to the observed data;  $C_d$  is the data covariance.

By assuming the solution of inversion using least square methods is The mean  $m_{mean}$ . Under second-order stationarity assumption the spatial correlation of geological properties is modeled by the variogram. The experimental variogram calculated along different space directions is given by :

$$\gamma(h, \theta) = \frac{1}{2N(h, \theta)} \sum_{i=1}^{N(h, \theta)} [Z(x_i) - Z(x_i + h)]^2 \quad (\text{II.13})$$

Where  $\gamma(h, \theta)$  is the semivariogram for direction in the *azimuth* $\theta$ ;  $N(h, \theta)$  is the number of pairs separated by a distance or lag  $h$  along the  $\theta$  direction,  $Z(x_i)$  variable under consideration;  $Z(x_i + h)$  is the lagged located at a distance of  $h$  in the considered direction  $\theta$ . Experimental variograms can be fit to theoretical models including spherical, Gaussian and exponential functions, and a several strategies can be used to

---

†. in this case by solving a linearized problem iteratively (Tarantola, 2005)

simulate possible models (realization) using geostatistical simulation algorithm ([Chilés et Delfiner, 1999](#)).

The stochastic inversion using the Sequential Gaussian Simulation (SGS) was implemented by the flowing steps :

1. find a posterior model with the maximum likelihood value using (equation [II.11](#)) ;
2. calculate histogram of the solution found in step (1) ;
3. select the parameter calibration called pilot points ([de Marsily et al., 1984](#)) or master points ([Gómez-Hernández et al., 1997](#)) ;
4. compute covariance of the model using (equation [II.12](#)) and the semivariogram using (equation [II.13](#)) ;
5. generate random realization using conditional or unconditional (SGS) algorithm ([Journel, 1999a](#)) ;
6. compute a posterior probability of each model using equation [II.10](#).

#### **II.4.5 Inversion of the synthetic data set**

In order to test the performance of the stochastic method, we create a complex geological body using a tetrahedral grid (Figure [II.2.a](#)). This reference model defined a 3D subsurface region of  $1.5 \times 1.6 \times 0.8 \text{ km}^3$  in size and the density inside of model varies from 0.4 and  $1 \text{ g/cm}^3$  (Figure [II.4](#) in top). First, we calculate the vertical component of the gravity field produced by the reference model at an altitude of 8'm and blurred by a random noise that is shown on Figure [II.3.a](#).

##### **II.4.5.1 Find a posterior model with the maximum likelihood using Least squares inversion**

From quick direct calculations fitting the gravity response of reference model we build up an initial density model as shown on Figure [II.2.b](#). This initial model has a volume of  $2.2 \times 2.7 \times 1.5 \text{ km}^3$  which is much larger than the true model with random distribution of density. And then, we used the data set calculated from reference model as observations. They were inverted using our own inversion algorithm, which is similar to that of ([Li et Oldenburg, 1998](#)) based on the least squares approach. Adding the initial model as *a priori* information into the inversion process, we reconstructed a three dimensional density model as Figure [II.2.c](#) shown. We compared the inversion result with the density

distribution of reference model at three depth levels (top view) : 150 m (Figure II.4.a), 350 m (Figure II.4.b) and 650 m (Figure II.4.c). The main geometry feature of source is well recovered by inversion, however, the accuracy of the density distribution is not precise enough. For example, the location of the maximum value of density is different in reference model from the inversion model. Consider the model size that is unit in kilometer, it is very important to know exactly where situated the ore bodies, more often they have high density for drilling location design.

The purpose of the first inversion is to reduce model space. The model proposed above is a posterior geometry for stochastic inversion methods that are then used to specify the density distribution for multiple models.

#### II.4.5.2 Stochastic inversion using Monte Carlo method

Based on the initial geometry model (Figure II.2.c), the Monte Carlo (MTC) method was applied. However, calculating the likelihood values for all the observed data for each model may be very long. So, in order to optimize the computing time, the likelihood value was calculated for just a parts of the data (selected critical points representing the field variation). Thus, if the computed likelihood value is close to zero, the simulated models are rejected (no need to calculate likelihood value for the remaining points), but if the likelihood value is close to one, there is a large probability to be close to one for the remaining points. After random realization of the density, the obtained models are pretty different. Figure II.5 shows the reference model and five selected MTC inversion results, respectively. The Figure II.6 shows the vertical component of the gravity fields of the three selected MTC models shown in Figure II.5.b, .c and .d. The gravity response of the selected models presents a good similarity with the reference gravimetric field. The comparison between the posterior models shows a large variety of possible models, in fact the distribution of the density in the posterior models varying from slightly to very heterogeneous model, as well as being an indication of the non-uniqueness solution of the inverse problem.

#### II.4.5.3 Optimized stochastic inversion using Sequential Gaussian Simulation

Based on a given solution the Sequential Gaussian Simulation (SGS). We consider 74 pilot points in the inverted model. Having a data set with the physical properties (pilot

points) and knowing the variogram model, the stochastic simulation is made on a temporary grid with a resolution of  $(100 \times 100 \times 75)$  cells, the simulated properties will be then the property transferred from the gridded model to the tetrahedral model for calculating the posterior probability in order to validate the simulation. Figure III.6.a, .b and c. shows the three selected experimental and modeled semivariograms for different azimuths and dips of the density distribution of the inverted model (Figure II.4 in the bottom), and the histogram of the distribution of density in the inverted model. For this example we use the anisotropic exponential variogram model with range of 500 to 800 m and without nugget effect. Figure II.8 shows 9 (out of 100) the simulated density distribution. The selected realizations have a likelihood value greater than 0.7. The three realizations shown in Figure II.8.a , b, and c are the result of simulation produced by the same initial pilot points, whose possible density values varying between 0.2 and 1 ( $g/cm^3$ ). The Figures II.8 .d, .e and .f shows three other accepted simulations after having changed the position of the pilot points and the possible density values between 0.2 and 0.7 ( $g/cm^3$ ). Figures II.8 .g, .h and i present another three other possible models using SGS from the result of MTC inversion shown in the Figure II.5.g.

All selected realizations have a global density mean of 0.4 ( $g/cm^3$ ) and variance of 0.018 ( $g/cm^3$ )<sup>2</sup>.

## II.4.6 Inversion of a real data set

### II.4.6.1 Geology and gravity data

The Blake River Group (BRG) of the Abitibi region (Canada) is bounded by the Porcupine Destor region fault in the north, and the Cadillac fault in the south. The BRG is a subdivision greenstone volcanogenic massive sulfide (VMS) deposits of the Noranda camp, Quebec, Canada. The BRG is composed of an andesite-rhyolite volcanic complex, felsic intrusions and diorite-gabbro sills and dykes (Bellefleur et Allard, 2007). It is host to 33 VMS deposits, 17 inside of Québec province, including the world class Noranda Mine. The tested area is around the Flavrian pluton, located 8 km West to the town of Noranda. This pluton is a synvolcanic intrusion. That has a felsic rocks composition with a significant proportion of tonalite (Paradis et al. (1988))(Figure II.9.a). The surface density samples measurements above the Flavrian Pluton shows a variation between 2.6 to  $3.05 g/cm^3$ , the interpolate density (Figure II.9.c) shows a variation comprised between 2.6 and  $2.9 g/cm^3$  with a median at  $2.74 g/cm^3$ .

The Bouguer anomaly of the BRG varying from  $-65.3 mGals$  to  $-23.5 mGals$  (Figure II.10.a). The residual anomaly was obtained by subtracting the regional field from a first

degree polynomial tend fitted on the regional of Bouguer anomaly (Figure II.10.b). The residual field varies between  $-8 \text{ mGals}$  and  $9 \text{ mGals}$  and has a negative value above the Flavrian pluton. We noticed that the anomaly in the southern part of the Pluton oriented along E-W direction with an extension of  $15 \text{ km}$ .

#### II.4.6.2 Stochastic inversion

##### II.4.6.2.1 Find a posterior model with the maximum likelihood

For this example the least square inversion by introducing a depth weight was used to find a posterior model with a maximum likelihood (Li et Oldenburg, 1998), this solution will be used as a starting model for the SGS. According to measurements of the samples of the density at the Flavrian Pluton, the average value is about  $2.78 \text{ g/cm}^3$ . The result of the least square inversion converges to a model with smooth density distribution illustrated on the Flavrain Pluton (Figure II.12.a). The distribution of the contrast density varies between  $-0.12$  and  $0.12 \text{ g/cm}^3$ .

##### II.4.6.2.2 Variogram and Histogram of density contrast

The variogram model is calculated on the density contrast distribution computed on the inverted model, Figure II.11 shows three selected variograms and density distribution histogram, the theoretical variogram model is fitted to a Gaussian one with a range about  $10^5 \text{ m}$ , the average sill is  $2.25 \times 10^{-3} (\text{g/cm}^3)^2$  and the nugget effect is  $0.12 \times 10^{-3} (\text{g/cm}^3)^2$ . The histogram shows the density contrast distribution ranging between  $-0.14$  and  $0.12$  with an average value of  $0$ .

This inversion provides a hypothesis on the irregular geometry and heterogeneity of the Flavrian Pluton. Its thickness reaches a maximum in the south at  $11 \text{ km}$ , rising to a depth of  $7 \text{ km}$  in the north (Figure II.12.a). According to the inverted structure, there are at least two phases of magmatic activity. The first phase forms the main body of the Flavrian Pluton which consists of felsic rocks that have a mass deficit relative to the mafic volcanic rocks that are concentrated at the base and the periphery of the pluton. The second magmatic and volcanic activity phase is at the center of the pluton.

##### II.4.6.2.3 Sequential simulation

The objective of the stochastic inversion is to generate several possible realizations in order to study the density heterogeneity distribution in the Flavrian pluton. Figure II.12

shows the result of the inversion of the five , the final selected realizations b, c, d, e, and f among 1000 simulated models. The result of the simulations show a contrast of  $-0.14 \text{ g/cm}^3$  in upper southern Western part of the Flavrian pluton corresponding to felsic rocks, and a positive contrast of  $0.02 \text{ g/cm}^3$  at the center of the pluton corresponding to mafic volcanic intrusion rocks. Figure II.13.a, .b, and .c shows the vertical component of the gravity field induced by the inverted model and simulations presented in Figure II.12.b, and .c, respectively. The analysis of *a posteriori* models, to estimate the probability of heterogeneities present in the pluton. The Figure II.14 a and b show that the density has the probability of  $2.64 \text{ g/cm}^3$  for the felsic rocks, and of  $2.8 \text{ g/cm}^3$  for the volcanic intrusion are the highest probable values for these rock types.

#### II.4.7 Discussion

An inversion method based on starting solution and Sequential Gaussian Simulation is presented. The simulation results depend on (i) the pilot points number, (ii) the type of modeled variogram (spherical, exponential and Gaussian) and the nugget effect. [Looms et al. \(2010\)](#) study the effect of the chosen *a priori* covariance matrix  $C_m$  on the inversion results. The synthetic example shows that not only the solution of inversion using least-squares can be used as the mean solution of the random realizations ( $\tilde{m}$ ), but also a solution found by the Monte Carlo can be used as an alternative median solution ( $\tilde{m}$ ) to generate multiple realizations using the Gaussian Simulation. The use of a tetrahedral mesh limits the choice of the geostatistical methods to algorithms as sequential indicator and sequential Gaussian simulation ([Remy et al., 2002; Manchuk, 2010](#)). However, the use of the underlying regular grid allows the use of much more simulation algorithm such as multi point geostatistics ([Strebelle et A., 2001](#)) and spectral simulation ([Pardo-Igùzquiza et Chica-Olmo, 1993](#)).

#### II.4.8 Conclusions

Various methods can be used to simulate the density distribution at the subsurface. The Monte Carlo inversion which consists in varying randomly the density distribution in the model, some models are rejected and others are accepted increasing considerably the possible number of models and the computation time. The models must be constrained by *a priori* information such as geological information (possible structures) and spatial densities variation. When the sequential simulation is applied to gravity linear inverse problems, this technique generates a large number of acceptable models. This allows

computing the posterior probability of the model and the probability of the density values in a given location and provides a useful tool for performing uncertainty studies on the simulation results. Such approaches may have important consequences on exploration decisions.

# References

- Afnimar, K., Koketsu, and K. Nakagawa, 2002, Joint inversion of refraction and gravity data for the three-dimensional topography of a sediment-basement interface : Geophysical Journal International, **151**, 243–254.
- Babak, O., and C. Deutsch, 2009, Collocated cokriging based on merged secondary attributes : Mathematical Geosciences, **41**, no. 8, 921–926. (10.1007/s11004-008-9192-2).
- Barbosa, V. C. F., and J. B. C. Silva, 1994, Generalized compact gravity inversion : Geophysics, **59**, 57–68.
- Barbosa, V. C. F., J. B. C. Silva, and W. E. Medeiros, 2002, Practical applications of uniqueness theorems in gravimetry : Part II—pragmatic incorporation of concrete geologic information : Geophysics, **67**, 795–800.
- Bellefleur, G., d. K. E. G. J., and M. Allard, 2007, A new look at the geological framework of the Central Noranda camp, Québec from industry high-resolution seismic profiles : Geological Survey of Canada Current Research, **C5**, 9p.
- Bertete-Aguirre, H., E. Cherkayev, and M. Oristaglio, 2002, Non-smooth gravity problem with total variation penalization functional : Geophysical Journal International, **149**, 499–507.
- Blakely, R. J., 1995, Potential theory in gravity and magnetic applications : Cambridge University Press.
- Bosch, M., 1999, Lithologic tomography : From plural geophysical data to lithology estimation : Journal of Geophysical Research B : Solid Earth, **104**, 749–766.
- Bosch, M., L. Cara, J. Rodrigues, A. Navarro, and M. Díaz, 2007, A Monte Carlo approach to the joint estimation of reservoir and elastic parameters from seismic amplitudes : Geophysics, **72**, Q29–Q39.
- Bosch, M., and J. McGaughey, 2001, Joint inversion of gravity and magnetic data under lithologic constraints : The Leading Edge, **20**, 877–881.

- Bosch, M., R. Meza, R. Jiménez, and A. Hönig, 2006, Joint gravity and magnetic inversion in 3D using Monte Carlo methods : *Geophysics*, **71**, G153–G156.
- Boulanger, O., and M. Chouteau, 2001, Constraints in 3D gravity inversion : *Geophysical Prospecting*, **49**, 265–280.
- Chasserau, P., and M. Chouteau, 2003, 3D gravity inversion using a model of parameter covariance : *Journal of Applied Geophysics*, **52**, 59 – 74.
- Chilés, J.-P., and P. Delfiner, 1999, *Geostatistics, Modeling Spatial Uncertainty.* : Wiley Series on Probability and Statistics.
- de Marsily, G. H., C. Lavada, M. Boucher, and G. Fasanino, 1984, Interpretation of interference tests in a well field using geostatistical techniques to fit the permeability distribution in a reservoir model : *Geostatistics for natural resources characterization, Part 2*.
- Franklin, J. N., 1970, Well posed stochastic extensions of ill posed linear problems : *Journal of the Institute of Mathematics and Its Applications*, **31**, 682–716.
- Fregoso, E., and L. A. Gallardo, 2009, Cross-gradients joint 3Dinversion with applications to gravity and magnetic data : *Geophysics*, **74**, L31–L42.
- Gallardo-Delgado, L. A., M. A. Pérez-Flores, and E. G.-T. no, 2003, A versatile algorithm for joint 3D inversion of gravity and magnetic data : *Geophysics*, **68**, 949–959.
- Gloaguen, E., D. Marcotte, M. Chouteau, and H. Perroud, 2005, Borehole radar velocity inversion using cokriging and cosimulation : *Journal of Applied Geophysics*, **57**, 242 – 259.
- Gloaguen, E., D. Marcotte, B. Giroux, C. Dubreuil-Boisclair, M. Chouteau, and M. Aubertin, 2007, Stochastic borehole radar velocity and attenuation tomographies using cokriging and cosimulation : *Journal of Applied Geophysics*, **62**, 141 – 157.
- Gómez-Hernández, J. J., A. Sahuquillo, and J. Capilla, 1997, Stochastic simulation of transmissivity fields conditional to both transmissivity and piezometric data—I. Theory : *Journal of Hydrology*, **203**, 162 – 174.
- Guillen, A., and V. Menichetti, 1984, Gravity and magnetic inversion with minimization of a specific functional : *Geophysics*, **49**, 1354–1360.
- Häggström, O., 2002, *Finite markov chains and algorithmic applications* : Cambridge University Press.
- Hansen, T. M., A. G. Journel, A. Tarantola, and K. Mosegaard, 2006, Linear inverse gaussian theory and geostatistics : *Geophysics*, **71**, R101–R111.
- Hansen, T. M., and K. Mosegaard, 2008, Visim : Sequential simulation for linear inverse problems : *Computers & Geosciences*, **34**, 53 – 76.

- Journel, A., 1999a, Conditioning geostatistical operations to nonlinear volume averages : Mathematical Geology, **31**, no. 8, 931–953. (10.1023/A:1007551529317).
- , 1999b, Markov models for cross-covariances : Mathematical Geology, **31**, no. 8, 955–964. (10.1023/A:1007553013388).
- Journel, A. G., and C. J. Huijbregts, 1978, Mining geostatistics : Academic Press.
- Lam, N. S., 1983, Spatial interpolation methods review : The American Cartographer, **10**, 129–149.
- Last, B. J., and K. Kubik, 1983, Compact gravity inversion : Geophysics, **48**, 713–721.
- Li, Y., and D. W. Oldenburg, 1998, 3-D inversion of gravity data : Geophysics, **63**, 109–119.
- Looms, M. C., T. M. Hansen, K. S. Cordua, L. Nielsen, K. H. Jensen, and A. Binley, 2010, Geostatistical inference using crosshole ground-penetrating radar : Geophysics, **75**, J29–J41.
- Mallet, J. L., 2002, Geomodeling : Inc. Oxford University Press.
- Manchuk, J. G., 2010, Geostatistical modeling of unstructured grids for flow simulation : PhD thesis, University of Alberta.
- Metropolis, N., A. W. Rosenbluth, M. N. Rosenbluth, A. H. Teller, and E. Teller, 1953, Equation of state calculations by fast computing machines : Journal of Chemical Physics, **21**, 1087–1092.
- Metropolis, N., and S. Ulam, 1949, The Monte Carlo method : J. Am. Stat. Assoc., **44**, 335–341.
- Mosegaard, K., and M. Sambridge, 2002, Monte Carlo analysis of inverse problems : Inverse Problems, **18**, R29–R54.
- Mosegaard, K., and A. Tarantola, 1995, Monte Carlo sampling of solutions to inverse problems : J. Geophys. Res., **100**, 12431–12447.
- Paradis, S., J. Ludden, and L. Gélinas, 1988, Evidence for contrasting compositional spectra in comagmatic intrusive and extrusive rocks of the late Archean Blake River Group, Abitibi, Québec : Canadian Journal of Earth Sciences, **25**, 134–144.
- Pardo-Igùzquiza, E., and M. Chica-Olmo, 1993, The Fourier Integral Method : An efficient spectral method for simulation of random fields : Mathematical Geology, **25**, no. 2, 177–217. (10.1007/BF00893272).
- Portniaguine, O., and M. S. Zhdanov, 1999, Focusing geophysical inversion images : Geophysics, **64**, 874–887.
- , 2002, 3-D magnetic inversion with data compression and image focusing : Geophysics, **67**, 1532–1541.

- Remy, N., A. Shtuka, B. Levy, and J. Caers, 2002, GSTL : the geostatistical template library in C++ : Computers & Geosciences, **28**, 971 – 979.
- Sambridge, M., and K. Mosegaard, 2002, Monte Carlo methods in geophysical inverse problems : Rev. Geophys., **40**, 1–29.
- Seneta, E., 1982, Non-Negative matrices and Markov Chains, 2nd ed. : Berlin : Springer.
- Shamsipour, P., D. Marcotte, M. Chouteau, and P. Keating, 2010, 3D stochastic inversion of gravity data using cokriging and cosimulation : Geophysics, **75**, I1–I10.
- Silva, J. B. C., and V. C. F. Barbosa, 2006, Interactive gravity inversion : Geophysics, **71**, J1–J9.
- Silva, J. B. C., W. E. Medeiros, and V. C. F. Barbosa, 2002, Practical applications of uniqueness theorems in gravimetry : Part I—constructing sound interpretation methods : Geophysics, **67**, 788–794.
- Strebelle, S., and J. A., 2001, Reservoir modeling using multiple-point statistics : SPE 71324 presented at the 2001 Society of Petroleum Engineers Annual Technical Conference and Exhibition, **New Orleans, Louisiana**, 30 September– 3 October.
- Tarantola, A., 2005, Inverse Problem Theory and Methods for Model Parameter Estimation : Society for Industrial and Applied Mathematics.
- , 2006, Popper, Bayes and the inverse problem : Nature Physics, **2**, 492–494.
- Tarantola, A., and B. Valette, 1982, Generalized nonlinear inverse problems solved using the least squares criterion : Reviews of Geophysics and Space Physics, **20**, 219–232.
- Xu, W., T. T. Tran, R. M. Srivastava, and A. G. Journel, 1992, Integrating Seismic Data in Reservoir Modeling : The Collocated Cokriging Alternative : Proceedings - SPE Annual Technical Conference and Exhibition, **Omega**, 833–842.

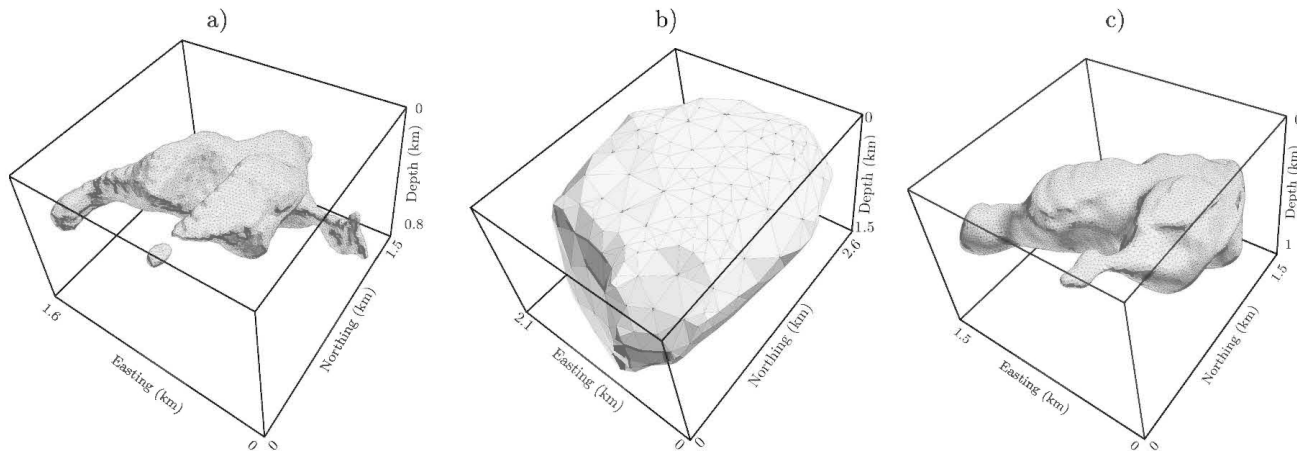


FIGURE II.2: Tetrahedral body. a) Reference model, b) initial model (prior information) and c) posterior model using least squares inversion.

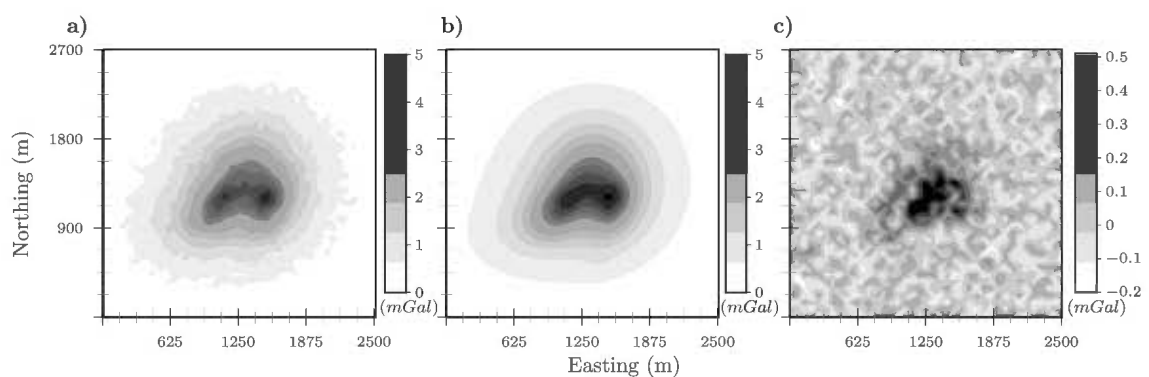


FIGURE II.3: The vertical component of the gravity field produced by the (a) reference model, contaminated by a random noise ; (b) prediction from inversion model ; and (c) the difference between reference model response and inverted model prediction.

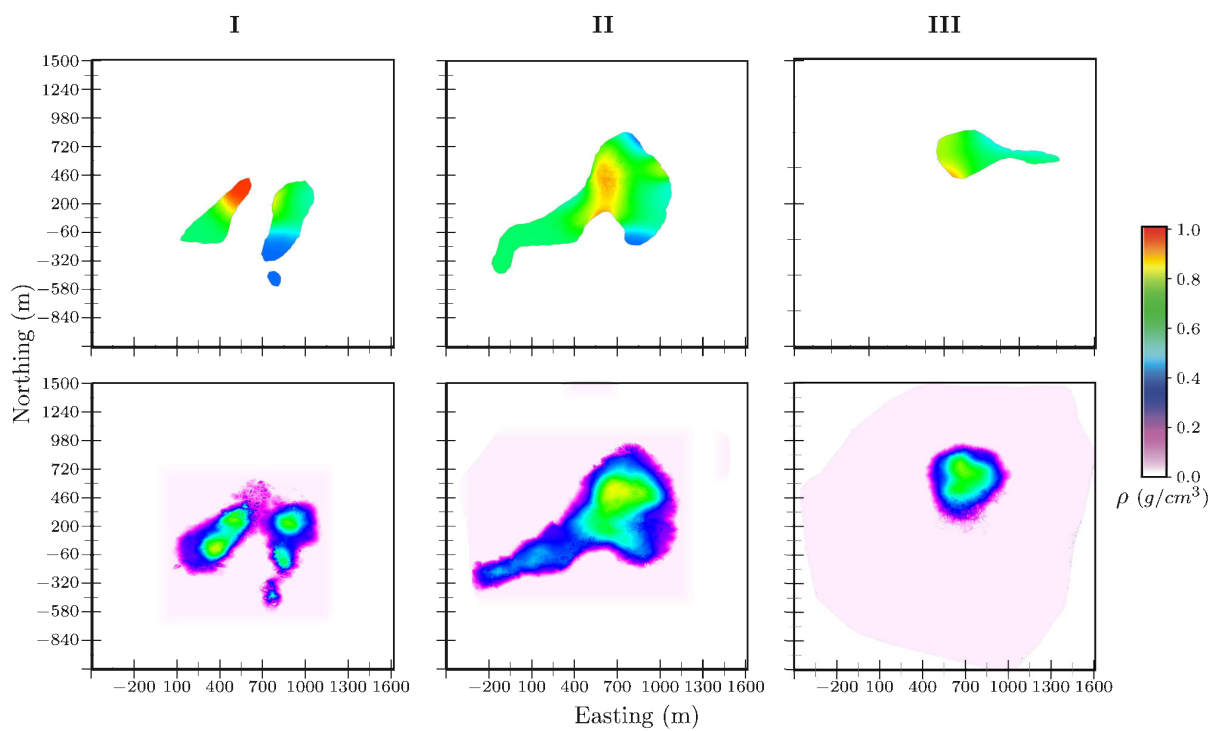


FIGURE II.4: Top view of density distribution between reference model (top) and inversion result (bottom) at (a) 150m, (b) 350m, (c) 650m of depth.

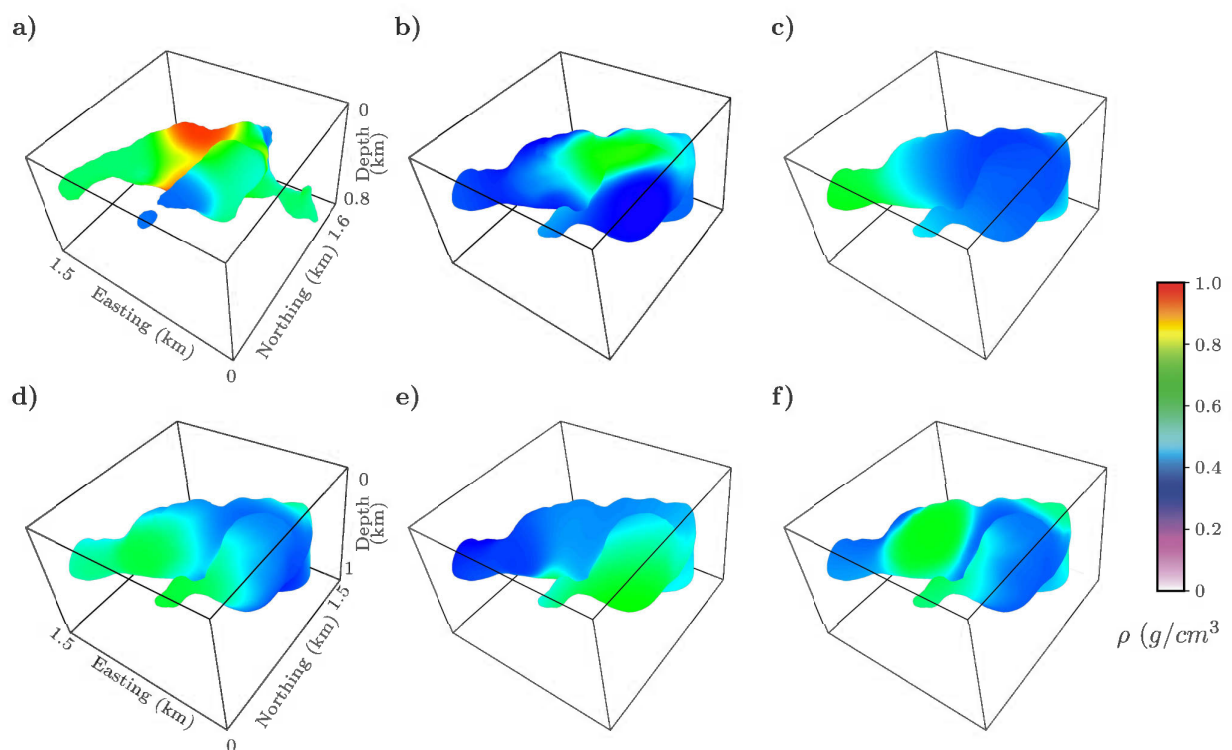


FIGURE II.5: Accepted models (density distribution) using Monte Carlo sampling (likelihood  $> 0.75$ )

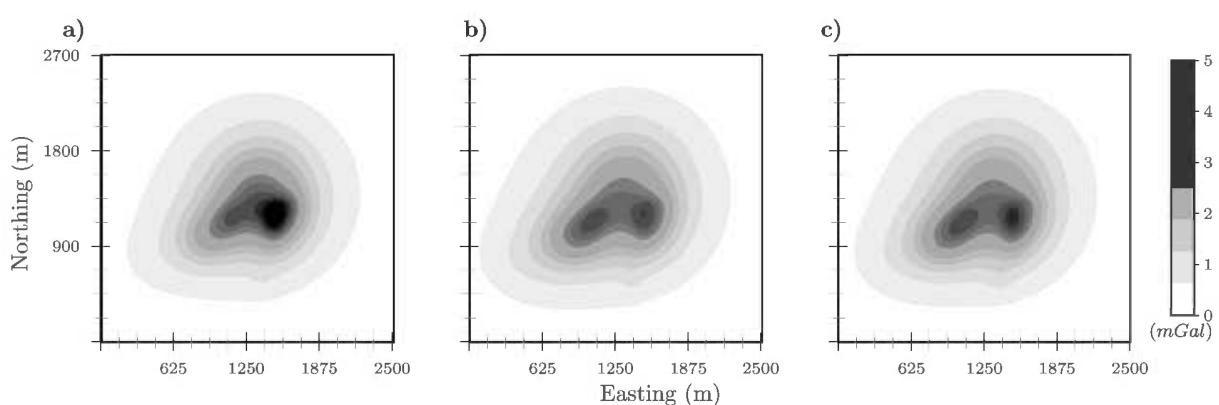


FIGURE II.6: Vertical component of the gravity field for the accepted MTC models  
(Figure II.5 b., c. and d.)

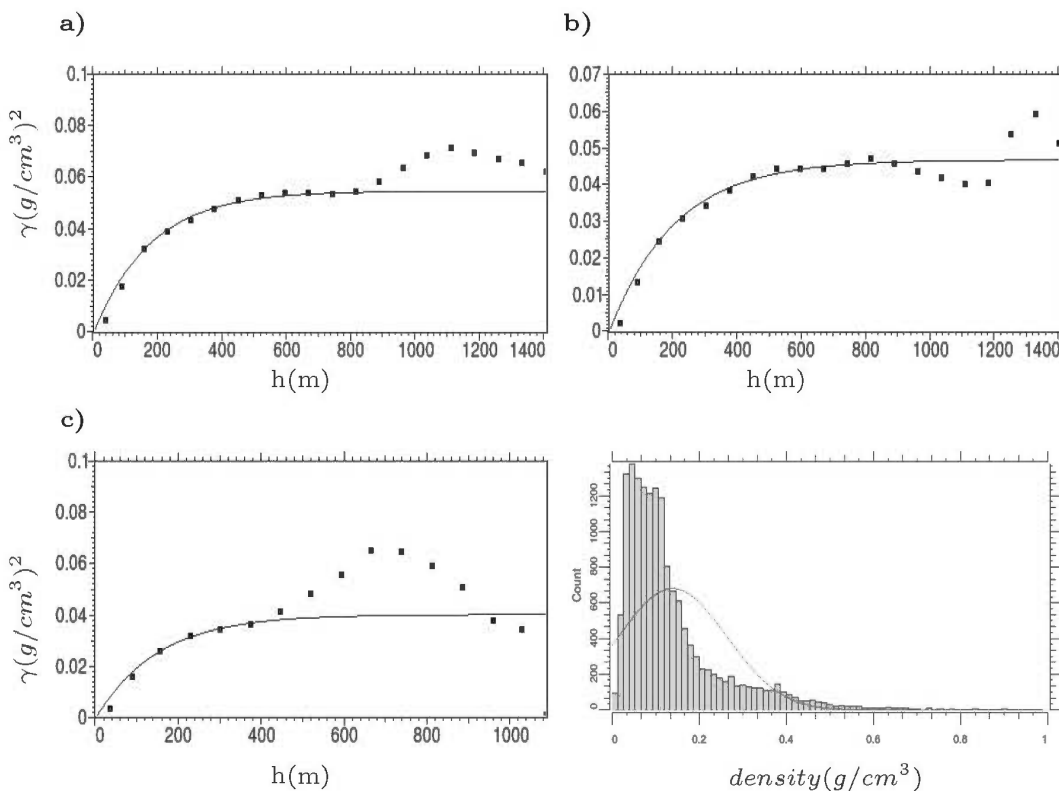


FIGURE II.7: Selected variograms (solid lines) of pilot points densities, Gaussian models are used for the variograms. a) Azimuth of  $0^\circ$  dip of  $0^\circ$ , b) azimuth of  $90^\circ$  dip of  $45^\circ$  and c) azimuth of  $45^\circ$  dip of  $85^\circ$ .

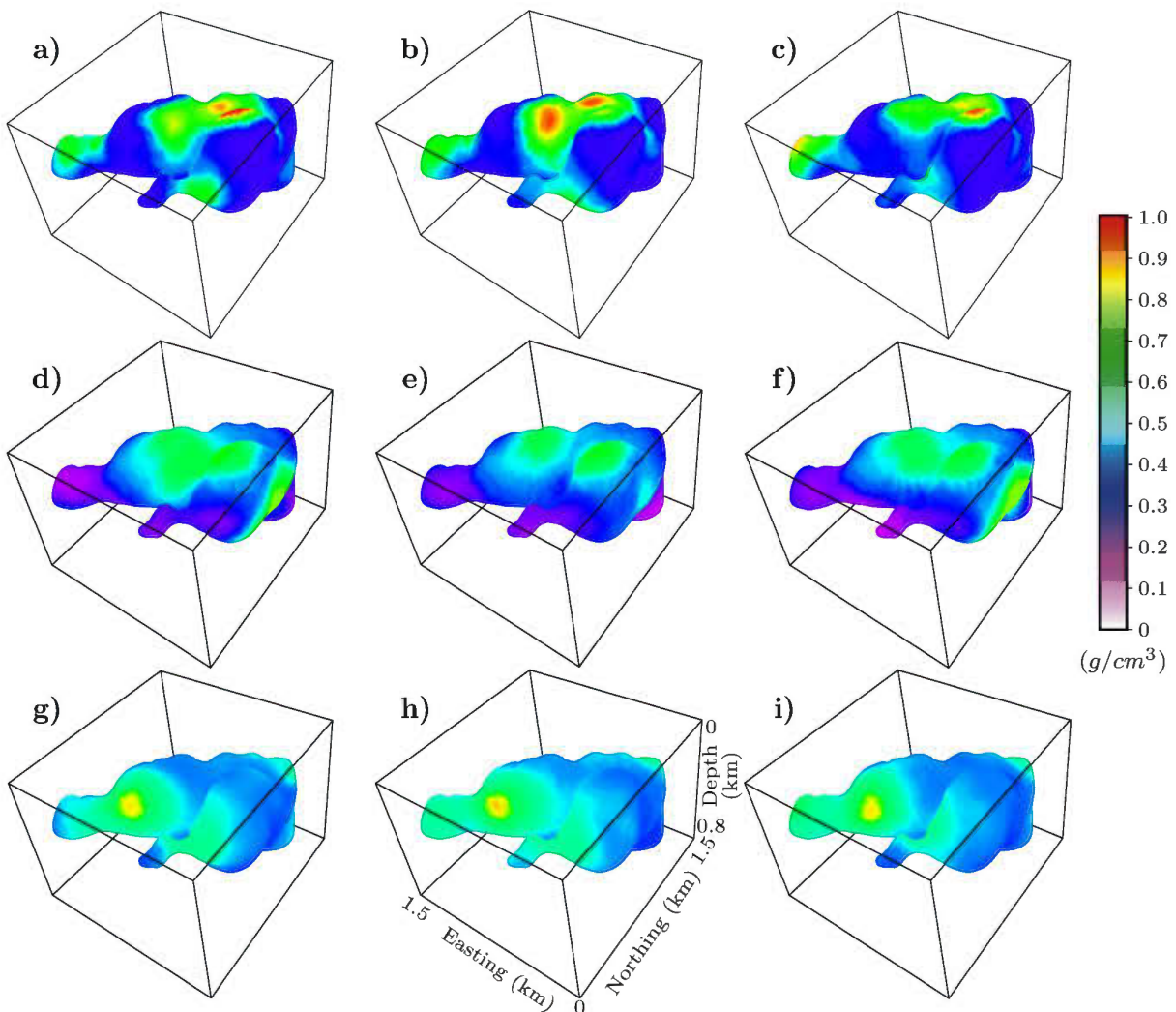


FIGURE II.8: Simulated density distribution in the posterior model using conditional Gaussian simulations (a, b, c, d, e and f) from inverted model and (g, h, and i) from model in Figure II.5.b (likelihood  $> 0.7$ ).

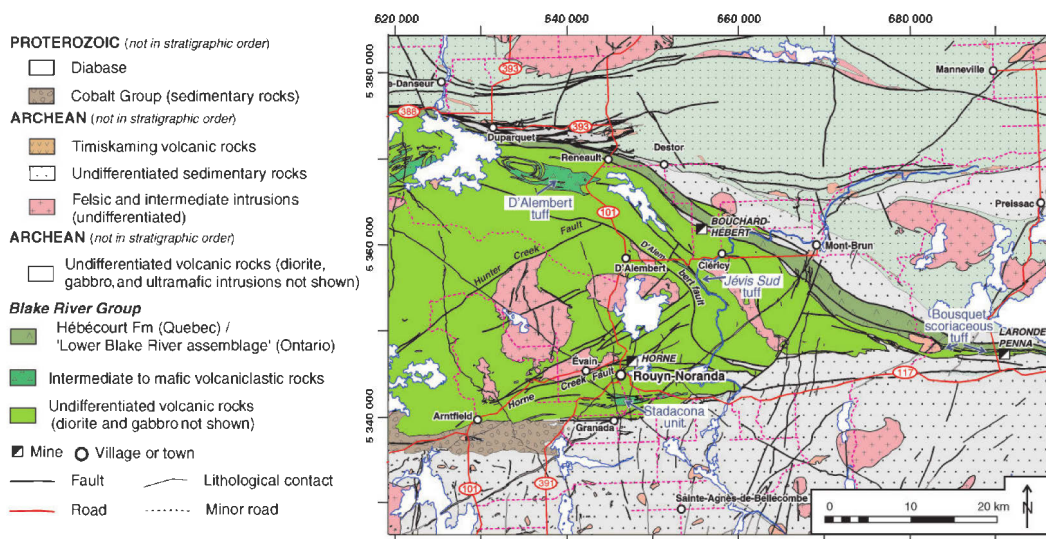


FIGURE II.9: Simplified geological map of central Noranda mining camp showing selected volcanogenic massive sulphide and major lithological contact.

then the simulation results is transferred to the tetrahedral mesh in order to compute the likelihood used to accept or reject the outcome of the simulation (Figure III.13.b and d and f). It is possible to manage several random realizations of the structural models whose average is other than the initial model found by zonation.

For an idea of the geometry of sources, Figure III.14 shows a top view of four possible density distributions of 1.6 km depth. As we can see for McIvor Pluton, the density contrast differs from one realization to another but remains the same tendency (the density decreases towards the center of the Pluton), it is also possible to sketch out the possible geometry shape (solid line). However it is more difficult to locate the diabase dyke due to low density contrast. Nevertheless it is possible to observe a slight tendency oriented northeast (dashed line) in the southern part of McIvor Pluton, which is not the case of the result found by the least squares method.

### III.3.7 Discussion

Inverting separately two set of potential field data leads in general to two different geological models. Some structures observed near the surface in the inversion of the magnetic data set may be invisible while inverting the gravimetric data, and vice versa. For instance dykes and diabases are absent in the inverted gravity model, and the McIvor Pluton, whose geometry is well defined by the gravimetric method is not present in the result of the inversion of the magnetic method.

The zonation method in the joint inversion allows imposing geometric constraint. The results of multiple inversion can be considered as *a priori* model whose the results are the average of several possible models. However an underestimation of the number of zones in the initial model should lead to a new zonation that could be recalculated from the model obtained by cokriging for example.

Considering the hypothesis that the smooth solution found by the least squares method is the average of several possible solutions in a Gaussian field, the result of the simulation is influenced by the number of pilot points used, by the type of the variogram (exponential, spherical or Gaussian), and by the simulation grid resolution. The correlation coefficient remains a difficult parameter to choose, in the presence of drilling data, Collocated Cokriging simulation could be used with a coefficient of correlation per zone. In other situations, it can be chosen by the user as an indicator of similarity between the gravity and the magnetism according to his interpretation and knowledge of the studied area. Otherwise, small correlation coefficients indicate independence between rocks density and susceptibility.

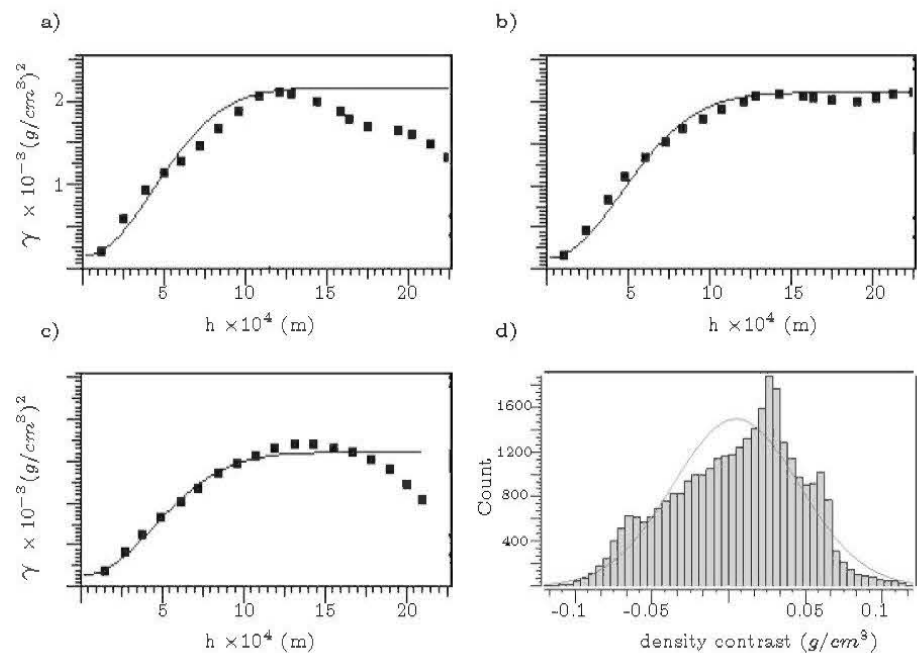


FIGURE II.11: Selected variograms (solid lines) of pilot points densities, Gaussian models are used for the variograms. a) Azimuth of  $0^\circ$  dip of  $0^\circ$ , b) azimuth of  $90^\circ$  dip of  $45^\circ$  and c) azimuth of  $45^\circ$  dip of  $85^\circ$ .

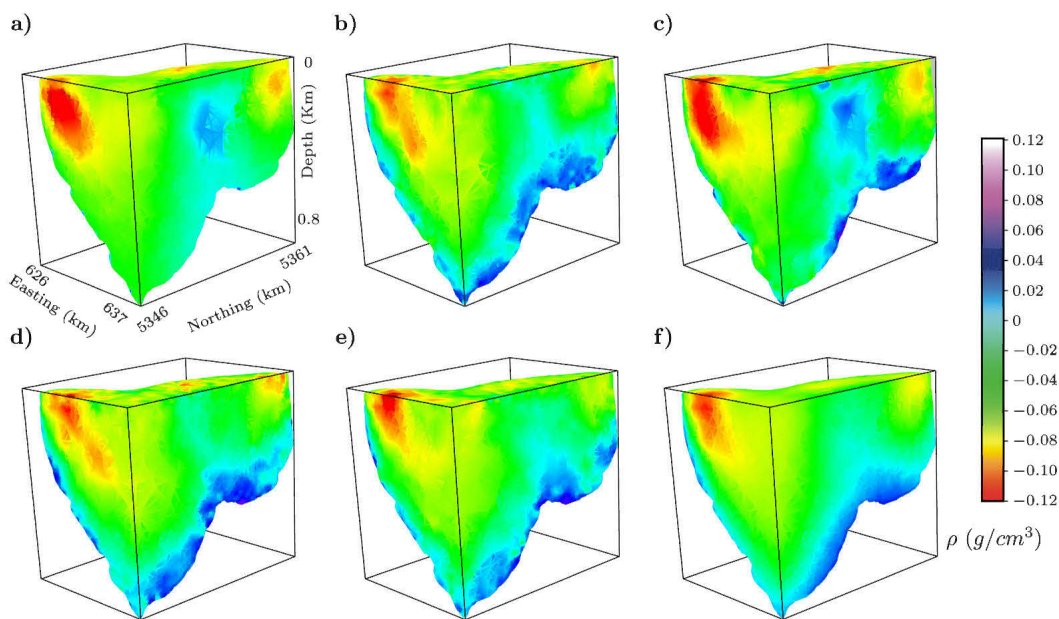


FIGURE II.12: Inversion result using a) least squares inversion (b), (c), (d), and (e)  
conditional Gaussian simulation, (f) mean of 100 random Gaussian simulation

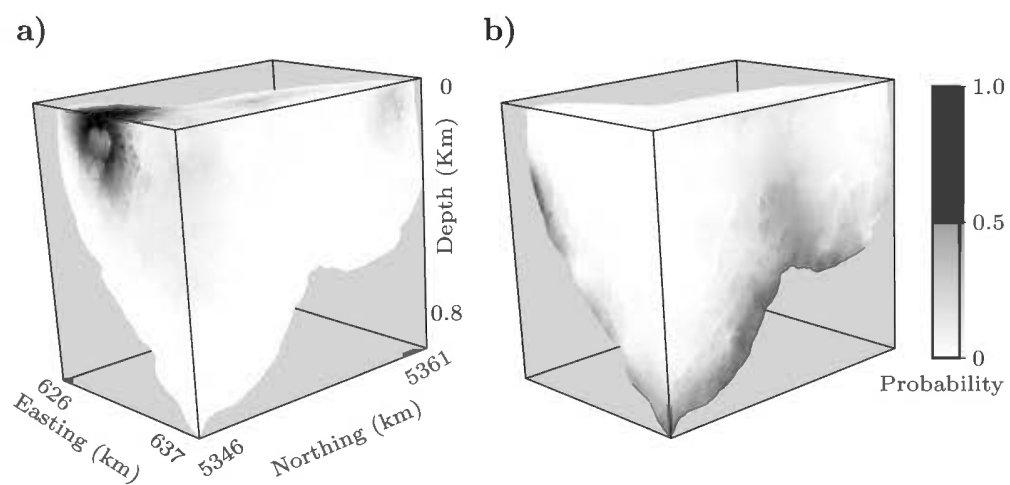


FIGURE II.14: Calculated probability from 100 realizations of the density of (a) 2.64 and (b) 2.8  $g/cm^3$ .

## II.5 Bilan

Il existe plusieurs techniques pour simuler la distribution de la propriété physique dans le sous-sol. La méthode proposée dans ce chapitre, offre une optimisation de la méthode de Monte Carlo. Les réalisations multiples proposées par les méthodes géostatistiques augmentent considérablement le nombre de modèles acceptés. Cependant, les modèles simulés doivent être inspirés par une information *a priori* telle que l'information géologique (structures possibles) et la variation spatiale de la propriété physique (solution de départ). Dans l'article proposé, la simulation séquentielle est appliquée au problème inverse en gravimétrie. Ceci permet de calculer la probabilité *a posteriori* des modèles et de la probabilité de la valeur de la densité au niveau d'une position donnée par sa fréquence de répétition. Par conséquence, la méthode proposée fournit un outil utile pour effectuer des études de l'incertitude sur les résultats de simulation. De telles approches peuvent avoir des conséquences importantes sur les décisions d'exploration. Néanmoins, il faut garder à l'esprit que les résultats de la simulation sont influencés par la solution de départ, le nombre et la position des points pilotes, le modèle de variogramme choisi, du niveau du bruit et enfin, de l'incertitude sur les mesures.



## CHAPITRE III

### INVERSION CONJOINTE

#### III.1 Introduction

La modélisation géologique et la compréhension des phénomènes mis en cause demandent une analyse complexe et très détaillée des informations géologiques, géochimiques ainsi que la répartition spatiale des propriétés physiques dans le sous-sol. Cette dernière est accessible d'une manière directe et ponctuelle par des trous de forage ou bien d'une manière indirecte par une interprétation des données géophysiques mesurées généralement en surface.

L'inversion est une des méthodes d'interprétation géophysique qui a pour but de quantifier les sources responsables des anomalies observées. Les modèles obtenus par inversions indépendantes de chaque méthode géophysique peuvent présenter des résultats différents les uns des autres, car chacune de ces méthodes est sensible à un contraste de propriété physique, dans le cas de la gravimétrie, la méthode est sensible à la répartition de la masse volumique (ou densité), par contre pour la magnétométrie, c'est la distribution de la aimantation (induite ou rémanente) dans le sous-sol.

Le résultat de l'inversion doit être confronté à la réalité géologique et souvent il est très difficile de répondre à toutes les questions en utilisant une seule méthode. D'autres facteurs viennent compliquer la modélisation tels que la limite de résolution de chaque méthode, le sur-dimensionnement du problème inverse, le bruit contaminant les données et le problème d'équivalence des sources responsables des anomalies observées en surface. Toutes ces causes augmentent ainsi le nombre de modèles possibles. Néanmoins, l'analyse combinée des paramètres géophysiques pourrait être utilisée, non seulement pour la discrimination lithologique telle que présentée par [Bosch \(1999\)](#) et [Ezzedine](#)

et al. (1999), mais aussi, pour augmenter la fiabilité du modèle géologique lorsque les propriétés interprétées sont estimées conjointement (Zeyen et Pous, 1993; Afnimar et al., 2002; Gallardo-Delgado et al., 2003; Linde et al., 2006; Tryggvason et Linde, 2006; Linde et al., 2008). Finalement en se basant sur l'interdépendance des propriétés physiques dans le sous-sol, l'inversion conjointe peut restreindre l'espace des modèles possibles.

### III.2 Inversion conjointe : état de l'art

L'inversion conjointe consiste à déterminer un ou plusieurs paramètres de modèle à partir des différentes données géophysiques mesurées. Les paramètres du modèle peuvent être représentés par de l'information structurale définie par les limites issues d'un contraste ou d'un changement de propriétés physiques dans le sous-sol. Dans ce dernier cas, les propriétés peuvent être de même nature, par exemple les vitesses de propagation des ondes de compression et de cisaillement respectivement pour les méthodes sismiques réfraction et réflexion, ou de nature différente comme par exemple la densité et la susceptibilité magnétique pour les méthodes de prospection gravimétrique et magnétique. Ainsi, le fait de résoudre le problème inverse en tenant compte d'un maximum d'informations et de plusieurs données géophysiques, augmente non seulement la fiabilité des résultats mais aussi facilite leur intégration dans une interprétation géologique et ou pétrophysique (Gallardo, 2004).

Lorsqu'une relation entre les différentes propriétés physiques à modéliser est définie, alors il est possible d'intégrer cette relation dans la fonction objective comme le propose Tondi et al. (2000). Ce qui permet de rendre le problème inverse plus simple et sa solution est équivalente à la résolution d'une inversion individuelle.

Certains auteurs utilisent les similarités structurales existantes entre les différents paramètres afin de lancer une inversion conjointe (Haber et Oldenburg, 1997; Musil et al., 2003; Gallardo-Delgado et al., 2003; Gallardo et Meju, 2004; Saunders et al., 2005). Les similarités sont exprimées sous forme de contrainte et la solution du problème inverse est obtenue en introduisant le concept du cross-gradients entre les différentes variables (Gallardo-Delgado et al., 2003; Gallardo et Meju, 2004; Tryggvason et Linde, 2006). L'information structurale peut être traduite en une matrice de pondération dont les éléments sont inversement proportionnels au gradient du modèle calculé. Les inversions sont effectuées séparément en permutant les coefficients de pondération

mutuellement à chaque itération (Günther et Rücker, 2006; Bouchet, 2010).

Une autre technique d'inversion est dite inversion en simultanée. Elle utilise une approche empirique pour passer d'un modèle issu d'une inversion dans un domaine, vers un autre modèle dans un autre domaine (Dell'Aversana, 2001; Jegen et al., 2009). Hu et al. (2009) propose une alternative qui consiste à imposer des contraintes puis à effectuer les inversions en commutant les contraintes entre les domaines à chaque fois. Stefano et al. (2011) offre une amélioration des techniques d'inversions simultanées, sans imposer de contrainte mais en introduisant une fonction objective qui permet de relier les différents domaines d'inversions.

Bosch (1999); Bosch et al. (2006, 2007) proposent d'intégrer les méthodes stochastiques dans le cadre d'une inversion conjointe. Basée sur une approche Bayésienne, la méthode résout le problème inverse en effectuant un échantillonnage de type Monte Carlo puis en calculant la probabilité *a posteriori* de chaque modèle sélectionné.

Dans l'article qui suit, nous présentons une amélioration de la méthode stochastique proposée par Tarantola (2005) et Bosch et al. (2006). Celle-ci se résume par une optimisation de la méthode d'échantillonnage des modèles *a posteriori* à l'aide des techniques géostatistiques. En effet, la co-simulation entre les valeurs de densité et d'aimantation est utilisée afin de procéder à une inversion conjointe, d'une part, et pour générer un grand nombre de réalisations tout en réduisant le temps de calcul comparativement à la méthode de Mont Carlo d'autre part.

### III.3 Joint Gravity and Magnetic Inversion using Collocated Cokriging Simulation

Nacim Foudil-Bey<sup>\*†</sup>, Li Zhen Cheng<sup>†</sup>, Jean-Jacques Royer<sup>\*</sup> and Guillaume Caumon<sup>\*</sup>

#### III.3.1 Résumé

Sachant que chaque méthode géophysique est sensible à un contraste de propriété physique dans le sous-sol, et que le pouvoir de résolution varie d'une méthode une autre, il n'est pas étonnant de trouver des résultats d'inversions différents par modélisation de chaque propriétés physique. Dans cet article nous proposons une méthode qui

exploite les résultats d'inversion séparée de chaque donnée pour effectuer une inversion conjointe. Toutes les informations structurales sont exprimer sous forme de contrainte géométrique. La méthode géostatistique utilisée permet d'intégrer deux sources d'information (densité et susceptibilité dans notre cas) et par conséquent de générer plusieurs distributions possibles de propriétés physiques dans dans un modèle en 3D par la technique de simulation par co-krigeage Colocalisé. Dans ce cas une propriété physique est considérée comme une variable primaire, et l'autre propriété est considérées comme variable secondaire. À la fin par une formulation bayésienne seul les modèles ayant une probabilité a posteriori acceptable sont gardés. En premier, la méthode à été testée sur exemple synthétique pour illustrer l'application de la méthode et de montrer l'influence du coefficient de corrélation entre la variable primaire et secondaire sur le résultat de la modélisation, Ensuite la méthode proposée a été appliquée au dessus du Pluton McIvor dans le camp minier de Matagami dans la province du Québec, Canada.

### **III.3.2 Abstract**

When two geophysical surveys or more are commonly available in a same area, it is often difficult to integrate their interpretation results together because they haven't same data resolution or they don't reflect same source distribution. By integrating calculation algorithms into such environment, it is possible to do interpretation of multiple data sets simultaneously with less limitation. In this paper we propose a method that carries the inversion results of each separate data and a geostatistical approach for joint inversion. First, all structural information are imposed as geometric constraint. Then, the geostatistical method are used allows to integrate two sources of information (density and susceptibility in our case) and consequently generate several possible distributions of physical properties in a common 3D model by Collocated Cokriging simulation technique. In this case one physical property is considered as primary variable and another property is considered as secondary variable. Finally, using Bayesian formulation only models with acceptable posterior probabilities will be kept. The method was tested on synthetic example to illustrate the application of the method, and to show the influence of the correlation factor between the primary and secondary variable how they affect the modelling result. By the end of this paper, we applied the method to the west of Matagami mining camp of Canada. The interpretation results showed a complex geological structure in which shallow and deep sources are clearly separated

### III.3.3 Introduction

Three dimensional geological modeling requires very detailed geological, geochemical prior information and spatial distribution analysis of the physical properties of the subsurface.

Consider the cost and the effect on the ecosystem, geophysical methods are the most efficient way to investigate the subsurface structures. After measurements in the field, the key question is how extract structural or lithologic informations from the data. The inversion of geophysical data is widely used in recovering a subsurface physical property distribution which has an intrinsic link to the geology. However the geological model produced by an inversion from individual data may present a different model depending on the geophysical method, because each one is sensitive to a specific physical property. For instance gravity method is sensitive to density contrast while magnetic method is sensitive to the magnetization. The result of the inversion must be confronted with the geological reality and it is often very difficult to answer questions using a single method. Other factors can make the modeling steps more complicated such as the resolution limit of each method, the over-sizing of the inverse problem, the noise and finally the problem of equivalence of sources causing anomalies which may increase the number of possible models.

Nevertheless, the combined analysis of geophysical parameters could be used not only for the lithological discrimination as presented by [Bosch \(1999\)](#) and [Ezzedine et al. \(1999\)](#), but also to increase the reliability of the 3D geophysical model when parameters are estimated together ([Zeyen et Pous, 1993](#); [Afnimar et al., 2002](#); [Gallardo-Delgado et al., 2003](#); [Linde et al., 2006](#); [Tryggvason et Linde, 2006](#); [Linde et al., 2008](#)). Consequently, based on the physical properties combination, joint inversion can restrict the space of possible models.

Some authors use the structural similarity between different parameters to launch a combined inversion ([Haber et Oldenburg, 1997](#); [Musil et al., 2003](#); [Gallardo-Delgado et al., 2003](#); [Gallardo et Meju, 2004](#); [Saunders et al., 2005](#)). The similarities are expressed as constraints and the solution of the inverse problem is obtained by introducing the concept of cross-gradients between differential variables ([Gallardo-Delgado et al., 2003](#); [Gallardo et Meju, 2004](#); [Tryggvason et Linde, 2006](#)). Another technique of simultaneous inversion uses the links between physical properties, either by linear relation ([Tondi et al., 2000](#)) or by an empirical approach allowing inversion model to switch from a domain to another model ([Dell'Aversana, 2001](#); [Jegen et al., 2009](#)). [Hu et al. \(2009\)](#) offers an alternative that consists in setting constraints , and then run the inversion by switching

constraints from the domain to the other every time steps. Stefano et al. (2011) proposed an alternative improves inversion technique that does not use constraints by introducing an objective function that allows linking the different inversion domain.

However, although the integration of multiple data sets during the inversion improves the inverted results, the oversized inversion remains a problem, the space of models is reduced but the problem of equivalent sources is still present. The multitude of equivalent models can be estimated by combination of priori information and stochastic methods, such as Monte Carlo (Bosch, 1999; Tarantola, 2005) or techniques of geostatistics simulations (Hansen et al., 2006; Gloaguen et al., 2007; Looms et al., 2010; Shamsipour et al., 2010b) mentioned as *a posteriori* probability in the literature.

In this paper, we propose a combined joint inversion methodology involving a geostatistical method. The structural information obtained from the inversion of each data set will be then co-simulated, between a primary variable and a secondary one, and the probability of realizations will be calculated. Only models with a value of higher likelihood than a prefixed threshold will be accepted. After introduce the co-simulation inversion methodology, we used synthetic data to illustrate the application of the method and to investigate the influence from different co-simulation parameters. Finally, the proposed method is applied to a data set collected over the McIvor Pluton in the Matagami mining camp in Québec, Canada.

### III.3.4 Theory

In the case of a model space ( $M$ ) common to two properties, the posterior probability is a function of *a priori* geological information  $\rho_M(m)$ , the likelihood function of data  $L(m_{var_1}, m_{var_2})$  and the probability density of the variable 1 ( $var_1$ ) conditioned by the variable 2 ( $var_2$ )  $\pi(m_{var_1}|m_{var_2})$ . For a given geological model  $i(m)$  the posterior probability can be written as following :

$$\sigma_i(m) = \underbrace{\frac{\rho_{iM}(m)}{prior} \cdot \frac{\pi_i(m_{var_1}|m_{var_2})}{correlation\ law} \cdot \frac{L_i(m_{var_1}, m_{var_2})}{likelihood}}_{information\ geostatistics} \quad (III.1)$$

Therefore solving the inverse problem amounts to sample models by varying the variables 1 and 2 simultaneously and then to calculate the posterior probability. However, finding an acceptable model by varying randomly two physical properties at the same time

remains difficult. Order to circumvent this problem, we propose, as a first step, to start with fixed and acceptable solution of the variable 2, then to seek a possible solutions to a variable 1. Once process is finished, it is possible to find plausible solutions of the variable 2 by considering the previously accepted solutions of a variable 1. In this case the inverse problem is simplified and the equation (III.1) can be written as :

$$\sigma(m) = \underbrace{\rho_M(m_{geo})}_{\text{geostatistics}} \underbrace{L(m_{var_1})}_{\text{likelihood}}_{var_2} \quad (\text{III.2})$$

where the first term ( $\rho_M(m_{geo}) = \rho_{iM}(m) \pi(m_{var_1}|m_{var_2})$ ) is satisfied by the geostatistical simulation and  $L(m_{var_1})_{var_2}$  is the likelihood value of data induced by a variable 1 when the solution of the variable 2 is fixed.

Solving the inverse problem by the classical least squares methods is translated by finding the maximum likelihood of the joint distribution  $(m, d)$  defined by the distribution of the a prior model and the observed data, respectively. In this case, the solution of inversion, is a model  $\tilde{m}$  with a maximum likelihood corresponding to the center of the distribution of the posterior probability which generalized solution was given by Tarantola (2005) as following :

$$\tilde{m} = \tilde{C}_m (G^t C_d^{-1} d_{obs} + C_m^{-1} m_{prior}) \quad (\text{III.3})$$

Where  $\tilde{m}$  is the posterior model with the maximum likelihood value ;  $\tilde{C}$  is the covariance of posterior model ;  $m_{prior}$  is the prior model ;  $C_m$  is the covariance of the subsurface model ;  $G$  is the linear (or non linear<sup>§</sup>) operator relating the model to the observed data ;  $C_d$  is the data covariance.

Assuming a Gaussian distribution of the *a priori* information whose mean is  $m_{prior}$ , the density probability function of unknown model  $m$  is given by :

$$\rho_M(m) = c_1 \frac{1}{2} (m - m_{prior})^t C_m^{-1} (m - m_{prior}) \quad (\text{III.4})$$

For a model ( $m_i \neq m_{prior}$ ) and satisfies the equation III.4, the solution of inversion must also converge to most probable model  $\tilde{m}$ , in this case the generalized solution can write as following :

---

§. in this case by solving a linearized problem iteratively Tarantola (2005)

$$\tilde{\mathbf{m}} = \tilde{\mathbf{C}}_m (\mathbf{G}^t \mathbf{C}_d^{-1} \mathbf{d}_{obs} + \mathbf{C}_{m_i}^{-1} \mathbf{m}_i) \quad (\text{III.5})$$

By making equality between equations III.3 and III.5, and taking prior model close to the maximum likelihood model ( $\mathbf{m}_{prior} \simeq \tilde{\mathbf{m}}$ ) it is possible to generate several equivalent models  $\mathbf{m}_i$  by the following formula :

$$\mathbf{m}_i \simeq \mathbf{C}_{m_i} \mathbf{C}_m^{-1} \tilde{\mathbf{m}} \quad (\text{III.6})$$

The geostatistical simulation produced many realizations which satisfy the equation III.6 in such way the arithmetic mean of the ( $m_i$ ) models is equal to ( $\tilde{m}$ ) model ( $\frac{\sum m_i}{\sum i} = \tilde{m}$ ).

However, in order to promote the structural similarities it is possible to integrate these correspondences as zones, the technique consists in extracting the structural information by zonation (Hyndman et al., 1994; Paasche et al., 2010), each zone being bounded by physical properties obtained by separates inversion. The model obtained summing gravity and magnetic models zonation can be used as *a priori* information, the result is expressed as structural constraint which can be considered as the average of *a priori* models in a Gaussian random field. The structural similarity can be imposed as geometric constraint by the cross gradient concept Gallardo-Delgado et al. (2003) whose function is given by :

$$\vec{t}(x, y, z) = \overrightarrow{\nabla m_1} \wedge \overrightarrow{\nabla m_2} \quad (\text{III.7})$$

The vectorial product  $t(x, y, z)$  is null when the physical properties changes are parallel, or when one of the two gradients is zero (one of the two medium is homogeneous). Consequently, the sum of the normalized cross gradient norms  $Sum_{t_n}$  over  $N$  cells calculated for two physical properties having the same structural similarity converges to zero and must satisfy the following equation :

$$Sum_{t_n} = \sum_{i=1}^N \|t_n(x, y, z)\| = 0 \quad (\text{III.8})$$

Incorporating the condition imposed by equation III.8 in equation III.2, the posterior probability can be written as follows :

$$\sigma(m) = \rho_M(m_{geo}) L(m_{var_1})_{var_2} (1 - Sum_{t_n}) \quad (\text{III.9})$$

Finally, the resulting simulated model is chosen randomly either by selecting the most likely model or by setting a likelihood threshold from which all greater values are considered. The technique consists in generating parameters distribution (density and magnetization) in a known model geometry. In order to reduce the number of parameters and thereby increase inversion performances, we have implemented the joint inversion between the density and magnetization uses a Collocated Cokriging Simulation with a Markov model Journel (1999b), the algorithm was performed by the following steps :

- find a posterior models with the maximum likelihood for gravity and magnetic data ;
- extracting structural information from the gravity and magnetic models and build the new geometry under constraint ;
- generating point of conditioning similar in spirit to the pilot point method in hydrogeology proposed by de Marsily et al. (1984) ;
- fix a secondary variable and calculate or impose the correlation factor between the density and magnetization in models regions ;
- compute the covariance of the model and the semivariogram for the primary variable ;
- perform a Gaussian Simulation with Collocated Cokriging as dataset (Xu, 1992; Babak et Deutsch, 2009) ;
- compute the posterior probability of simulated model using eqation III.9 ;
- accept or reject the posterior model ;
- go to first step iteratively till the algorithm converge.

### III.3.5 Inversion on synthetic data

#### III.3.5.1 The reference model and prior information

The gravity (Figures III.1.a) and magnetic (Figure III.5.a) data produced by the reference model are considered as observations. The density contrast in the reference model varies between 0.3 and 1.3  $g/cm^3$  (Figure III.3 top) and the magnetic susceptibility between 0 and 0.016  $SI$  (Figure III.4.a). For this example the prior information is chosen by calculating the vertical derivative of the gravity and magnetic vertical components (Figures III.2.a and III.2.b). Knowing that the vertical derivative accentuate the effect of the shallow sources, these values have been re-normalized between 0 and 1, while the vertical derivatives of magnetic field were re-normalized between 0 and 1 for the first 100 meters near the surface and the vertical derivative of gravity field between 100 and 300 meters by vertical projection into the initial geometry. The density contrast of the prior model is shown in the cross-sections (Figure III.3 medium) and the gravity effect of this prior model illustrated in Figures III.1.b.

### III.3.5.2 Find a posterior models with the maximum likelihood

The initial model play a role a prior information inversion that we performed using our own inversion algorithm, similar to [Li et Oldenburg \(1996, 1998\)](#) methods which are based on the least squares principle. The inversion results are shown on Figure [III.3](#) (bottom). This step is necessary to reduce the model space (Foudil-Bey et al., 2012, in press) in order to apply stochastic methods to study accurately the density and the magnetic susceptibility distributions. As we expected, the results of inversion are not identical to the reference model, but there is a similarity in model geometry. Consequently, we can use those density and susceptibility models recovered by inversions as posterior models for stochastic methods' application.

### III.3.5.3 Joint stochastic inversion using Collocated Cokriging simulation

An example of sequential simulation is an application of the conditional simulation of the magnetic susceptibility (primary variable) cokriged with density data used as secondary conditioning variable. In this example the magnetic susceptibility taken as hard data averaging on 1000 Monte Carlo (MTC) realizations and the density (soft data) is the result of the inverted model using least squares inversion. Figure [III.7.a, .b, and .c](#) show the histogram, the variogram model (one selected Gaussian variogram model according azimuth of  $0^0$  and dip of  $45^0$ ) and the density versus magnetic susceptibility cross-plot, respectively. The mean model is an arithmetic averaging of 1000 Mtc realisations (Figure [III.7.g](#)), it has an average magnetic susceptibility of  $0.008 \text{ SI}$  with variance of  $10^{-7} \text{ SI}^2$ . The weak correlation coefficient ( $-0.2$ ) is calculated by linear regression and would leave a substantial residual misfit between the two data sets (Figure [III.7.c](#)). The Figure [III.7.d, .e and .f](#) present 3 posterior models using Collocated Cokriging Simulation with a correlation coefficient of  $-0.2$ , as showing very similar models. The magnetic susceptibility is higher in the South-West part and lower in the superior North part of the models. The correlation coefficient impacts the simulation results, as we can see in the Figure [III.7.h and .i](#). The low posterior models are very different, this is due to the correlation coefficients used at  $0.8$  and  $-0.8$ , respectively. Indeed, as a high correlation coefficient ( $0.8$ ) between the hard and soft data is used, the distribution of the magnetic susceptibility obtained on the simulated models (Figure [III.7.h](#)) is very similar to the distribution of the density on the inverted model (i.e. physical property decreases with depth).

### III.3.6 Inverting real dataset data

#### III.3.6.1 Geological context

The study area is situated in the western part of the Matagami mining camp which is located in the North of the Abitibi Archean greenstone belt of Canada (Figure III.8), where a Volcanogenic Massive Sulfide (VMS) deposits have been identified ([MacGeehan, 1978](#)). The Matagami volcanic complex is formed by two major volcanic phases ([Piche et al., 1993](#)). The rhyolites of the Watson Lake Group (WLG) were produced at the end of the first phase dated at given age while the Watson Lake Group was formed at the beginning of the late volcanic phase dated from  $2\ 724.6 \pm 2.5$  Ma ([Mortensen, 1993](#)). The WLG and upper Wabasse marks the discontinuity between these groups ([Calvert et Li, 1999](#)). The volcanic sequences consist of the WLG that composed mainly felsic rocks as rhyolites and the intermediate to mafic volcanic rocks of the Wabasse Group ([Bosczuk et al., 2011](#)). In this region, the Galinée Anticline is a major regional structure ([Beaudry and Gaucher, 1986; Hammouche et al., 2010; Rhéaume, 2010](#)). Two Plutons (McIvor and Cavelier) in the south-west of this anticline, were interpreted as synvolcanic by [Rhéaume \(2010\)](#) and postvolcanic by [Lacroix et al. \(1990\)](#) intrusions respectively. The composition of the McIvor Pluton varies from tonalitic to dioritic, however the Cavelier Pluton is more felsic with high-magnetic ring. Since the favorable rhyolite horizon of the WLG hosts the VMS-type mineralization, the extension at depth of the WLG is one of goals to study.

#### III.3.6.2 Inversion of gravity data

The gravity data used in present inversion come from a ground survey between October 2006 and March 2007, performed by GEOSIG within IGC-3 research project of Natural Resources of Canada. The data had been collected by 3 gravimeters (LaCoste and Romberg) of Geomatics, compiled and the Bouguer anomalies were calculated by Geological Survey of Canada (DP-2007, MRNF). No terrain correction was applied as the study area consists mostly in a flat surface. The residual Bouguer anomaly is obtained after removing a second order polynomial trend to the Bouguer anomaly. The range of variations the residual Bouguer anomaly is between  $-8mGals$  and  $9mGals$ . As expected the McIvor composed by the felsic rocks has a lower density contrast which decreases to the center of the Pluton to reach a value of about  $-7.5mGals$  (Figure III.9.a).

[Bosczuk et al. \(2011\)](#) measured the density on 150 rock samples in the study area.

They have shown that the mean value of density of basalts and andesites are very similar,  $2.87 \text{ g/cm}^3$  to  $2.88 \text{ g/cm}^3$  respectively. The density of rhyolites is relatively low ( $2.75 \pm 0.036 \text{ g/cm}^3$ ). Based on this density contrast between felsic and mafic rocks, we try to use gravity inversion method for investigating the structure of the first  $4.5 \text{ km}$  of the upper crust.

The first vertical derivative of the Bouguer anomaly (Figure III.9.c) represents the shallow sources geometry of the study area, and the limits of the McIvor Pluton. The gravity data inversion was performed using the classical least squares inversion technique described by Li et Oldenburg (1998), who introduced a depth weight. Figure III.10.a shows the gravity inversion results and the modeled density contrast varies from  $-0.15$  to  $0.15 \text{ g/cm}^3$  (relative to the average of  $2.87 \text{ g/cm}^3$ ), where there is a mass deficiency inside of the McIvor Pluton and sediments, but an excess density in volcanic rocks units. The Figure III.10.c shows the geological model constructed from the inversion result, as we can see, the geometry of the McIvor Pluton is well defined, but it is difficult to distinguish between sedimentary rocks (observed on the surface on the geologic map) and underlying formation which have the same density contrast.

### III.3.6.3 Inversion of magnetic data

All available airborne magnetic data in Québec before 1997 for NTS map sheets 32E and 32L (Matagami area) were compiled by Denis-Jacques Dion and Denis L. Lefebvre (DP – 2006 – 07). The magnetic field is reduced to pole and a regional trend has been removed. The residual magnetic anomaly in the study area varies from  $-250 \text{ nT}$  to  $200 \text{ nT}$  (Figure III.9.b). The Proterozoic diabase dykes along the  $NE - SW$  direction have the most visible positive magnetic signature. The vertical derivative of the magnetic anomaly displays the boundaries of the dyke (Figure III.9.d).

By using the classical least squares inversion technique (Li et Oldenburg, 1996) the magnetic data is inverted in term of a susceptibility distribution in three dimensions. Two bands of high magnetic susceptibility resulted from the inversion correspond to the subvertical diabase dykes. We can see two types of geometries : (1) the first one contains two structures striking to  $NE - SW$  direction with depths varying from  $800 \text{ m}$  to  $4000 \text{ m}$  (the deeper towards  $NE$  direction). This part of the model corresponds to the diabase dykes with an average magnetic susceptibility of  $0.01 \text{ SI}$ ; (2) the second type of geometry is a structure along the  $N - S$  direction of the study area with a positive contrast of  $0.01 \text{ SI}$  that increases in depth to a maximum value of  $0.03 \text{ SI}$ .

The second group is characterized by a single structure with a maximum depth of  $4500 \text{ m}$

with negative magnetic susceptibility contrast (an average of  $-0.01 \text{ SI}$ ) which surrounds all the structures having a positive contrast. Magnetic inversion presents very low magnetic susceptibility contrast at the surface but this contrast decreases in depth to reach a minimum value of  $-0.03 \text{ SI}$

### III.3.6.4 Joint inversion by Collocated Cokriging simulation

The initial structural model (Figure III.11) was built by considering that the models found by separate inversions converge to a model with a maximum likelihood and includes all the interpreted structural information.

#### III.3.6.4.1 Simulation parameters

In order to perform the stochastic joint inversion, the density contrast was considered as the primary variable where the magnetic susceptibility was used as a secondary variable, as we can see in the Figure III.12.c the linear regression has a low coefficient of correlation between density contrast and magnetic susceptibility in the pilot points. This low coefficient of 0.2 could be explained either by the lithology or by the effect of the weight factor used within the mean squares inversion which tends to decrease the sensitivity of the sources in depth.

The variogram model is obtained from the distribution of density contrast in the inverted gravity model. By way of example the Figure III.12.a shows one selected variogram (azimuth of  $45^0$  and dip of  $45^0$ ), the chosen variogram is a spherical model without nugget effect, his range of  $900\text{m}$  and his average sill of  $0.0035 \text{ (g/cm}^3)^2$ . The histogram (Figure III.12.b) shows the density contrast distribution with variation between  $-0.15 \text{ g/cm}^3$  and  $0.15 \text{ g/cm}^3$  and an average of  $0 \text{ g/cm}^3$ .

#### III.3.6.4.2 Simulation results

The Collocated Cokriging simulation is used to manage 1000 realisations. The simulated tests were used with several correlations factors with a maximum value not exceeding 0.5 (Figure III.13.c and d). The Collocated Cokriging is used for embedded secondary variable (magnetic susceptibility) for the prediction of the primary variable (density) for gravity models obtained with different values of correlation coefficient. The value limit of the coefficient is reached when the gravity response of the model differs from the reference data. The co-simulation is carried out on a 3D grid with resolution of  $100 \times 80 \times 30$ ;

then the simulation results is transferred to the tetrahedral mesh in order to compute the likelihood used to accept or reject the outcome of the simulation (Figure III.13.b and d and f). It is possible to manage several random realizations of the structural models whose average is other than the initial model found by zonation.

For an idea of the geometry of sources, Figure III.14 shows a top view of four possible density distributions of 1.6 km depth. As we can see for McIvor Pluton, the density contrast differs from one realization to another but remains the same tendency (the density decreases towards the center of the Pluton), it is also possible to sketch out the possible geometry shape (solid line). However it is more difficult to locate the diabase dyke due to low density contrast. Nevertheless it is possible to observe a slight tendency oriented northeast (dashed line) in the southern part of McIvor Pluton, which is not the case of the result found by the least squares method.

### III.3.7 Discussion

Inverting separately two set of potential field data leads in general to two different geological models. Some structures observed near the surface in the inversion of the magnetic data set may be invisible while inverting the gravimetric data, and vice versa. For instance dykes and diabases are absent in the inverted gravity model, and the McIvor Pluton, whose geometry is well defined by the gravimetric method is not present in the result of the inversion of the magnetic method.

The zonation method in the joint inversion allows imposing geometric constraint. The results of multiple inversion can be considered as *a priori* model whose the results are the average of several possible models. However an underestimation of the number of zones in the initial model should lead to a new zonation that could be recalculated from the model obtained by cokriging for example.

Considering the hypothesis that the smooth solution found by the least squares method is the average of several possible solutions in a Gaussian field, the result of the simulation is influenced by the number of pilot points used, by the type of the variogram (exponential, spherical or Gaussian), and by the simulation grid resolution. The correlation coefficient remains a difficult parameter to choose, in the presence of drilling data, Collocated Cokriging simulation could be used with a coefficient of correlation per zone. In other situations, it can be chosen by the user as an indicator of similarity between the gravity and the magnetism according to his interpretation and knowledge of the studied area. Otherwise, small correlation coefficients indicate independence between rocks density and susceptibility.

### III.3.8 Conclusions

By Using a geostatistical method (Collocated Cokriging Cosimulation), we proposed a joint inversion method based on a Bayesian approach. The performance of individual inversions are imposed as a structural and as *a priori* information for the joint inversion, so that the inversion results are in harmony with the structural geology.

Through the synthetic example, we saw the influence of the a prior information, especially with the choice of the correlation factor between the primary and secondary variables. In the absence of this information, you can find several models with different distributions of physical properties that reproduce the same calculated field.

We applied the method on real data in the Matagami area. The inversions of the two separate gravity and magnetic methods offer two different models of the structural point view. This difference may be explained by the low contrast of physical properties in some areas, and by the method used to resolve the inverse problem that uses a smoothing factor which increases in depth. However, the joint inversion amongst to take into consideration all the structural information, and to simulate several possible realizations of density contrast, the smooth distributions by the CoKriging method or disrupting property by Collocated cosimulation Simulation technique.

# References

- Afnimar, K., Koketsu, and K. Nakagawa, 2002, Joint inversion of refraction and gravity data for the three-dimensional topography of a sediment-basement interface : Geophysical Journal International, **151**, 243–254.
- Babak, O., and C. Deutsch, 2009, Collocated Cokriging Based on Merged Secondary Attributes : Mathematical Geosciences, **41**, no. 8, 921–926.
- Barbosa, V. C. F., and J. B. C. Silva, 1994, Generalized compact gravity inversion : Geophysics, **59**, 57–68.
- Barbosa, V. C. F., J. B. C. Silva, and W. E. Medeiros, 2002, Practical applications of uniqueness theorems in gravimetry : Part II—Pragmatic incorporation of concrete geologic information : Geophysics, **67**, 795–800.
- Beaudry, C., and E. Gaucher, 1986, Cartographie géologique dans la région de matagami : Technical report, Ministère de l’Énergie et des Ressources du Québec.
- Bellefleur, G., d. K. E. G. J., and M. Allard, 2007, A new look at the geological framework of the central Noranda camp, Québec from industry high-resolution seismic profiles : Geological Survey of Canada Current Research, **C5**, 9p.
- Bertete-Aguirre, H., E. Cherkayev, and M. Oristaglio, 2002, Non-smooth gravity problem with total variation penalization functional : Geophysical Journal International, **149**, 499–507.
- Bhattacharyya, B. K., 1964, Magnetic anomalies due to prism-shaped bodies with arbitrary polarization : Geophysical Prospecting, **24**, 633–649.
- Blakely, R. J., 1995, Potential Theory in Gravity and Magnetic Applications : Cambridge University Press.
- Bosch, M., 1999, Lithologic tomography : From plural geophysical data to lithology estimation : Journal of Geophysical Research B : Solid Earth, **104**, 749–766.
- Bosch, M., L. Cara, J. Rodrigues, A. Navarro, and M. Díaz, 2007, A Monte Carlo approach to the joint estimation of reservoir and elastic parameters from seismic amplitudes : Geophysics, **72**, O29–O39.

- Bosch, M., and J. McGaughey, 2001, Joint inversion of gravity and magnetic data under lithologic constraints : The Leading Edge, **20**, 877–881.
- Bosch, M., R. Meza, R. Jiménez, and A. Höning, 2006, Joint gravity and magnetic inversion in 3D using Monte Carlo methods : Geophysics, **71**, G153–G156.
- Boszczuk, P., L. Z. Cheng, H. Hammouche, P. Roy, S. Lacroix, and A. Cheillettz, 2011, A 3D gravity data interpretation of the Matagami mining camp, Abitibi Subprovince, Superior Province, Québec, Canada. Application to VMS deposits exploration : Journal of Applied Geophysics.
- Boulanger, O., and M. Chouteau, 2001, Constraints in 3D gravity inversion : Geophysical Prospecting, **49**, 265–280.
- Calvert, A. J., and Y. Li, 1999, Seismic reflection imaging over a massive sulfide deposit at the Matagami mining camp, Québec : Geophysics, **64**, 24–32.
- Chasserau, P., and M. Chouteau, 2003, 3D gravity inversion using a model of parameter covariance : Journal of Applied Geophysics, **52**, 59 – 74.
- Chilès, J.-P., and P. Delfiner, 1999, Geostatistics, Modeling Spatial Uncertainty. : Wiley Series on Probability and Statistics.
- Colombo, D., and M. D. Stefano, 2007, Geophysical modeling via simultaneous joint inversion of seismic, gravity, and electromagnetic data : Application to prestack depth imaging : The Leading Edge, **26**, 326–331.
- de Marsily, G. H., C. Lavadan, M. Boucher, and G. Fasanino, 1984, Interpretation of interference tests in a well field using geostatistical techniques to fit the permeability distribution in a reservoir model : Geostatistics for natural resources characterization, **Part 2**.
- Dell'Aversana, P., 2001, Integration of seismic, MT and gravity data in a thrust belt interpretation : First Break, **19**, 335–341.
- Ezzedine, S., Y. Rubin, and J. Chen, 1999, Bayesian Method for hydrogeological site characterization using borehole and geophysical survey data : Theory and application to the Lawrence Livermore National Laboratory Superfund Site : Water resources research, **35**, 2671–2683.
- Fregoso, E., and L. A. Gallardo, 2009, Cross-gradients joint 3D inversion with applications to gravity and magnetic data : Geophysics, **74**, L31–L42.
- Gallardo, L. A., 2004, Joint Two-Dimensional Inversion of Geoelectromagnetic and Seismic Refraction Data With Cross-Gradients Constraint : PhD thesis, Lancaster University.
- Gallardo, L. A., and M. A. Mejú, 2004, Joint two-dimensional DC resistivity and seismic travel time inversion with cross-gradients constraints : Journal of Geophysical Research

- B : Solid Earth, **109**, B03311 1–11.
- , 2007, Joint two-dimensional cross-gradient imaging of magnetotelluric and seismic traveltimes data for structural and lithological classification : Geophysical Journal International, **169**, 1261–1272.
- Gallardo-Delgado, L. A., M. A. Pérez-Flores, and E. G.-T. no, 2003, A versatile algorithm for joint 3D inversion of gravity and magnetic data : Geophysics, **68**, 949–959.
- Gloaguen, E., D. Marcotte, M. Chouteau, and H. Perroud, 2005, Borehole radar velocity inversion using cokriging and cosimulation : Journal of Applied Geophysics, **57**, 242 – 259.
- Gloaguen, E., D. Marcotte, B. Giroux, C. Dubreuil-Boisclair, M. Chouteau, and M. Aubertin, 2007, Stochastic borehole radar velocity and attenuation tomographies using cokriging and cosimulation : Journal of Applied Geophysics, **62**, 141 – 157.
- Guillen, A., and V. Menichetti, 1984, Gravity and magnetic inversion with minimization of a specific functional : Geophysics, **49**, 1354–1360.
- Günther, T., and C. Rücker, 2006, A general approach for introducing information into inversion and examples from dc resistivity inversion : European Association of Geoscientists & Engineers. Near Surface Geophysics, **12th European Meeting of Environmental and Engineering Geophysics, Helsinki (Finland)**.
- Haber, E., and D. Oldenburg, 1997, Joint inversion : a structural approach : Inverse Problems, **13**, 63.
- Häggström, O., 2002, Finite Markov Chains and algorithmic applications : Cambridge University Press.
- Hammouche, H., P. Boszczuk, and P. Roy, 2010, Géologie des feuillets île bancroft (32f12-200-0202) et lac macivor (32f13-200-0101), région de matagami : Technical report, Ministère des Ressources naturelles et de la Faune du Québec.
- Hansen, T. M., A. G. Journel, A. Tarantola, and K. Mosegaard, 2006, Linear inverse Gaussian theory and geostatistics : Geophysics, **71**, R101–R111.
- Hansen, T. M., and K. Mosegaard, 2008, VISIM : Sequential simulation for linear inverse problems : Computers & Geosciences, **34**, 53 – 76.
- Hu, W., A. Abubakar, and T. M. Habashy, 2009, Joint electromagnetic and seismic inversion using structural constraints : Geophysics, **74**, R99–R109.
- Hyndman, D. W., J. M. Harris, and S. M. Gorelick, 1994, Coupled seismic and tracer test inversion for aquifer property characterization : Water resources research, **30**, 1965–1977.
- Jegen, M. D., R. W. Hobbs, P. Tarits, and A. Chave, 2009, Joint inversion of marine magnetotelluric and gravity data incorporating seismic constraintspreliminary results

- of sub-basalt imaging off the Faroe Shelf : Earth and Planetary Science Letters, **282**, 47–55.
- Johnson, W. W., 1969, A least-squares method of interpreting magnetic anomalies caused by two-dimensional structures : Geophysics, **34**, 65–74.
- Journel, A., 1999a, Conditioning Geostatistical Operations to Nonlinear Volume Averages : Mathematical Geology, **31**, no. 8, 931–953.
- , 1999b, Markov Models for Cross-Covariances : Mathematical Geology, **31**, no. 8, 955–964.
- Journel, A. G., and C. J. Huijbregts, 1978, Mining geostatistics : Academic Press.
- K. Mosegaard, and M. Sambridge, 2002, Monte Carlo analysis of inverse problems : Inverse Problems, **18**, R29–R54.
- Lacroix, S., A. Simard, P. Pilote, and L. M. Dubé, 1990, Regional geologic elements and mineral resources of the Harricana Turgeon Belt, Abitibi of NW Québec, The northwestern Quebec polymetallic belt ; a summary of 60 years of mining exploration. Poceeding of the Rouyn-Noranda 1990 symposium. Canadian Institute of Mining and Metallurgy. ed. : Rive, M., Verpaelst, P., Gagnon, Y., Lulin, J.M., Riverin, G., Simard, A. , **43**.
- Lam, N. S., 1983, Spatial interpolation methods review : The American Cartographer, **10**, 129–149.
- Last, B. J., and K. Kubik, 1983, Compact gravity inversion : Geophysics, **48**, 713–721.
- Li, Y., and D. W. Oldenburg, 1996, 3-D inversion of magnetic data : Geophysics, **61**, 394–408.
- , 1998, 3-D inversion of gravity data : Geophysics, **63**, 109–119.
- , 2010, Rapid construction of equivalent sources using wavelets : Geophysics, **75**, L51–L59.
- Linde, N., A. Binley, A. Tryggvason, L. B. Pedersen, and A. Revil, 2006, Improved hydrogeophysical characterization using joint inversion of cross-hole electrical resistance and ground-penetrating radar travelttime data : Water resources research, **42**, W12404.
- Linde, N., A. Tryggvason, J. E. Peterson, and S. S. Hubbard, 2008, Joint inversion of crosshole radar and seismic traveltimes acquired at the South Oyster Bacterial Transport site : Geophysics, **73**, G29–G37.
- Looms, M. C., T. M. Hansen, K. S. Cordua, L. Nielsen, K. H. Jensen, and A. Binley, 2010, Geostatistical inference using crosshole ground-penetrating radar : Geophysics, **75**, J29–J41.

- MacGeehan, P. J., 1978, The geochemistry of altered volcanic rocks at Matagami, Québec : a geothermal model for massive sulphide genesis : Canadian Journal of Earth Sciences, **15**, 551–570.
- Mallet, J. L., 2002, Geomodeling : Inc. Oxford University Press.
- Manchuk, J. G., 2010, Geostatistical Modeling of Unstructured grids for flow Simulation : PhD thesis, University of Alberta.
- Metropolis, N., A. W. Rosenbluth, M. N. Rosenbluth, A. H. Teller, and E. Teller, 1953, Equation of state calculations by fast computing machines : Journal of Chemical Physics, **21**, 1087–1092.
- Metropolis, N., and S. Ulam, 1949, The Monte Carlo method : Journal of the American Statistical Association, **44**, 335–341.
- Mortensen, J. K., 1993, U-Pb geochronology of the eastern Abitibi Subprovince. Part 1 : Chibougamau-Matagami-Joutel region : Canadian Journal of Earth Sciences, **30**, 11–28.
- Mosegaard, K., and A. Tarantola, 1995, Monte Carlo sampling of solutions to inverse problems : Journal of Geophysical Research, **100**, 12431–12447.
- Musil, M., H. R. Maurer, and A. G. Green, 2003, Discrete tomography and joint inversion for loosely connected or unconnected physical properties : application to crosshole seismic and georadar data sets : Geophysical Journal International, **153**, 389–402.
- Paasche, H., J. Tronicke, and P. Dietrich, 2010, Automated integration of partially collocated models : Subsurface zonation using a modified fuzzy c-means cluster analysis algorithm : Geophysics, **75**, P11–P22.
- Paradis, S., J. Ludden, and L. Gélinas, 1988, Evidence for contrasting compositional spectra in comagmatic intrusive and extrusive rocks of the late Archean Blake River Group, Abitibi, Québec : Canadian Journal of Earth Sciences, **25**, 134–144.
- Piche, M., J. Guha, and R. Daigneault, 1993, Stratigraphic and structural aspects of the volcanic rocks of the Matagami mining camp, Québec ; implications for the Norita ore deposit : Economic Geology, **88**, 1542–1558.
- Pilkington, M., 1997a, 3-D magnetic imaging using conjugate gradients : Geophysics, **62**, 1132–1142.
- , 1997b, 3-D magnetic imaging using conjugate gradients : Geophysics, **62**, 1132–1142.
- , 2006, Joint inversion of gravity and magnetic data for two-layer models : Geophysics, **71**, L35–L42.
- Plouff, D., 1976, Gravity and magnetic fields of polygonal prisms and application to magnetic terrain corrections : Geophysics, **41**, 727–741.

- Portniaguine, O., and M. S. Zhdanov, 1999, Focusing geophysical inversion images : Geophysics, **64**, 874–887.
- , 2002, 3-D magnetic inversion with data compression and image focusing : Geophysics, **67**, 1532–1541.
- Remy, N., A. Shtuka, B. Levy, and J. Caers, 2002, GSTL : the geostatistical template library in C++ : Computers & Geosciences, **28**, 971 – 979.
- Rhéaume, P., 2010, Géologie du feuillet lac Watson (32f12-200-0201), et des portions 611 attenantes des feuillets rivière Subercase (32e09-200-0202), lac de la Gauchetière (32e16- 612 200-0102) et lac McIvor (32f13-200-0101), région de Matagami : Technical report, Ministère des Ressources naturelles et de la Faune du Québec, GM 64950 (in French).
- Sambridge, M., and K. Mosegaard, 2002, Monte Carlo methods in geophysical inverse problems : Reviews of Geophysics, **40**, 1–29.
- Saunders, J. H., J. V. Herwanger, C. C. Pain, M. H. Worthington, and C. R. E. De Oliveira, 2005, Constrained resistivity inversion using seismic data : Geophysical Journal International, **160**, 785–796.
- Seneta, E., 1982, Non-Negative Matrices and Markov Chains, 2nd ed. : Berlin : Springer.
- Shamsipour, P., M. Chouteau, P. Keating, and D. Marcotte, 2010a, Three-dimensional stochastic inversion of gravity data : application to gravity data from the Matagami region, Québec : Geological Survey of Canada, **Current Research 2010-12**, 10 p.
- Shamsipour, P., D. Marcotte, M. Chouteau, and P. Keating, 2010b, 3D stochastic inversion of gravity data using cokriging and cosimulation : Geophysics, **75**, I1–I10.
- Silva, J. B. C., and V. C. F. Barbosa, 2006, Interactive gravity inversion : Geophysics, **71**, J1–J9.
- Silva, J. B. C., W. E. Medeiros, and V. C. F. Barbosa, 2002, Practical applications of uniqueness theorems in gravimetry : Part I—Constructing sound interpretation methods : Geophysics, **67**, 788–794.
- Stefano, M. D., F. G. Andreasi, S. Re, M. Virgilio, and F. F. Snyder, 2011, Multiple-domain, simultaneous joint inversion of geophysical data with application to subsalt imaging : Geophysics, **76**, R69–R80.
- Tarantola, A., 2005, Inverse Problem Theory and Methods for Model Parameter Estimation : Society for Industrial and Spplied Mathematics.
- , 2006, Popper, Bayes and the inverse problem : Nature Physics, **2**, 492–494.
- Tarantola, A., and B. Valette, 1982, Generalized Nonlinear Inverse Problems Solved Using the Least Squares Criterion : Reviews of Geophysics and Space Physics, **20**, 219–232.

- Tondi, R., R. De Franco, and R. Barzaghi, 2000, Sequential integrated inversion of refraction and wide-angle reflection traveltimes and gravity data for two-dimensional velocity structures : *Geophysical Journal International*, **141**, 679–698.
- Tryggvason, A., and N. Linde, 2006, Local earthquake (LE) tomography with joint inversion for P- and S-wave velocities using structural constraints : *Geophysical Research Letters*, **33**, L07303.
- Xu, Wenlong, T. T. S. R. J. A., 1992, Integrating seismic data in reservoir modeling : The collocated cokriging alternative : *Proceedings - SPE Annual Technical Conference and Exhibition, Omega*, 833–842.
- Zeyen, H., and J. Pous, 1993, 3-D Joint Inversion of Magnetic and Gravimetric Data With A Priori Information : *Geophysical Journal International*, **112**, 244–256.

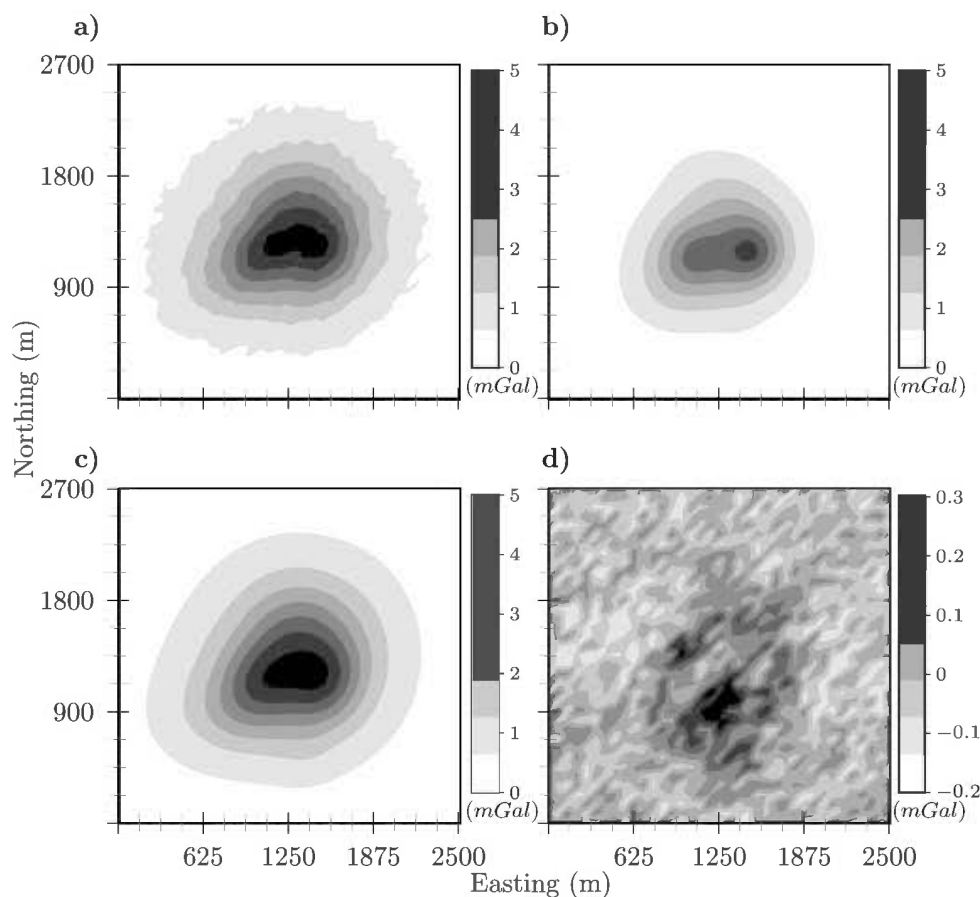


FIGURE III.1: The vertical component of gravity field produced by the (a) reference model contaminated with random noise, (b) prior model , (c) inverted model and (d) the difference between the gravimetric inverted and reference field .

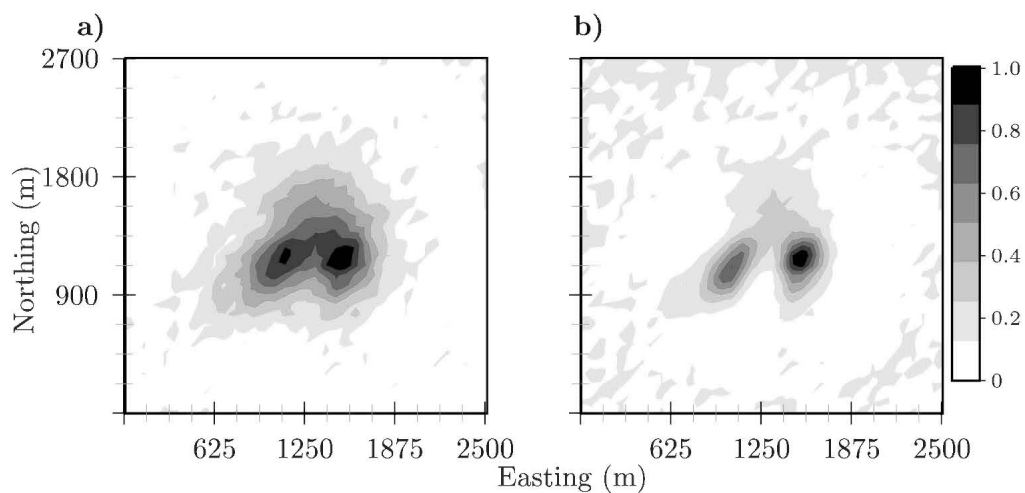


FIGURE III.2: The first vertical derivative of the vertical component of the (a) gravity and (b) magnetic fields produced by the reference model.

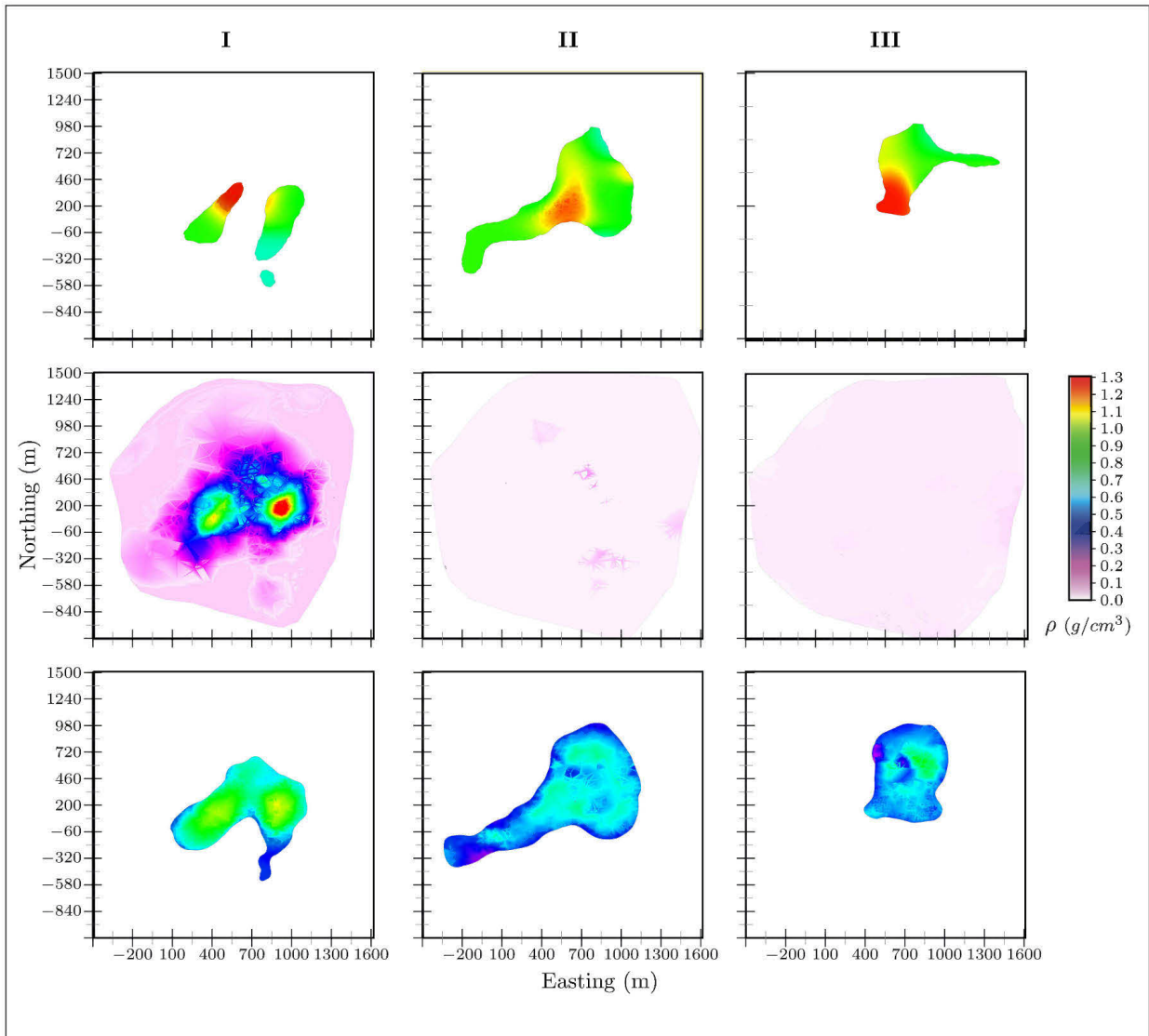


FIGURE III.3: Comparison between the reference model (in top), prior model (in medium) and inversion result (in bottom) along horizontal cross sections at depth of column (I) 150 m (II) 350 and (III) 650 m.

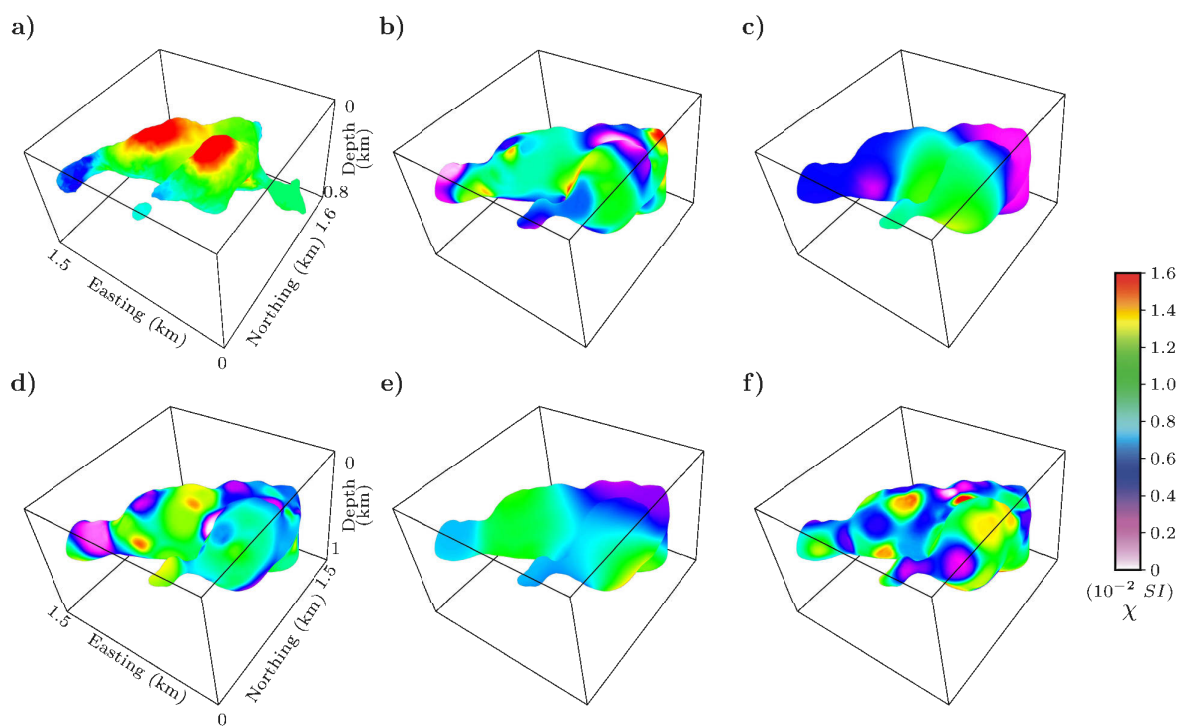


FIGURE III.4: Magnetic susceptibility distributions in the a) Reference model and b), c), d), e) and f) accepted realizations.

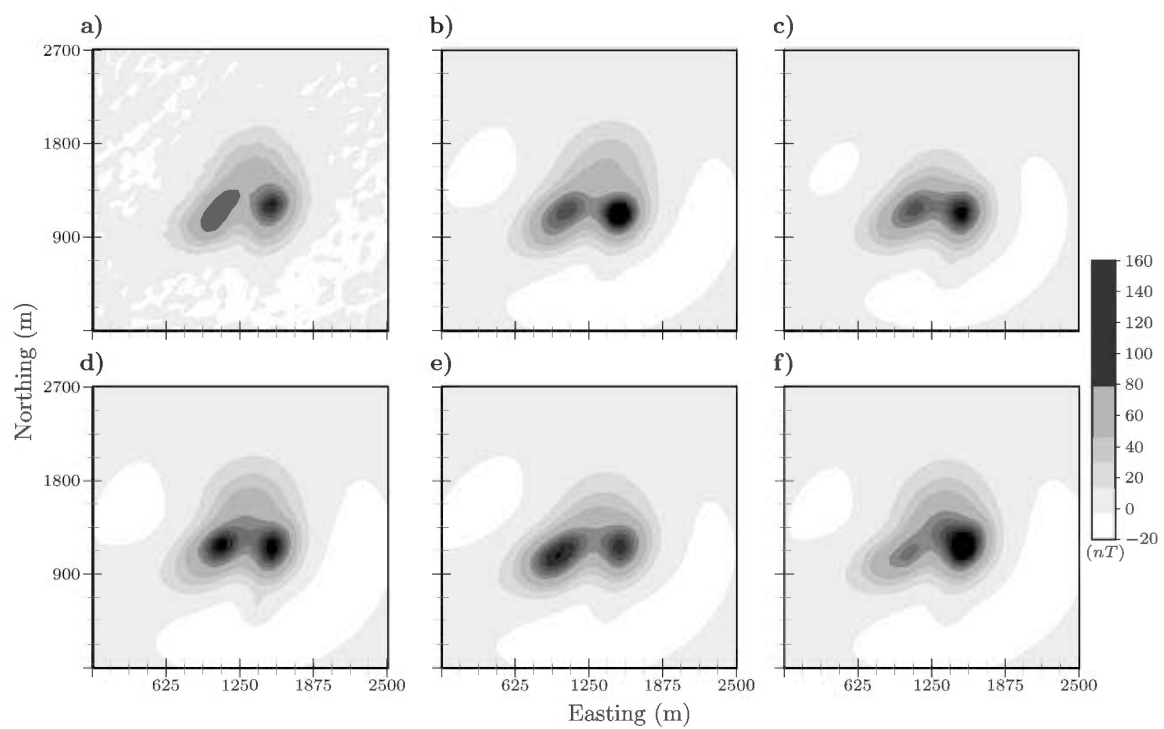


FIGURE III.5: Vertical component of the magnetic field for a) reference model and b), c), d), e) and f) accepted models (Figure III.4)

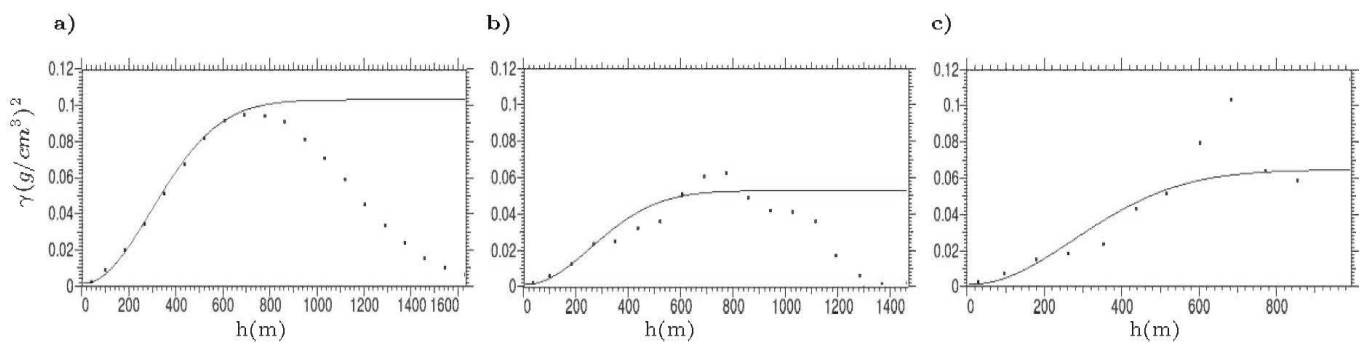


FIGURE III.6: Selected variograms (solid lines) of pilot points densities, Gaussian models are used for the variograms. a) Azimuth of  $0^\circ$  dip of  $0^\circ$ , b) azimuth of  $90^\circ$  dip of  $45^\circ$  and c) azimuth of  $45^\circ$  dip of  $85^\circ$ .

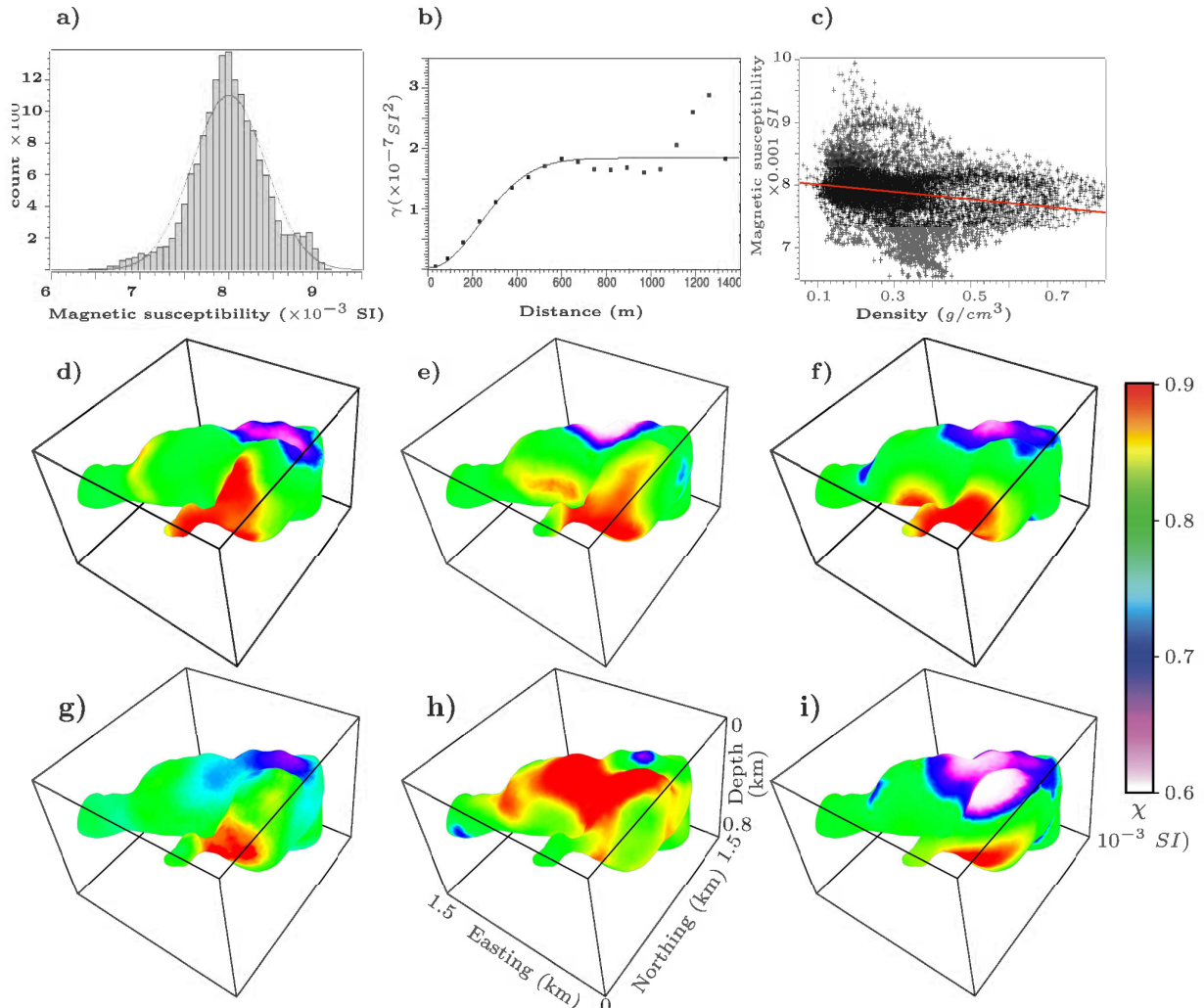


FIGURE III.7: Simulated magnetic susceptibility distribution in the posterior model. a), Histogram of distribution b) semivariogram model , c) magnetic susceptibility-density cross plot, d), e), and f) collocated cokriged simulations with correlation coefficient of  $-0.2$ , g) mean of mtc realizations, and collocated cokriged simulations with correlation coefficient of h)  $0.8$  and i)  $-0.8$  . (likelihood values of models  $> 0.7$ ).

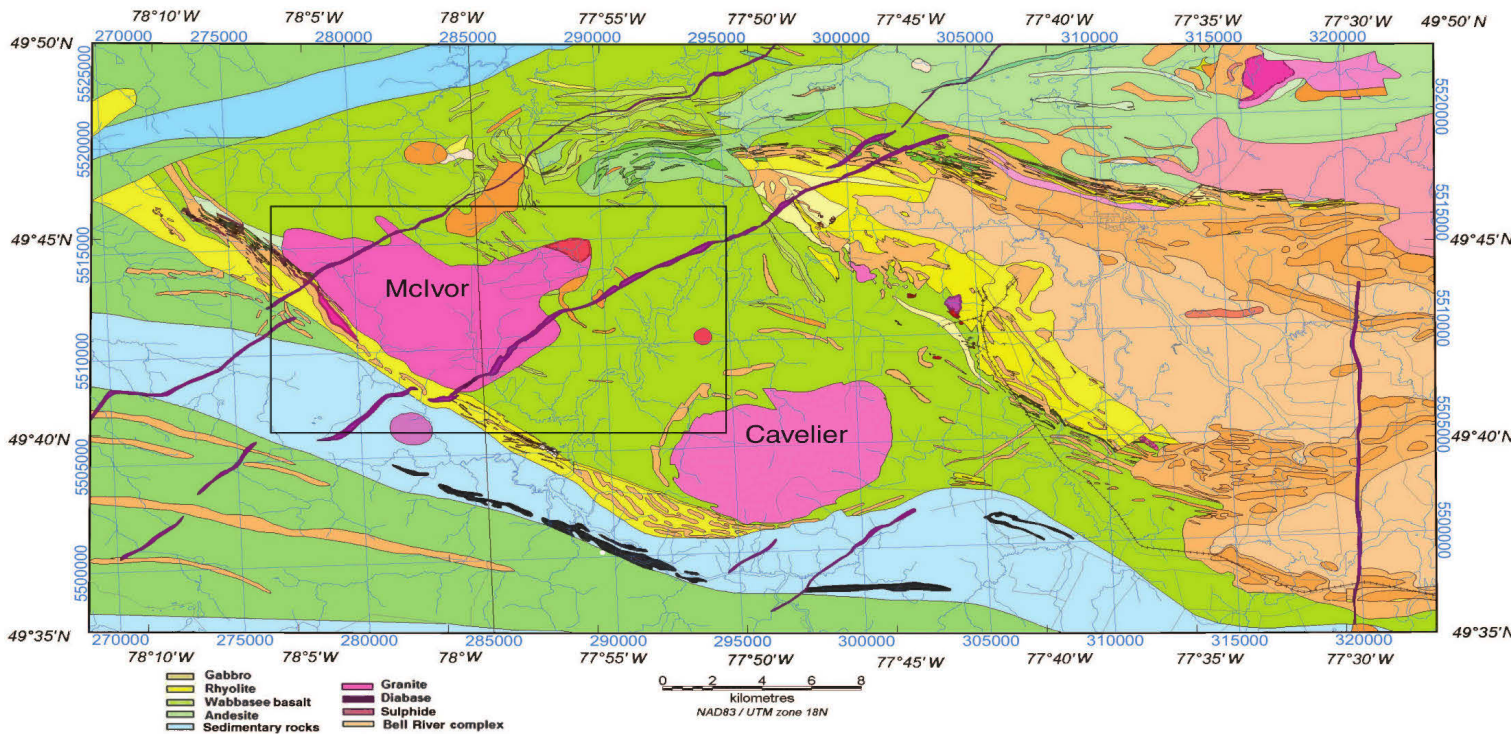


FIGURE III.8: Geologic setting of matagami from ([Shamsipour et al., 2010a](#)). The study area define with the solid line

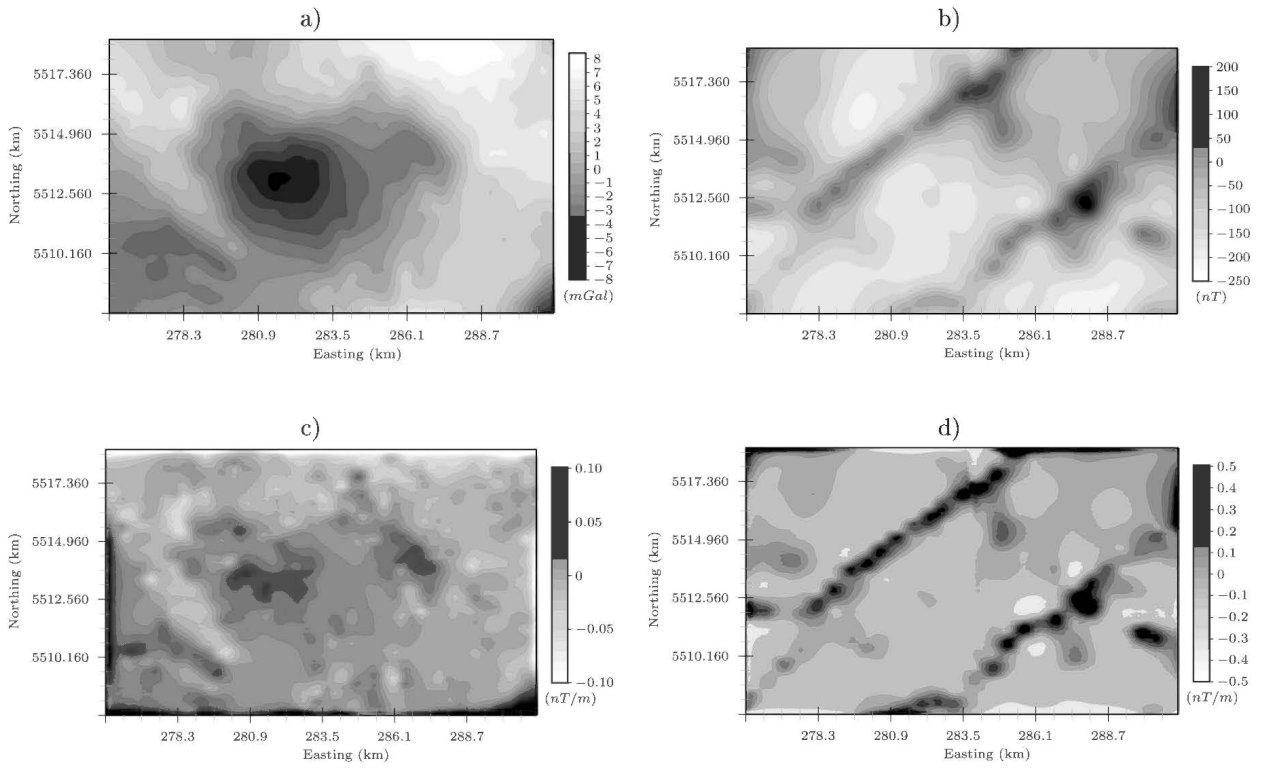


FIGURE III.9: Potential field data. a) residual gravity anomaly, b) residual magnetic anomaly and vertical derivative of c) gravi and d) magnetic anomalies.

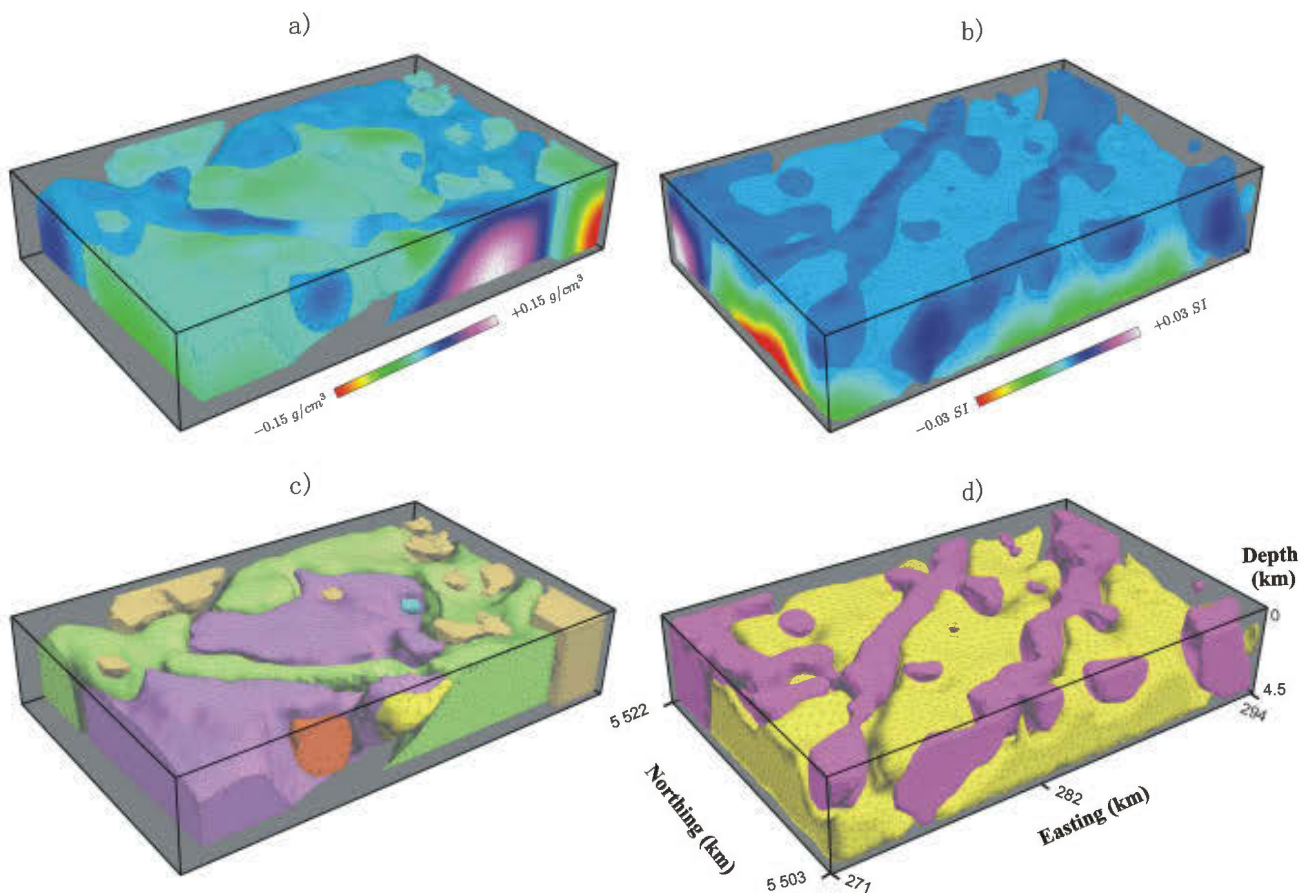


FIGURE III.10: Three-dimensional results using least square separate inversion. a) Density distribution , b) magnetic susceptibility distribution, and structural model given by gravity and structural model using c) density , d) magnetic susceptibility distributions.

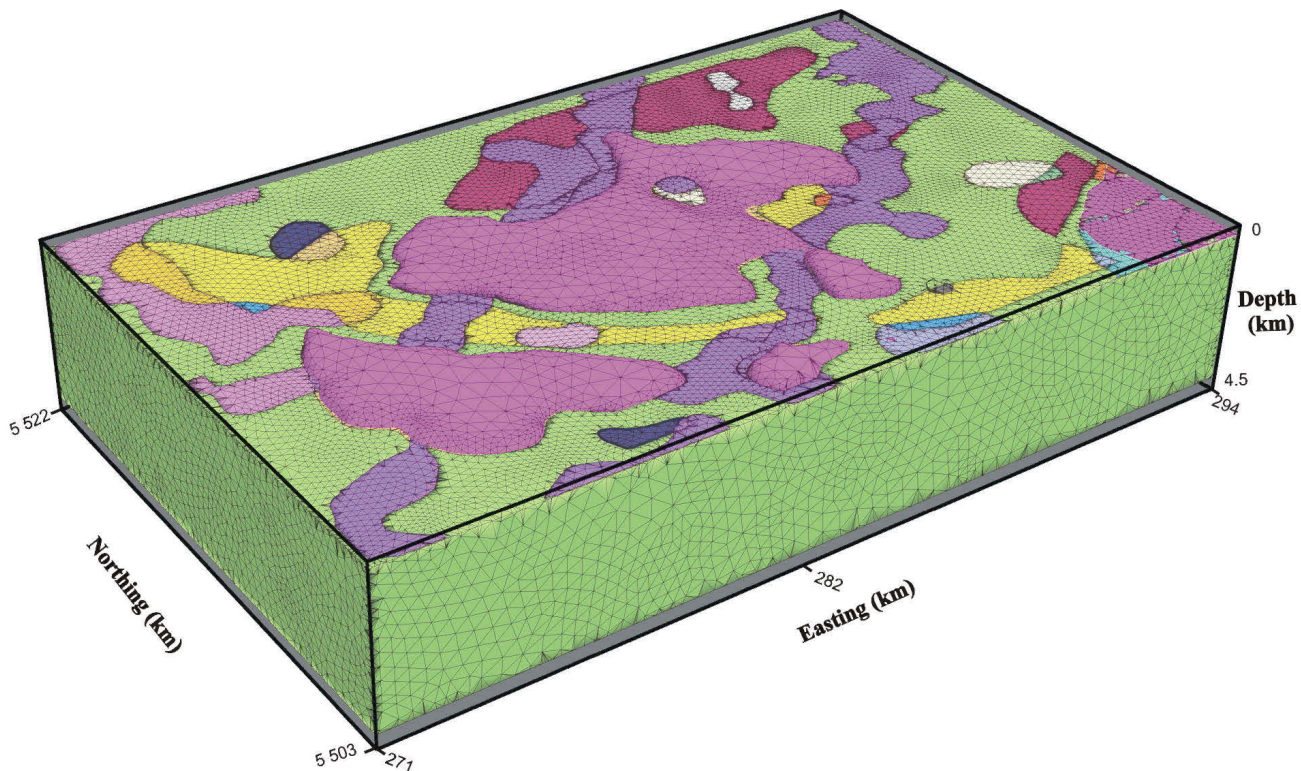


FIGURE III.11: Result of zonation between the magnetic and gravimetric structural models

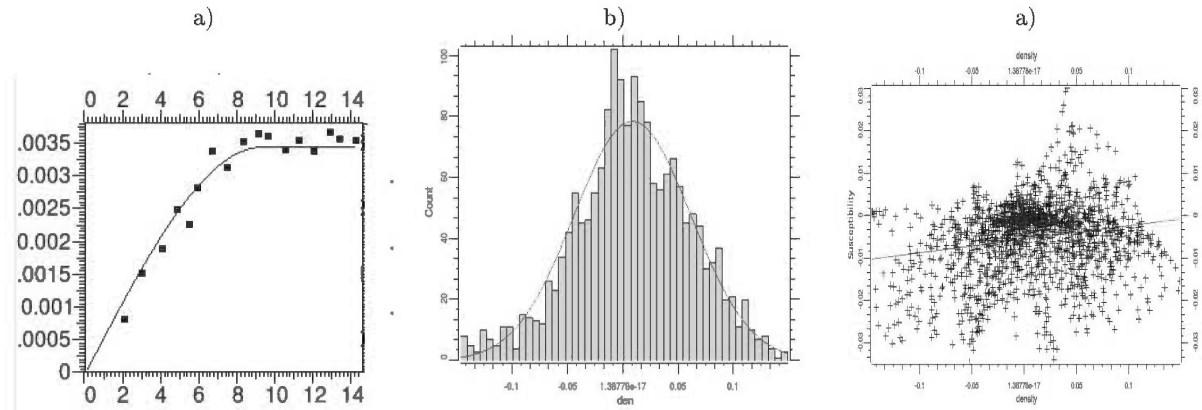


FIGURE III.12: Selected Cosimulation parameters. a) histogram of density contrast , b) selected variogram (Azimuth of  $45^0$  dip of  $45^0$ ) c) density and magnetic cross-correlation.

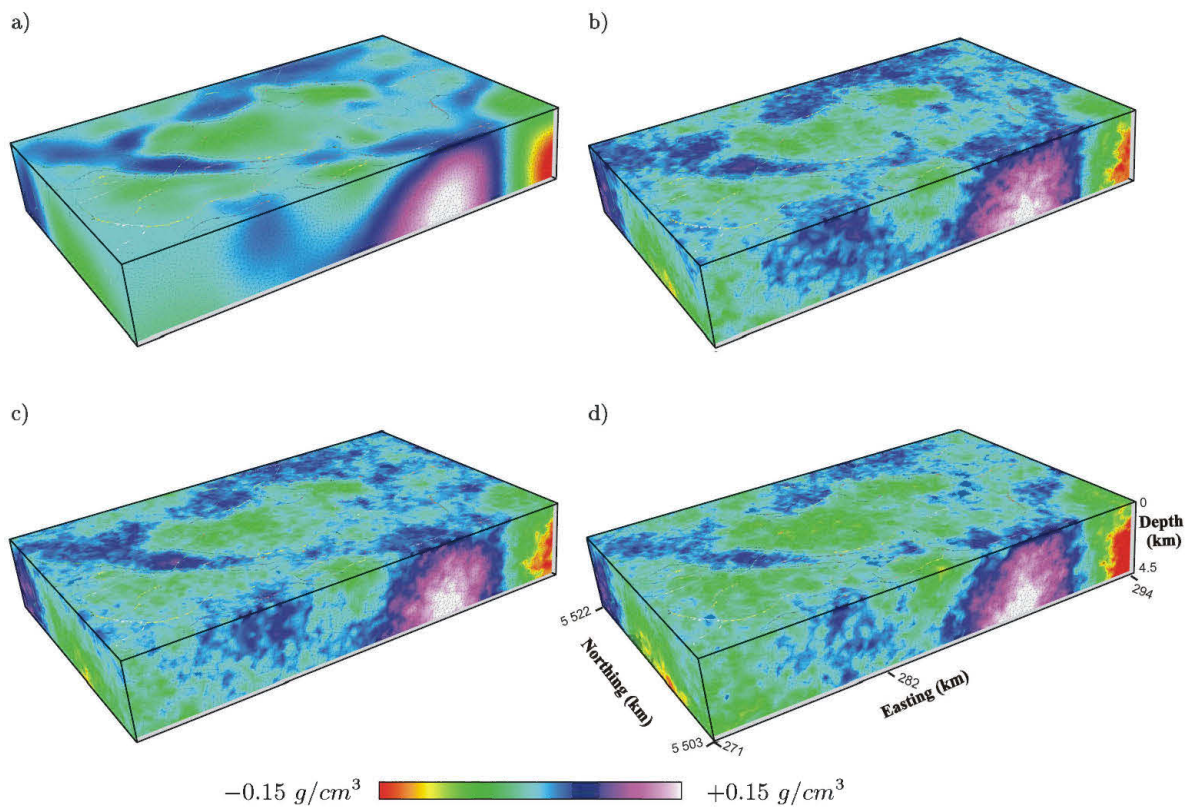


FIGURE III.13: Inversion result using a) Least squares , and b) c) d) Collocated Cokriging Simulation.

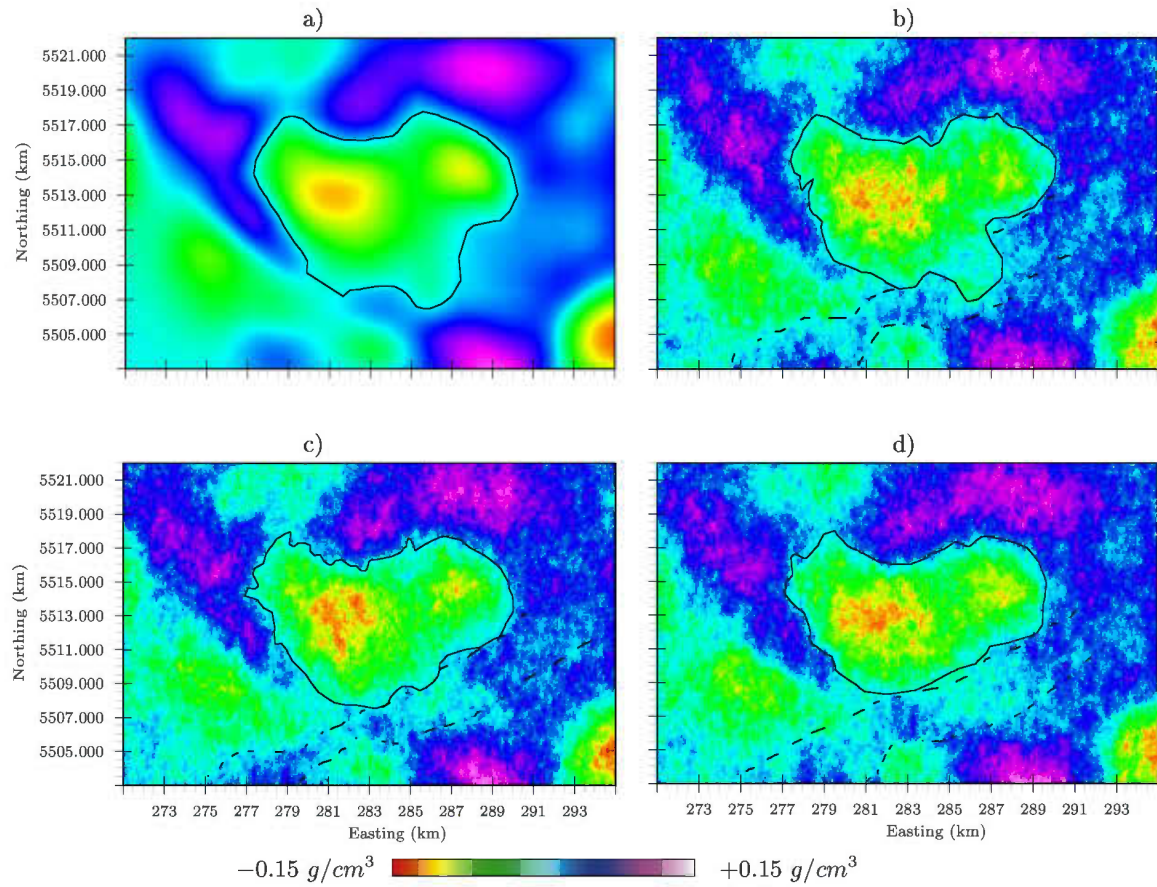


FIGURE III.14: Top view of density distribution in the inversion results. (a) Least squares (b) , (c) and (d) Collocated Cokriging Simulation

### III.4 Bilan

En utilisant une méthode géostatistique (Collocated Cosimulation Simulation), nous avons proposé une méthode d'inversion conjointe basée sur une formulation bayésienne. Les résultats obtenus par inversions individuelles sont exprimés sous forme de contraintes structurales et sont considérés comme une information *a priori* pour l'inversion conjointe afin que les résultats d'inversions soient en accord avec la géologie structurale.

A travers l'exemple synthétique, nous avons pu constater l'influence de l'information *a priori*, notamment avec le choix du coefficient de corrélation entre la variable primaire et secondaire. En l'absence de cette information, il est possible de trouver plusieurs modèles avec des distributions de propriétés physiques différentes qui reproduisent les données observées.

A titre d'exemple, nous avons appliqué la méthode sur des données réelles prélevées de la région de Matagami. Les inversions séparées des deux méthodes, gravimétrie et magnétique, proposent deux modèles différents du point de vue structural. Cette différence peut s'expliquer par le faible contraste de propriétés physiques dans certaines zones et par la méthode de résolution du problème inverse qui utilise un facteur de lissage croissant avec la profondeur. Néanmoins, l'inversion conjointe a permis de prendre en considération toutes les informations structurales et de simuler plusieurs répartitions possibles du contraste de densité : des distributions, soit lisses par la méthode du Co-Kriging, soit perturbées avec la technique de Co-simulation.



**CHAPITRE IV**  
**RESEAUX DE NEURONES APPLIQUÉS POUR LA QUANTIFICATION DES**  
**INCERTITUDES**

**IV.1 Neural Network Stochastic Simulation Applied for Quantifying Uncertainties**

Nacim Foudil-Bey<sup>\*†</sup>, Jean-Jacques Royer\*, Li Zhen Cheng<sup>†</sup>, Fouad Erchiqui<sup>†</sup>, and Jean-Claude Mareschal<sup>‡</sup>

**IV.1.1 Abstract**

Generally the geostatistical simulation methods are used to generate several realizations of physical properties in the sub-surface, these methods are based on the variogram analysis and limited to measures correlation between variables at two locations only. In this paper, we propose a simulation of properties based on supervised Neural network training at the existing drilling data set. The major advantage is that this method does not require a preliminary geostatistical study and takes into account several points. As a result, the geological information and the diverse geophysical data can be combined easily. To do this, we used a neural network with multi-layer perceptron architecture like feed-forward, then we used the back-propagation algorithm with conjugate gradient technique to minimize the error of the network output. The learning process can create links between different variables, this relationship can be used for interpolation of the properties on the one hand, or to generate several possible distribution of physical properties on the other hand, changing at each time and a random value of the input neurons, which was kept constant until the period of learning. This method was tested on real data to simulate multiple realizations of the density and the magnetic susceptibility in three-dimensions at the mining camp of Val d'Or, Québec (Canada).

**keyword :** Artificial Neural Networks, Stochastic, Simulation, Geophysics, Density, Magnetic susceptibility.

#### IV.1.2 Introduction

During the last 20 years, predictions based on statistical learning processes had been applied with great success in a wide range of applications, including character recognition, shape classification or partitioning, filtering, predictions, etc. One of the most popular methods is artificial neural networks which mimic the neurons behavior of human brain. This work aims at applying these methods to quantify uncertainties of results obtained during geophysical inversion.

Geophysical data inversion is a key step in interpreting geological underground structures. Inversion methods are generally classified in two groups : (i) the deterministic approaches, and (ii) the stochastic ones. Deterministic inversions based on global minimum search offer a unique solution called the *best model* or the *most likely model* (Tarantola, 2006). They are based on the iterative least squares minimization of some objective function (Tarantola et Valette, 1982) often improved by introducing a weighting function (Menke, 1984). Another class of methods suggest solving the inverse problem by applying a neural network algorithm to faster the search of the optimum. They have been applied in geophysics for locating ground targets from electromagnetic field data (Poulton et al., 1992), estimating basement resistivity distribution (Gad et Ushijima, 2001; Calderón-Macias et al., 2000; Neyamadpour et al., 2009), seismic wavelength inversion (Röth et Tarantola, 1994). At the opposite of these last methods, stochastic methods such as Monte Carlo (Metropolis et Ulam, 1949), genetic algorithms (Holland, 1975), and simulated annealing (Kirkpatrick et al., 1983) offer the possibility of generating several models that can fit to the observations and therefore to estimate the *a posteriori* probability model.

Geostatistical simulations such as *sequential Gaussian simulation* (SGS) (Deutsch et Journel, 1998) or *sequential indicator simulations* (SIS) (Journel et Isaaks, 1984), are based on a variogram analysis. They simulate several equiprobable realizations of a random variable. The integration of geostatistical simulation methods during the inversion process increases the performance of the stochastic inversion as it accounts for the rock spatial variability (Hansen et al., 2006; Looms et al., 2010). Furthermore, co-simulations simulate several possible realizations of a random variable accounting for secondary parameters, and generally give better results than the simulation of a single variate. Co-simulations integrate more information in the process of the inversion (Gloaguen et

al., 2005; Shamsipour et al., 2010b). In theory, it would be more interesting to integrate several geophysical properties to account for the geological complexity. However in practice, it is very difficult to take into account these secondary variables. In general, it is impossible to find deterministic relationships which combine all the physical properties, and requires the use of empirical relationships to link a property to another, or physical properties to the geology or to the lithology. Multiple point statistics integrating both the spatial variability and the multivariate aspects allow simulating variables accounting for several secondary parameters Strebelle (2002).

As suggested by Caers et Journel (1998), neural networks can be an alternative for simulating several variables. The advantages are : (i) to define statistical relationships either between two points of the spaces, or/ and between several points of the space variables, (ii) variables can be of various nature and (iii) to integrate non-linearity relationships between variables. Caers et Journel (1998) and Caers (2001) suggest using a 2D smooth gridded shape recognition method at the learning step, and then, a multi-grid approach (Tran, 1994; Strebelle, 2002) is used to simulate several realizations at the prediction step. In this work, we propose a different approach based on pattern recognition neural networks (Caers, 2001; Wong et Shibli, 2001) for simulating the sub-surface physical properties. In this method, the analysis of physical properties is conditioned by an existing drilling data set and the results of independent inversions. Their distributions are used for a supervised training of the neural network, then the simulation is processed by injecting the distributions available at the prediction step.

#### IV.1.3 Neural networks

The neural network is a linear combination of non-linear functions that tries to solve complex problems. Conceptually, this approach mimic the human brain activity. Their architectures are interconnected networks similarly to the synapse connections. They request a learning phase before being able to make forecasts (Haykin, 1999; Nigrin, 1993; Zurada, 1992). The number of input and output neurons correspond to the number of observed or predictive variables and of variable to be predicted, respectively. There are several types of neural networks, the most popular ones being the multi-layer perceptron (MLP) (Rummelhart et al., 1986). The choice of the neural network architecture depends on phenomena and problems to be solved. In this work, we used a multi-layer perceptron (MLP) architecture with a feed-forward approach that is well adapted for spatial modeling. This approach has been successfully tested for predicting the metal content of ore deposits (Singer et Kouda, 1996; Brown et al., 2000; Porwal et al., 2003).

A back-propagation method is implemented for optimizing weights at the learning stage using a mean squares criteria to minimize the errors between the observations and the predicted output, coupled to a conjugate gradient method (Werbos, 1994) to find the optimal values for the connections.

#### IV.1.3.1 Network architecture

The input and output layers are of fixed size and are conditioned by the number of observed variables and by the number of variables to be predicted, respectively. Input variables are of various nature. It includes among others : coordinates  $(x, y, z)$ , the magnetic susceptibility contrast  $\chi_1$  at the drilling level and  $\chi_2$  found by the inversion, the density contrast  $\rho$  at the drilling level found by the inversion, the coded geological unit  $\kappa$  for the different rocks types, a standard error  $\sigma = 0.5$  for accounting for uncertainties of input variables (Taylor, 1997) ; the network outputs are the predicted susceptibility  $\chi$  or the density  $\rho$ . Figure IV.1 shows the architecture used for the neural network.

#### IV.1.3.2 Training network and back propagation

The neural network training process aims at calibrating the optimum weights of the different connections between neurons by minimizing the error between the predicted output and the observed values. In this work, we used a back-propagation algorithm (Rummelhart et al., 1986) together with a conjugate gradient method. At the beginning of the learning stage, the weights are initialized by a random number generator with uniform distribution between  $-0.1$  to  $0.1$  (Yam et Chow, 2000). The errors corresponding to the difference between the predicted and the observed output are then estimated at each step of the learning process. Then, the weights of each layer are recurrently modified during the learning stage using back-propagation techniques in order to reduce these errors.

The convergence rate of the algorithm depends on (i) the problem to be solved, (ii) the number of connections between the various entities and, of course, (iii) on the input and output layers sizes (based on the available data). The output level of a neuron  $X_j$  is given by :

$$Y_j = f\left(\sum_1^N X_i w_{ij} + b_j\right); \quad (\text{IV.1})$$

where  $f$  is the sigmoid function  $f(\alpha) = \frac{1}{1+e^{-\alpha}}$ ;  $X_i$  is the  $i^{th}$  input value;  $w_{ij}$  the synaptic weight between neurons  $i$  and  $j$ ,  $N$  the total number of neurons and  $b_j$  is the input bias often fixed to 0 early the learning stage.

The total error  $\varepsilon$  between the output and the observations is evaluated as the mean squared error  $e_i$  between the output of neurons  $i$  and the  $i^{th}$  observation :

$$\varepsilon = \frac{1}{N} \sum_{i=1}^N e_i^2. \quad (\text{IV.2})$$

with  $e_i = (d_i - Y_i)$  being the difference between the observation  $d_i$  and the prediction  $Y_i$  at the neuron level  $i$ . Finally the error calculated at the level of a neuron is distributed on the related synapses and neurons by the conjugate gradient algorithm (Johansson et al., 1991).

Let  $\Delta w_{ij}^t$  be the correction to be made on weight  $w_{ij}$  at iteration  $t$  connecting the neurons  $i$  to  $j$ , it is given by :

$$\Delta w_{ij}^t = \mu e_i f' \left( \sum_{k=1}^m w_{kj} + b_j \right) X_i + \Omega \Delta w_{ij}^{t-1} \quad (\text{IV.3})$$

where  $w_{kj}$  is an intermediate path between neuron  $i$  and neuron  $j$  passing through neuron  $k$ ;  $\mu$  and  $\Omega$  are factor ranging between 0 and 1 called the *rate* and *momentum*, respectively.  $\Omega$  is an added coefficient used to increase the convergence speed of the back-propagation algorithm, it accelerates the learning stage and forces to search minima out of local minima.

#### IV.1.4 Application

A single case study was chosen to demonstrate the ability of the proposed method to integrate different types of data when interpolating and simulating multi variables. The study area is located in the Val d'Or mining camp in the Abitibi province, Québec, Canada (Figure IV.2). The geological formations are composed of volcanic rocks and volcano clastic Archaean mafic to ultramafic and felsic formations (Wong et al., 1991; Scott et al., 2002). These volcanic formations are separated by a narrow band of younger sedimentary units (Mortensen, 1993). The major part of the ore deposits are of Volcanogenic Massive Sulfide (VMS) type. During the learning stage, the neural network establishes non linear complex relationships between the different rock types defined in the input

and the location of ore deposits in the output, especially regarding the spatial distribution of the susceptibility in the sub-surface. The neural weights obtained after the learning stage can then be studied carefully to better understand the link between each rock type and the known mineralizations, and thus can be used to derive 3D potential maps.

#### **IV.1.4.1 Interpolation**

Integrating several variables impacts the interpolation results given by the neural network. In this example, only the magnetic susceptibility and the density contrast obtained from the magnetic and gravity inversions have been considered as the primary variable together with the rock types as secondary variables. Figures IV.3 .a), .b) and .c) show the horizontal predicted geological map at a depth of 930 m, the prediction is compatible with the inverted density contrast and magnetization, respectively. As seen in Figures IV.3 e) and f), properties interpolated using neural network account for rock types. Integrating the geological information at the prediction step had improved the property estimation especially in low contrast zones. These interpolations are conditioned by boreholes data as they have been included at the training stage. Predictions respect data conditioning as shown in Figures IV.3. d).

#### **IV.1.4.2 Simulation**

The position of the selected points, rock types, magnetization, density contrast and neurons with a constant value of 0.5 for the learning process are taken as input to the neural network. In order to simulate several rock types, magnetic susceptibility and density realizations after the training stage of the neural network, the prediction is performed by injecting an input data set and by randomly varying between 0 and 1 the neuron values of the last layer at each realization. Figures IV.4.a .b and .c give three selected possible realizations for the rock types. Figures IV.5 .a .b and .c show three possible realizations of the sub surface magnetic susceptibility. The most upper figures show horizontal maps at a depth of 930 m, at the center, vertical cross-sections down to a depth of 1600 m. Lower figures show the total magnetic field induced by the three selected realizations. The magnetic field produced by the selected models are very similar, the latter step is essential to validate the simulations, and thus for keeping the most realistic models that have similar potential field (gravity or magnetic) considered as a reference.

#### IV.1.4.3 Computer performances

The study area is modeled using a centered regular 3D grids (Voxet) comprising  $150 \times 150 \times 75$  elementary cells. The magnetic susceptibility and the density calculated from the inversion are stored at the center of each elementary cells. Ore deposits are retrieved using a regular 2D grid. The learning stage takes about 15 mn on the Intel Core 2 Duo (2.40 GHz). This is the longest step in implementing the suggested method. The prediction of a 3D cube is relatively fast, this prediction time depends on the number of simulations and the spatial resolution of the study area.

#### IV.1.5 Discussions and Conclusions

This work proposes to use a stochastic simulation method based on training neural networks. The benefits of this method are : (i) to be available to integrate several variables, (ii) it does not request a preliminary geostatistical study such as the variograms analysis to capture the spatial variability, (iii) it does not need empirical relationships between the different input and output variables. The spatial correlations are studied capture during the training stage of the neural network. These same benefits could be viewed as disadvantages as neural networks behave like black box and need a set of training images including both the sub-surface geophysical responses and a careful knowledge of the underground regarding ore deposits. Posterior analysis of the predictions allow to cross validate the results. However, other advantages of the proposed methodology are the ability of neural networks to be used not only as predictors but also as simulators. This is a very interesting tool to quantify the uncertainty related to a given exploration area. Once the neural network is completely trained, changing randomly weight neurons values of the output layer impacts the predicted results and allow generating several realizations which are conditioned by the drill holes data (considered as points). in some case, up-scaling procedure might be necessary depending on the cell sizes of the grid. Neural networks are well adapted to investigate mature brownfields in which several deposits are already been discovered at the learning stage. Assuming green fields behave like brown ones, it is then possible to apply this methodology to investigate new areas containing potential undiscovered deposits and to produce potential 3D map accounting for uncertainty.

## References

- Brown, W. M., T. D. Gedeon, D. I. Groves, and R. G. Barnes, 2000, Artificial neural networks : a new method for mineral prospectivity mapping : Australian Journal of Earth Sciences, **47**, 757–770.
- Caers, J., 2001, Geostatistical reservoir modelling using statistical pattern recognition : Journal of Petroleum Science and Engineering, **29**, 177 – 188. ( Soft Computing and Earth Sciences ).
- Caers, J., and A. G. Journel, 1998, Stochastic Reservoir Simulation using Neural Networks Trained on Outcrop data : Society of Petroleum Engineers, 27–30 September. (Annual Technical Conference and Exhibition).
- Calderón-Macías, C., M. K. Sen, and P. L. Stoffa, 2000, Artificial neural networks for parameter estimation in geophysics : Geophysical Prospecting, **48**, 21–47.
- Deutsch, C. V., and A. G. Journel, 1998, GSLIB : Geostatistical Software Library and User's Guide : Oxford University Press, New York, *2<sup>nd</sup> Edition*.
- Gad, E.-Q., and K. Ushijima, 2001, Inversion of DC resistivity data using neural networks : Geophysical Prospecting, **49**, 417–430.
- Gloaguen, E., D. Marcotte, M. Chouteau, and H. Perroud, 2005, Borehole radar velocity inversion using cokriging and cosimulation : Journal of Applied Geophysics, **57**, 242 – 259.
- Goldberg, D. E., 1989, Genetic Algorithms in Search, Optimization, and Machine Learning : Addison-Wesley, Reading, MA.
- Hansen, T. M., A. G. Journel, A. Tarantola, and K. Mosegaard, 2006, Linear inverse Gaussian theory and geostatistics : Geophysics, **71**, R101–R111.
- Haykin, S., 1999, Neural Networks A Comprehensive Foundation : Prentice Hall, New Jersey.
- Holland, J. H., 1975, Adaptation in Natural and Artificial Systems : University of Michigan Press.

- Johansson, E., F. Dowla, and D. Goodman, 1991, Backpropagation Learning for Multi-layer Feed-Forward Neural Networks Using the Conjugate Gradient Method : International Journal of Neural Systems, **2**, 291–301.
- Journel, A., and E. Isaaks, 1984, Conditional Indicator Simulation : Application to a Saskatchewan uranium deposit : Mathematical Geology, **16**, 685–718.
- Kirkpatrick, S., C. D. Gelatt, and M. P. Vecchi, 1983, Optimization by Simulated Annealing : Science, **220**, 671–680.
- Loomis, M. C., T. M. Hansen, K. S. Cordua, L. Nielsen, K. H. Jensen, and A. Binley, 2010, Geostatistical inference using crosshole ground-penetrating radar : Geophysics, **75**, J29–J41.
- Menke, W., 1984, Geophysical Data Analysis : Discrete Inverse Theory : Academic Press, Inc. New York.
- Metropolis, N., and S. Ulam, 1949, The Monte Carlo method : Journal of the American Statistical Association, **44**, 335–341.
- Mortensen, J. K., 1993, U-Pb geochronology of the eastern Abitibi Subprovince. Part 1 : Chibougamau–Matagami–Joutel region : Canadian Journal of Earth Sciences, **30**, 11–28.
- Mueller, W., and J. Mortensen, 2002, Age constraints and characteristics of subaqueous volcanic construction, the Archean Hunter Mine Group, Abitibi greenstone belt : Precambrian Research, **115**, 119 – 152.
- Neyamadpour, A., W. A. T. W. Abdullah, and S. Taib, 2009, Use of Artificial Neural Networks to Invert 3D Electrical Resistivity Imaging Data : AIP Conference Proceedings, **1150**, 210–213.
- Nigrin, A., 1993, Neural Networks for Pattern Recognition : Cambridge, MA : The MIT Press.
- Porwal, A., E. J. M. Carranza, and M. Hale, 2003, Artificial Neural Networks for Mineral-Potential Mapping : A Case Study from Aravalli Province, Western India : Natural Resources Research, **12**, no. 3, 155–171.
- Poulton, M., K. Sternberg, and C. Glass, 1992, Neural network pattern recording of the subsurface EM images : Journal of Applied Geophysics, **29**, 21–36.
- Röth, G., and A. Tarantola, 1994, Neural networks and inversion of seismic data. : Journal of Geophysical Research, **99**, 811–822.
- Rummelhart, D. E., G. E. Hinton, and R. Williams, 1986, Learning internal representation by backpropagating errors : Nature, **332**, 533–536.
- Scott, C. R., W. U. Mueller, and P. Pilote, 2002, Physical volcanology, stratigraphy, and lithogeochemistry of an Archean volcanic arc : evolution from plume-related volcanism

- to arc rifting of SE Abitibi Greenstone Belt, Val d'Or, Canada : Precambrian Research, **115**, 223 – 260.
- Shamsipour, P., D. Marcotte, M. Chouteau, and P. Keating, 2010, 3D stochastic inversion of gravity data using cokriging and cosimulation : Geophysics, **75**, I1–I10.
- Singer, D., and R. Kouda, 1996, Application of a feedforward neural network in the search for Kuroko deposits in the Hokuroku district, Japan : Mathematical Geology, **28**, no. 8, 1017–1023.
- Strebelle, S., 2002, Conditional Simulation of Complex Geological Structures Using Multiple-Point Statistics : Mathematical Geology, **34**, no. 1, 1–21.
- Tarantola, A., 2006, Popper, Bayes and the inverse problem : Nature Physics, **2**, 492–494.
- Tarantola, A., and B. Valette, 1982, Generalized Nonlinear Inverse Problems Solved Using the Least Squares Criterion : Reviews of Geophysics and Space Physics, **20**, 219–232.
- Taylor, J. R., 1997, An Introduction to Error Analysis : The Study of Uncertainties in Physical Measurements : 2<sup>nd</sup> Edition, University Science Books.
- Tran, T. T., 1994, Improving variogram reproduction on dense simulation grids : Computers and Geosciences, **20**, no. 7-8, 1161–1168.
- Werbos, E., 1994, The roots of back-propagation : John Wiley Sons, Inc.
- Wong, L., D. Davis, T. Krogh, and F. Robert, 1991, U–Pb zircon and rutile chronology of Archean greenstone formation and gold mineralization in the Val d'Or region, Québec : Earth and Planetary Science Letters, **104**, 325 – 336.
- Wong, P., and S. Shibli, 2001, Modelling a fluvial reservoir with multipoint statistics and principal components : Journal of Petroleum Science and Engineering, **31**, 157 – 163. ( Soft Computing and Earth Sciences (Part 2) ).
- Yam, J. Y. F., and T. W. S. Chow, 2000, A weight initialization method for iproving training speed in feedforward neural network : Neurocomputing, **30**, 219–232.
- Zurada, J., 1992, Introduction To Artificial Neural Systems : Boston : PWS Publishing Company.

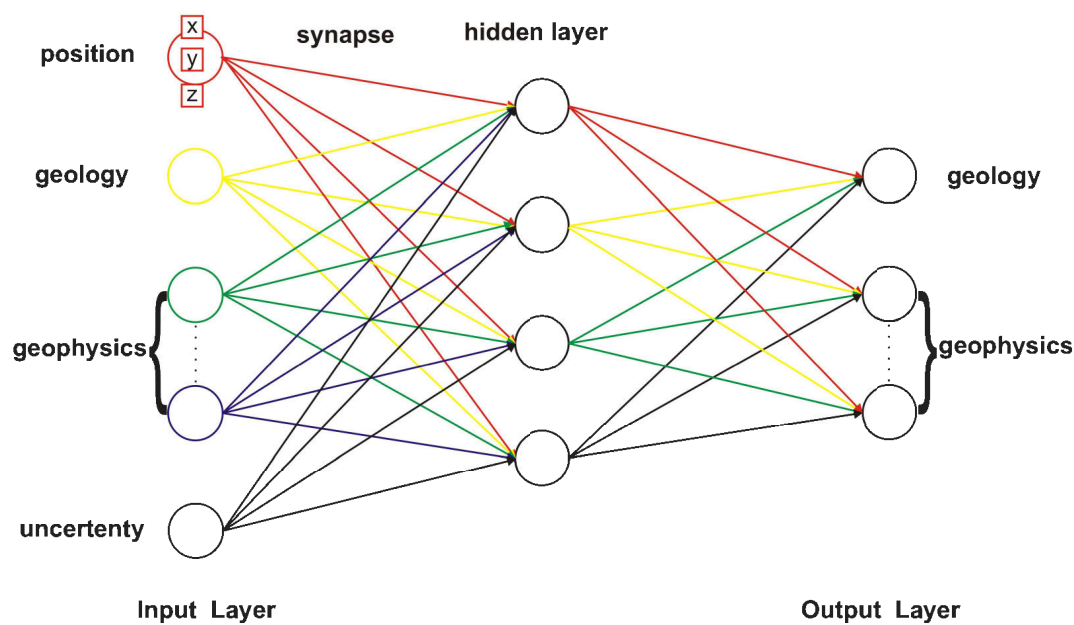


FIGURE IV.1: Neural network architecture.

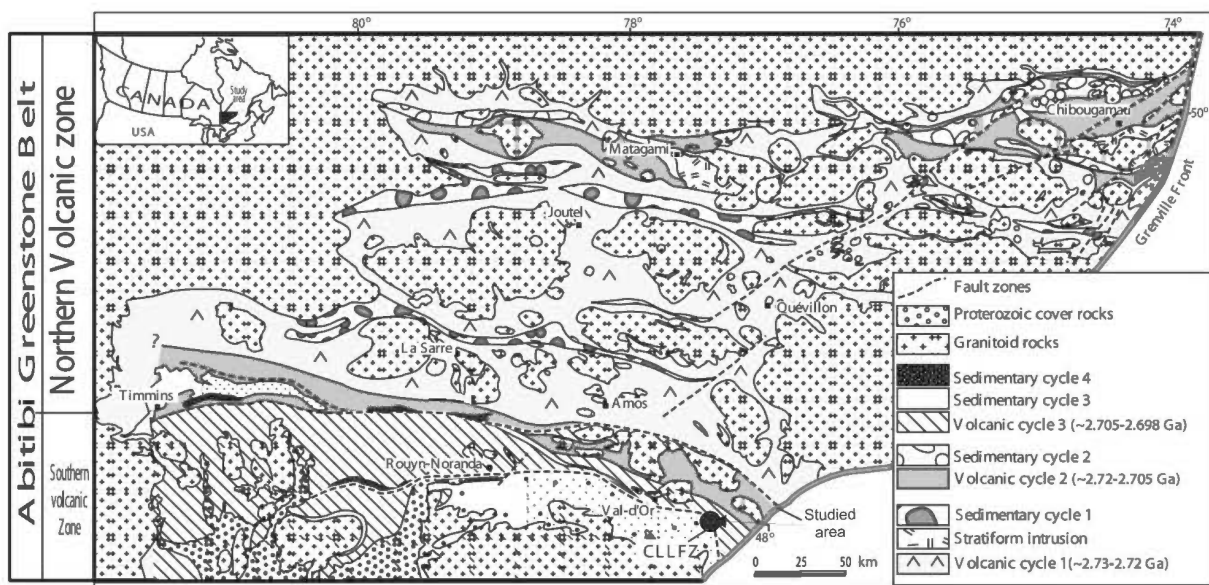


FIGURE IV.2: Geology of the Abitibi greenstone belt, Québec, Canada. From ([Mueller et Mortensen, 2002](#))

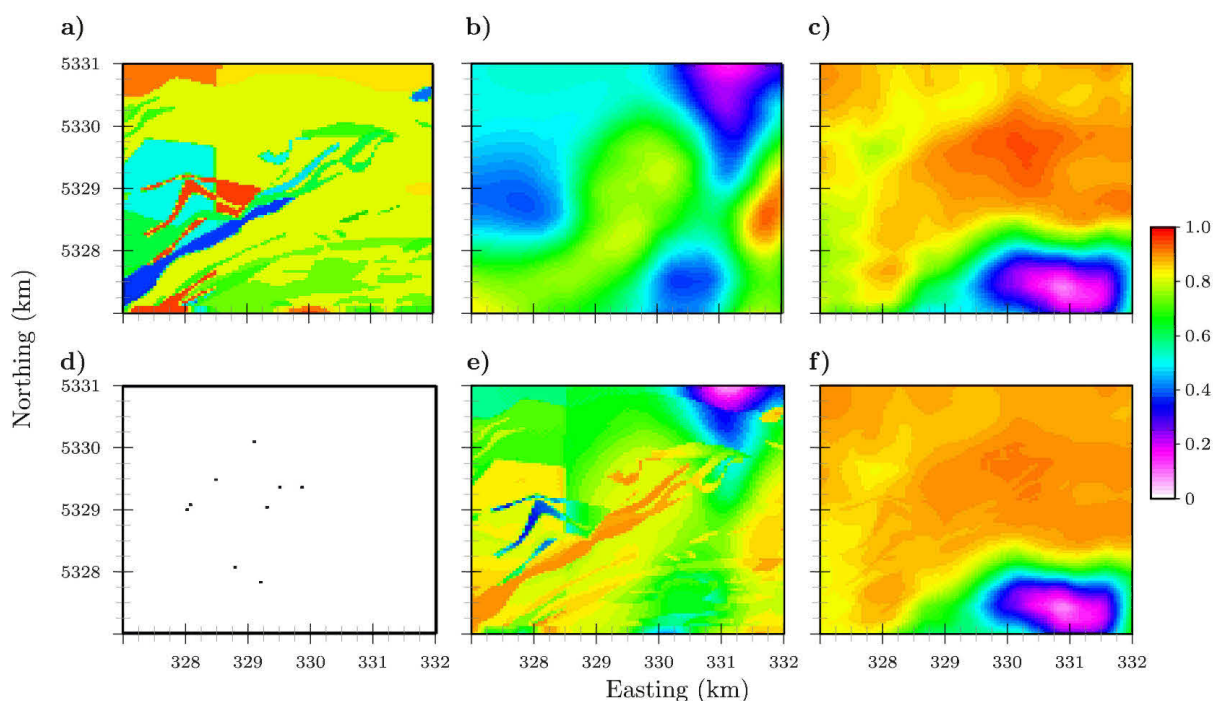


FIGURE IV.3: Normalized (a) coded geological map (b) density contrast , (c) magnetic susceptibility, (e) interpolated density contrast using (ANN), training point and (f) interpolated magnetic susceptibility (ANN).

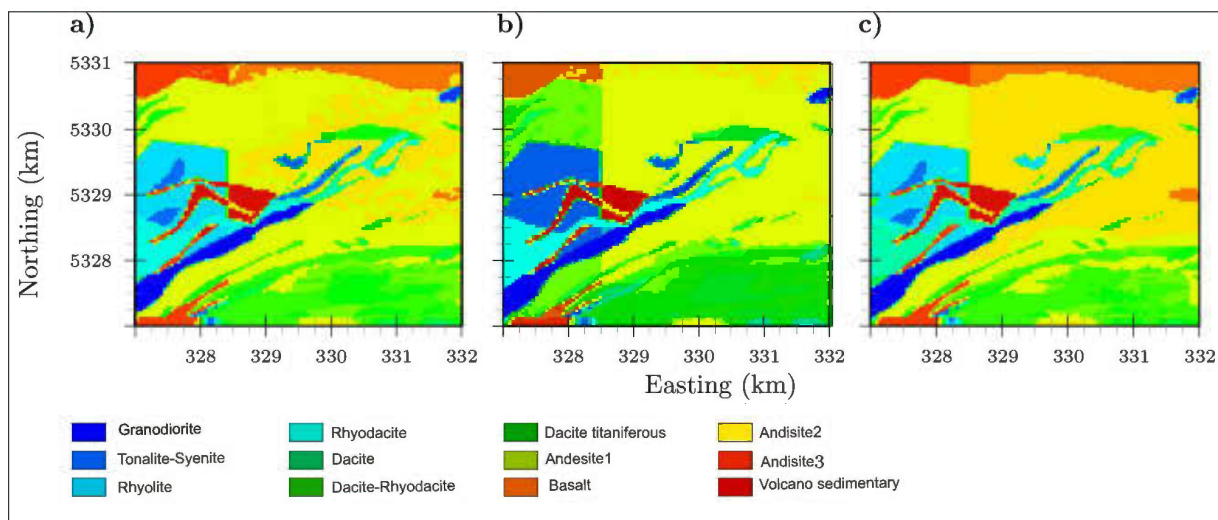


FIGURE IV.4: Horizontal cross-sections showing three possible geological maps simulated by ANN at a depth of 930 m.

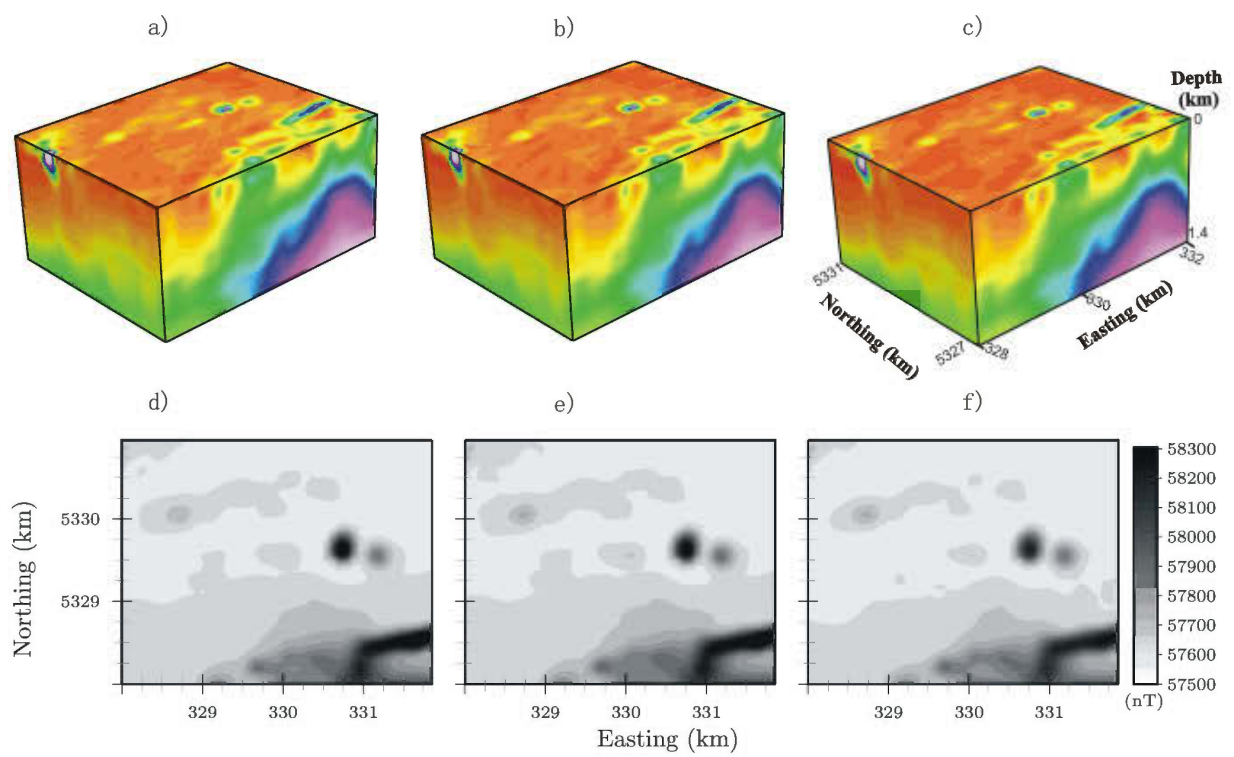


FIGURE IV.5: 3 selected realizations of simulated magnetization



## CONCLUSION GÉNÉRALE

Les objectifs de cette thèse étaient de développer des méthodes d'interprétations de données géophysiques. Pour passer des données mesurées sur le terrain à un modèle géologique et ou géophysique plusieurs étapes sont nécessaires.

Dans le chapitre I, une méthode basée sur une approximation simple a été développée pour le calcul des composantes des champs de potentiels (gravimétrique et magnétique) créées par n'importe quel modèle possédant une géométrie complexe et une distribution hétérogène de propriétés physiques. La structure géologique est modélisée pas une grille à base de tétraèdre et l'algorithme de subdivision proposée permet de raffiner le maillage au voisinage des points d'observation afin que l'approximation utilisée dans le calcul direct soit toujours valable.

Le chapitre II, offre une optimisation de la méthode d'inversion de Monte Carlo par l'utilisation des méthodes de simulations géostatistiques et le résultat de l'inversion obtenu par la méthode des moindres carrés. Le but de la méthode proposée est d'échantillonner un maximum de modèles avec différentes distributions de la propriété physique, afin de favoriser les réalisations dont la densité de probabilité *a posteriori* sera acceptable. Ainsi, la méthodologie consiste à l'intégration de l'information *a priori*, à l'utilisation d'un modèle de variogramme qui prend en considération la répartition spatiale de la propriété physique, à l'utilisation d'un algorithme de simulation séquentielle, et enfin au calcul de la réponse *a posteriori* de chaque modèle simulé. Les résultats d'inversions sont influencé par : l'information *a priori*, la solution de départ (trouvé par la méthode des moindre carrés ou Monte Carlo), le nombre de points pilotes, le modèle de variogramme choisi, l'incertitude sur les mesures, la méthode de simulation et la résolution spatiale du modèle.

Pour sa part le chapitre III, a mis l'accent sur l'inversion stochastique conjointe entre les données gravimétrique et magnétique. Sachant que l'inversion séparée de chaque donnée géophysique peut présenter un résultat différent en fonction de la méthode utilisée,

une contrainte sur la géologie structurale est extraite à partir des résultats obtenus par inversion séparée, puis imposée sous forme de géométrie commune pour l'inversion conjointe. La géostatistique utilisée par la technique de simulation co-localisé par co-krigeage a permis d'intégrer les deux sources d'information à savoir les distributions du contraste de densité et la susceptibilité magnétique et par conséquence de générer plusieurs distributions possibles de propriétés physiques dans un modèle 3D. En plus des mêmes facteurs cités dans la méthode d'inversion stochastique et qui influence le résultat de l'inversion, le coefficient de corrélation entre la variable primaire et secondaire a une grande emprise sur les résultats de la co-simulation. Néanmoins, ce coefficient peut être utilisé avec des valeurs différentes par région et dans l'absence d'information *a priori* des variables pour tester certaine hypothèses.

Enfin dans le chapitre IV, une méthode basée sur l'apprentissage des réseaux de neurones artificiels est utilisée pour générer plusieurs distributions possibles de variables (propriétés physiques ou unités géologiques). En effet, l'analyse des variables supervisée en un certain nombre de points permet de trouver la relation complexe qui pourrait exister entre les variables de différentes natures. L'avantage majeur est que cette méthode ne demande pas une étude géostatistique préalable et tient compte de plusieurs points. Lors de processus d'apprentissage un neurone d'incertitude est gardé constant avec une valeur de 0.5 qui correspond à l'abscisse du maximum de la fonction de densité de probabilité normalisée entre 0 et 1. Ainsi, plusieurs distributions possibles de variables peuvent être générées en changeant à chaque fois et de manière aléatoire la valeur du neurone d'incertitude lors de l'étape de prédiction.

## BIBLIOGRAPHIE

- AFNIMAR, KOKETSU, K., ET NAKAGAWA, K., 2002, JOINT INVERSION OF REFRACTION AND GRAVITY DATA FOR THE THREE-DIMENSIONAL TOPOGRAPHY OF A SEDIMENT-BASEMENT INTERFACE : *Geophysical Journal International*, **151** (1), 243–254.
- BABAK, O., ET DEUTSCH, C., 2009, COLLOCATED COKRIGING BASED ON MERGED SECONDARY ATTRIBUTES : *Mathematical Geosciences*, **41**, 921–926.
- BACKUS, G., ET GILBERT, F., 1968, THE RESOLVING POWER OF GROSS EARTH DATA : *Geophysical Journal of the Royal Astronomical Society*, **16** (2), 169–205.
- BARBOSA, V. C. F., AO B. C. SILVA, J., ET MEDEIROS, W. E., 1999, GRAVITY INVERSION OF A DISCONTINUOUS RELIEF STABILIZED BY WEIGHTED SMOOTHNESS CONSTRAINTS ON DEPTH : *Geophysics*, **64** (5), 1429–1437.
- BARBOSA, V. C. F., SILVA, J. B. C., ET MEDEIROS, W. E., 2002, PRACTICAL APPLICATIONS OF UNIQUENESS THEOREMS IN GRAVIMETRY : PART II—PRAGMATIC INCORPORATION OF CONCRETE GEOLOGIC INFORMATION : *Geophysics*, **67** (3), 795–800.
- BARBOSA, V. C. F., ET SILVA, J. B. C., 1994, GENERALIZED COMPACT GRAVITY INVERSION : *Geophysics*, **59** (1), 57–68.
- BARNETT, C. T., 1976, THEORETICAL MODELING OF THE MAGNETIC AND GRAVITATIONAL FIELDS OF AN ARBITRARILY SHAPED THREE-DIMENSIONAL BODY : *Geophysics*, **41** (6), 1353–1364.
- BELLEFLEURG., D. K. E. G. J., ET ALLARD, M., 2007, A NEW LOOK AT THE GEOLOGICAL FRAMEWORK OF THE CENTRAL NORANDA CAMP, QUÉBEC FROM INDUSTRY HIGH-RESOLUTION SEISMIC PROFILES : *Geological Survey of Canada Current Research*, **C5**, 9p.

- BERTETE-AGUIRRE, H., CHERKAEV, E., ET ORISTAGLIO, M., 2002, NON-SMOOTH GRAVITY PROBLEM WITH TOTAL VARIATION PENALIZATION FUNCTIONAL : Geophysical Journal International, **149** (2), 499–507.
- BHATTACHARYYA, B. K., 1964, MAGNETIC ANOMALIES DUE TO PRISM-SHAPED BODIES WITH ARBITRARY POLARIZATION : Geophysical Prospecting, **24**, 633–649.
- BLAKELY, J. R., 1996, POTENTIAL THEORY IN GRAVITY & MAGNETIC APPLICATIONS, Cambridge University Press.
- BOSCH, M., MEZA, R., JIMÉNEZ, R., ET HÖNIG, A., 2006, JOINT GRAVITY AND MAGNETIC INVERSION IN 3D USING MONTE CARLO METHODS : Geophysics, **71** (4), G153–G156.
- BOSCH, M., CARA, L., RODRIGUES, J., NAVARRO, A., ET DÍAZ, M., 2007, A MONTE CARLO APPROACH TO THE JOINT ESTIMATION OF RESERVOIR AND ELASTIC PARAMETERS FROM SEISMIC AMPLITUDES : Geophysics, **72** (6), O29–O39.
- BOSCH, M., 1999, LITHOLOGIC TOMOGRAPHY : FROM PLURAL GEOPHYSICAL DATA TO LITHOLOGY ESTIMATION : Journal of Geophysical Research B : Solid Earth, **104**, 749–766.
- BOSZCZUK, P., CHENG, L. Z., HAMMOUCHE, H., ROY, P., LACROIX, S., ET CHEILLETZ, A., JUL 2011, A 3D GRAVITY DATA INTERPRETATION OF THE MATAGAMI MINING CAMP, ABITIBI SUBPROVINCE, SUPERIOR PROVINCE, QUÉBEC, CANADA. APPLICATION TO VMS DEPOSITS EXPLORATION : Journal of Applied Geophysics.
- BOTT, M. H. P., 1963, TWO METHODS APPLICABLE TO COMPUTERS FOR EVALUATING MAGNETIC ANOMALIES DUE TO FINITE THREE DIMENSIONAL BODIES : Geophysical Prospecting, **11** (3), 292–299.
- BOUCHEDDA, A., 2010, INVERSION CONJOINTE DES DONNÉES ÉLECTRIQUES ET DE RADAR EN FORAGE : PhD. thesis, École Polytechnique de Montréal.
- BOULANGER, O., ET CHOUTEAU, M., 2001, CONSTRAINTS IN 3D GRAVITY INVERSION : Geophysical Prospecting, **49**, 265–280.
- BROWN, W. M., GEDEON, T. D., GROVES, D. I., ET BARNES, R. G., 2000, ARTIFICIAL NEURAL NETWORKS : A NEW METHOD FOR MINERAL PROSPECTIVITY MAPPING : Australian Journal of Earth Sciences, **47** (4), 757–770.
- CADY, J. W., 1980, CALCULATION OF GRAVITY AND MAGNETIC ANOMALIES OF FINITE-LENGTH RIGHT POLYGONAL PRISMS : Geophysics, **45** (10), 1507–1512.

- CAERS, J., ET JOURNEL, A. G., 1998, STOCHASTIC RESERVOIR SIMULATION USING NEURAL NETWORKS TRAINED ON OUTCROP DATA : Society of Petroleum Engineers, pages 27–30 September.
- CAERS, J., 2001, GEOSTATISTICAL RESERVOIR MODELLING USING STATISTICAL PATTERN RECOGNITION : Journal of Petroleum Science and Engineering, **29**, 177 – 188.
- CALDERÓN-MACÍAS, C., SEN, M. K., ET STOFFA, P. L., 2000, ARTIFICIAL NEURAL NETWORKS FOR PARAMETER ESTIMATION IN GEOPHYSICS : Geophysical Prospecting, **48** (1), 21–47.
- CAIVERT, A. J., ET LI, Y., 1999, SEISMIC REFLECTION IMAGING OVER A MASSIVE SULFIDE DEPOSIT AT THE MATAGAMI MINING CAMP, QUÉBEC : Geophysics, **64** (1), 24–32.
- CAUMON, G., LEPAGE, F., SWORD, C., ET MALLET, J.-L., 2004, BUILDING AND EDITING A SEALED GEOLOGICAL MODEL : Mathematical Geology, **36**, 405–424.
- CAUMON, G., COLLON-DROUAILLET, P., LE CARLIER DE VESLUD, C., VISEUR, S., ET SAUSSE, J., 2009, SURFACE-BASED 3D MODELING OF GEOLOGICAL STRUCTURES : Mathematical Geosciences, **41**, 927–945.
- CAUMON, G., 2003, PRÉSENTATION, VISUALISATION ET MODIFICATION DE MODÈLES VOLUMIQUES POUR LES GÉOSCIENCES : PhD. thesis, Institut National Polytechnique de Lorraine. Nancy, France.
- CAUMON, G., 2009, VERS UNE INTÉGRATION DES INCERTITUDES ET DES PROCESSES EN GÉOLOGIE NUMÉRIQUE : PhD. thesis, Institut National Polytechnique de Lorraine (France).
- CAUMON, G., 2010, TOWARDS STOCHASTIC TIME-VARYING GEOLOGICAL MODELING : Mathematical Geosciences, **42** (5), 555–569.
- CHAI, Y., ET HINZEW., J., 1988, GRAVITY INVERSION OF AN INTERFACE ABOVE WHICH THE DENSITY CONTRAST VARIES EXPONENTIALLY WITH DEPTH : Geophysics, **53**, 837–845.
- CHASSERIAU, P., ET CHOUTEAU, M., MAY 2003, 3D GRAVITY INVERSION USING A MODEL OF PARAMETER COVARIANCE : Journal of Applied Geophysics, **52** (1), 59 – 74.
- CHENG, L. Z., FALLARA, F., FOUDIL-BEY, N., GOUTIER, J., DION, C., ET PETRELLA, L., ETUDE TRIDIMENSIONNELLE DES ÉLÉMENTS STRUCTURAUX MAJEURS

- DU GROUPE DE BLAKE RIVER :, Technical report, Rapport de travaux statutaires, Ressources naturelles et Faune du Québec, 2010.
- CHILÉS, J.-P., ET DELFINER, P., 1999, GEOSTATISTICS, MODELING SPATIAL UNCERTAINTY : Wiley Series on Probability and Statistics.
- DE MARSILY, G. H., LAVADAN, C., BOUCHER, M., ET FASANINO, G., 1984, INTERPRETATION OF INTERFERENCE TESTS IN A WELL FIELD USING GEOSTATISTICAL TECHNIQUES TO FIT THE PERMEABILITY DISTRIBUTION IN A RESERVOIR MODEL :, volume Part 2 Geostatistics for natural resources characterization.
- DELL'AVERSANA, P., 2001, INTEGRATION OF SEISMIC, MT AND GRAVITY DATA IN A THRUST BELT INTERPRETATION : First Break, **19** (6), 335–341.
- DEUTSCH, C. V., ET JOURNEL, A. G., 1998, GSLIB : GEOSTATISTICAL SOFTWARE LIBRARY AND USER'S GUIDE :, volume 2<sup>nd</sup> Edition Oxford University Press, New York.
- EULEUR, N., 1999, MODÉLISATION VOLUMIQUE, CONTRAINTES ET LIBERTÉS : PhD. thesis, Institut National Polytechnique de Lorraine. Nancy, France.
- EVJEN, H. M., 1936, THE PLACE OF THE VERTICAL GRADIENT IN GRAVITATIONAL INTERPRETATIONS : Geophysics, **1** (1), 127–136.
- EZZEDINE, S., RUBIN, Y., ET CHEN, J., 1999, BAYESIAN METHOD FOR HYDROGEOLOGICAL SITE CHARACTERIZATION USING BOREHOLE AND GEOPHYSICAL SURVEY DATA : THEORY AND APPLICATION TO THE LAWRENCE LIVERMORE NATIONAL LABORATORY SUPERFUND SITE : Water resources research, **35** (9), 2671–2683.
- FRANK, T., TERTOIS, A.-L., ET MALLET, J.-L., 2007, 3D-RECONSTRUCTION OF COMPLEX GEOLOGICAL INTERFACES FROM IRREGULARLY DISTRIBUTED AND NOISY POINT DATA : Computers and Geosciences, **33**, 932–943.
- FRANKLIN, J. N., 1970, WELL POSED STOCHASTIC EXTENSIONS OF ILL POSED LINEAR PROBLEMS : Journal of the Institute of Mathematics and Its Applications, **31**, 682–716.
- FREGOSO, E., ET GALLARDO, L. A., 2009, CROSS-GRADIENTS JOINT 3D INVERSION WITH APPLICATIONS TO GRAVITY AND MAGNETIC DATA : Geophysics, **74** (4), L31–L42.
- GAD, E.-Q., ET USHIJIMA, K., 2001, INVERSION OF DC RESISTIVITY DATA USING NEURAL NETWORKS : Geophysical Prospecting, **49** (4), 417–430.

- GALLARDO-DELGADO, L. A., PÉREZ-FLORES, M. A., ET NO, E. G.-T., 2003, A VERSATILE ALGORITHM FOR JOINT 3D INVERSION OF GRAVITY AND MAGNETIC DATA : *Geophysics*, **68** (3), 949–959.
- GALLARDO, L. A., ET MEJU, M. A., 2004, JOINT TWO-DIMENSIONAL DC RESISTIVITY AND SEISMIC TRAVEL TIME INVERSION WITH CROSS-GRADIENTS CONSTRAINTS : *Journal of Geophysical Research B : Solid Earth*, **109** (3), B03311 1–11.
- GALLARDO, L. A., 2004, JOINT TWO-DIMENSIONAL INVERSION OF GEOELECTROMAGNETIC AND SEISMIC REFRACTION DATA WITH CROSS-GRADIENTS CONSTRAINT : PhD. thesis, Lancaster University.
- GARCÍA-ABDESEM, J., 1992, GRAVITATIONAL ATTRACTION OF A RECTANGULAR PRISM WITH DEPTH-DEPENDENT DENSITY : *Geophysics*, **57** (3), 470–473.
- GEMAN, S., ET GEMAN, D., 1984, STOCHASTIC RELAXATION, GIBBS DISTRIBUTIONS, AND THE BAYESIAN RESTORATION OF IMAGES : *IEEE Transactions*.
- GJØYSTDAL, H., REINHARDSEN, J. E., , ET ÅSTEBØL, K., 1985, COMPUTER REPRESENTATION OF COMPLEX THREE-DIMENSIONAL GEOLOGICAL STRUCTURES USING A NEW SOLID MODELING TECHNIQUE : *Geophysical Prospecting*, **33** (8), 1195–1211.
- GLOAGUEN, E., MARCOTTE, D., CHOUTEAU, M., ET PERROUD, H., 2005, BOREHOLE RADAR VELOCITY INVERSION USING COKRIGING AND COSIMULATION : *Journal of Applied Geophysics*, **57** (4), 242 – 259.
- GLOAGUEN, E., MARCOTTE, D., GIROUX, B., DUBREUIL-BOISCLAIR, C., CHOUTEAU, M., ET AUBERTIN, M., 2007, STOCHASTIC BOREHOLE RADAR VELOCITY AND ATTENUATION TOMOGRAPHIES USING COKRIGING AND COSIMULATION : *Journal of Applied Geophysics*, **62** (2), 141 – 157.
- GOLDBERG, D. E., 1989, GENETIC ALGORITHMS IN SEARCH, OPTIMIZATION, AND MACHINE LEARNING : Addisonâ€“Wesley, Reading, MA.
- GÓMEZ-HERNÁNEZ, J. J., SAHUQUILLO, A., ET CAPILLA, J., 1997, STOCHASTIC SIMULATION OF TRANSMISSIVITY FIELDS CONDITIONAL TO BOTH TRANSMISSIVITY AND PIEZOMETRIC DATA—I. THEORY : *Journal of Hydrology*, **203**, 162 – 174.
- GOOVAERTS, P., 1997, GEOSTATISTICS FOR NATURAL RESOURCES EVALUATION : Oxford University Press, New York.
- GUILLEN, A., ET MENICHETTI, V., 1984, GRAVITY AND MAGNETIC INVERSION WITH MINIMIZATION OF A SPECIFIC FUNCTIONAL : *Geophysics*, **49** (8), 1354–1360.

- GÜNTHER, T., ET RÜCKER, C., 2006, A GENERAL APPROACH FOR INTRODUCING INFORMATION INTO INVERSION AND EXAMPLES FROM DC RESISTIVITY INVERSION : European Association of Geoscientists & Engineers. Near Surface Geophysics, **12th European Meeting of Environmental and Engineering Geophysics, Helsinki (Finland)**.
- HABER, E., ET OLDENBURG, D., 1997, JOINT INVERSION : A STRUCTURAL APPROACH : Inverse Problems, **13** (1), 63.
- HANSEN, T. M., JOURNEL, A. G., TARANTOLA, A., ET MOSEGAARD, K., 2006, LINEAR INVERSE GAUSSIAN THEORY AND GEOSTATISTICS : Geophysics, **71** (6), R101–R111.
- HANSEN, T. M., ET MOSEGAARD, K., 2008, VISIM : SEQUENTIAL SIMULATION FOR LINEAR INVERSE PROBLEMS : Computers & Geosciences, **34** (1), 53 – 76.
- HANSEN, R. O., ET WANG, X., 1988, SIMPLIFIED FREQUENCY-DOMAIN EXPRESSIONS FOR POTENTIAL FIELDS OF ARBITRARY THREE-DIMENSIONAL BODIES : Geophysics, **53** (3), 365–374.
- HAYKIN, S., 1999, NEURAL NETWORKS A COMPREHENSIVE FOUNDATION : Prentice Hall, New Jersey.
- HENDERSON, R. G., ET ZIETZ, I., 1949, THE COMPUTATION OF SECOND VERTICAL DERIVATIVES OF GEOMAGNETIC FIELDS : Geophysics, **14** (4), 508–516.
- HOLLAND, J. H., 1975, ADAPTATION IN NATURAL AND ARTIFICIAL SYSTEMS : University of Michigan Press.
- HOLSTEIN, H., SCHURHOLZ, P., STARR A., J., ET CHAKRABORTY, M., 1999, COMPARISON OF GRAVIMETRIC FORMULAS FOR UNIFORM POLYHEDRA : Geophysics, **64** (5), 1438–1446.
- HU, W., ABUBAKAR, A., ET HABASHY, T. M., 2009, JOINT ELECTROMAGNETIC AND SEISMIC INVERSION USING STRUCTURAL CONSTRAINTS : Geophysics, **74** (6), R99–R109.
- HYNDMAN, D. W., HARRIS, J. M., ET GORELICK, S. M., 1994, COUPLED SEISMIC AND TRACER TEST INVERSION FOR AQUIFER PROPERTY CHARACTERIZATION : Water resources research, **30** (7), 1965–1977.
- JEGEN, M. D., HOBBS, R. W., TARITS, P., ET CHAVE, A., 2009, JOINT INVERSION OF MARINE MAGNETOTELLURIC AND GRAVITY DATA INCORPORATING SEISMIC

- CONSTRAINTS PRELIMINARY RESULTS OF SUB-BASALT IMAGING OFF THE FAROE SHELF : *Earth and Planetary Science Letters*, **282**, 47–55.
- JESSELL, M., 2001, THREE-DIMENSIONAL GEOLOGICAL MODELLING OF POTENTIAL-FIELD DATA : *Computers & Geosciences*, **27** (4), 455 – 465.
- JOHANSSON, E., DOWLA, F., ET GOODMAN, D., 1991, BACKPROPAGATION LEARNING FOR MULTILAYER FEED-FORWARD NEURAL NETWORKS USING THE CONJUGATE GRADIENT METHOD : *International Journal of Neural Systems*, **2** (4), 291–301.
- JOURNAL, A., ET ALABERT, F., 1989, NON-GAUSSIAN DATA EXPANSION IN THE EARTH SCIENCES : *Terra Nova*, **1** (2), 123–134.
- JOURNEL, A., ET ISAAKS, E., 1984, CONDITIONAL INDICATOR SIMULATION : APPLICATION TO A SASKATCHEWAN URANIUM DEPOSIT : *Mathematical Geology*, **16**, 685–718.
- JOURNEL, A., 1999A, CONDITIONING GEOSTATISTICAL OPERATIONS TO NONLINEAR VOLUME AVERAGES : *Mathematical Geology*, **31**, 931–953.
- 1999B, MARKOV MODELS FOR CROSS-COVARIANCES : *Mathematical Geology*, **31**, 955–964.
- KEILIS-BOROK, V. I., ET YANOVSKAJA, T. B., 1967, INVERSE PROBLEMS OF SEISMOLOGY (STRUCTURAL REVIEW) : *Geophysical Journal of the Royal Astronomical Society*, **13**, 223–234.
- KIRKPATRICK, S., GELATT, C. D., ET VECCHI, M. P., MAY 1983, OPTIMIZATION BY SIMULATED ANNEALING : *Science*, **220** (4598), 671–680.
- LAST, B. J., ET KUBIK, K., 1983, COMPACT GRAVITY INVERSION : *Geophysics*, **48** (6), 713–721.
- LEE, T.-C., ET BIEHLER, S., 1991, INVERSION MODELING OF GRAVITY WITH PRISMATIC MASS BODIES : *Geophysics*, **56** (9), 1365–1376.
- LI, Y., ET OLDENBURG, D. W., 1996, 3-D INVERSION OF MAGNETIC DATA : *Geophysics*, **61** (2), 394–408.
- LI, Y., ET OLDENBURG, D. W., 1998, 3-D INVERSION OF GRAVITY DATA : *Geophysics*, **63** (1), 109–119.

- LI, Y., ET OLDENBURG, D. W., 2003, FAST INVERSION OF LARGE-SCALE MAGNETIC DATA USING WAVELET TRANSFORMS AND A LOGARITHMIC BARRIER METHOD : Geophysical Journal International, **152** (2), 251–265.
- LINDE, N., BINLEY, A., TRYGGVASON, A., PEDERSEN, L. B., ET REVIL, A., 2006, IMPROVED HYDROGEOPHYSICAL CHARACTERIZATION USING JOINT INVERSION OF CROSS-HOLE ELECTRICAL RESISTANCE AND GROUND-PENETRATING RADAR TRAVELTIME DATA : Water resources research, **42**,, W12404.
- LINDE, N., TRYGGVASON, A., PETERSON, J. E., ET HUBBARD, S. S., 2008, JOINT INVERSION OF CROSSHOLE RADAR AND SEISMIC TRAVELTIMES ACQUIRED AT THE SOUTH OYSTER BACTERIAL TRANSPORT SITE : Geophysics, **73** (4), G29–G37.
- LOOMS, M. C., HANSEN, T. M., CORDUA, K. S., NIELSEN, L., JENSEN, K. H., ET BINLEY, A., 2010, GEOSTATISTICAL INFERENCE USING CROSSHOLE GROUND-PENETRATING RADAR : Geophysics, **75** (6), J29–J41.
- MACGEEHAN, P. J., 1978, THE GEOCHEMISTRY OF ALTERED VOLCANIC ROCKS AT MATAGAMI, QUEBEC : A GEOTHERMAL MODEL FOR MASSIVE SULPHIDE GENESIS : Canadian Journal of Earth Sciences, **15** (4), 551–570.
- MALLET, J. L., 2002, GEOMODELING : Oxford University Press.
- MANCHUK, J. G., 2010, GEOSTATISTICAL MODELING OF UNSTRUCTURED GRIDS FOR FLOW SIMULATION : PhD. thesis, University of Alberta.
- MASSOT, J., 2002, IMPLÉMENTATION DE MÉTHODES DE RESTAURATION ÉQUILIBRÉE : PhD. thesis, Institut National Polytechnique de Lorraine (France).
- MENKE, W., 1984, GEOPHYSICAL DATA ANALYSIS : DISCRETE INVERSE THEORY : Academic Press, Inc. New York.
- METROPOLIS, N., ROSENBLUTH, A. W., ROSENBLUTH, M. N., TELLER, A. H., ET TELLER, E., 1953, EQUATION OF STATE CALCULATIONS BY FAST COMPUTING MACHINES : Journal of Chemical Physics, **21** (6), 1087–1092.
- METROPOLIS, N., ET ULAM, S., 1949, THE MONTE CARLO METHOD : Journal of the American Statistical Association, **44**, 335–341.
- MORTENSEN, J. K., 1993, U–Pb GEOCHRONOLOGY OF THE EASTERN ABITIBI SUB-PROVINCE. PART 1 : CHIBOUGAMAU–MATAGAMI–JOUTEL REGION : Canadian Journal of Earth Sciences, **30** (1), 11–28.

- MOSEGAARD, K., ET SAMBRIDGE, M., 2002, MONTE CARLO ANALYSIS OF INVERSE PROBLEMS : *Inverse Problems*, **18**, R29–R54.
- MOSEGAARD, K., ET TARANTOLA, A., 1995, MONTE CARLO SAMPLING OF SOLUTIONS TO INVERSE PROBLEMS : *Journal of Geophysical Research*, **100**, 12431–12447.
- MOSEGAARD, K., ET TARANTOLA, A., 2002, PROBABILISTIC APPROACH TO INVERSE PROBLEMS, INTERNATIONAL HANDBOOK OF EARTHQUAKE & ENGINEERING SEISMOLOGY, PART A, : Academic Press, New York, 237–265.
- MUELLER, W., ET MORTENSEN, J., 2002, AGE CONSTRAINTS AND CHARACTERISTICS OF SUBAQUEOUS VOLCANIC CONSTRUCTION, THE ARCHEAN HUNTER MINE GROUP, ABITIBI GREENSTONE BELT : *Precambrian Research*, **115**, 119 – 152.
- MUFTI, I. R., 1973, RAPID DETERMINATION OF CUBE'S GRAVITY FIELD : *Geophysical Prospecting*, **21** (4), 724–735.
- MUSIL, M., MAURER, H. R., ET GREEN, A. G., 2003, DISCRETE TOMOGRAPHY AND JOINT INVERSION FOR LOOSELY CONNECTED OR UNCONNECTED PHYSICAL PROPERTIES : APPLICATION TO CROSSHOLE SEISMIC AND GEORADAR DATA SETS : *Geophysical Journal International*, **153** (2), 389–402.
- NAGY, D., 1966, THE GRAVITATIONAL ATTRACTION OF A RIGHT RECTANGULAR PRISM : *Geophysics*, **31** (2), 362–371.
- NEYAMADPOUR, A., ABDULLAH, W. A. T. W., ET TAIB, S., 2009, USE OF ARTIFICIAL NEURAL NETWORKS TO INVERT 3D ELECTRICAL RESISTIVITY IMAGING DATA, *AIP Conference Proceedings*, **1150** (1), 210–213.
- NIGRIN, A., 1993, NEURAL NETWORKS FOR PATTERN RECOGNITION : Cambridge, MA : The MIT Press.
- OKABE, M., 1979, ANALYTICAL EXPRESSIONS FOR GRAVITY ANOMALIES DUE TO HOMOGENEOUS POLYHEDRAL BODIES AND TRANSLATIONS INTO MAGNETIC ANOMALIES : *Geophysics*, **44** (4), 730–741.
- PAASCHE, H., TRONICKE, J., ET DIETRICH, P., 2010, AUTOMATED INTEGRATION OF PARTIALLY COLOCATED MODELS : SUBSURFACE ZONATION USING A MODIFIED FUZZY C-MEANS CLUSTER ANALYSIS ALGORITHM : *Geophysics*, **75** (3), P11–P22.
- PARADIS, S., LUDDEN, J., ET GÄLLINAS, L., 1988, EVIDENCE FOR CONTRASTING COMPOSITIONAL SPECTRA IN COMAGMATIC INTRUSIVE AND EXTRUSIVE ROCKS OF

- THE LATE ARCHEAN BLAKE RIVER GROUP, ABITIBI, QUÉBEC : Canadian Journal of Earth Sciences, **25**, 134–144.
- PARDO-IGÙZQUIZA, E., ET CHICA-OLMO, M., 1993, THE FOURIER INTEGRAL METHOD : AN EFFICIENT SPECTRAL METHOD FOR SIMULATION OF RANDOM FIELDS : Mathematical Geology, **25**, 177–217.
- PICHE, M., GUHA, J., ET DAIGNEAULT, R., 1993, STRATIGRAPHIC AND STRUCTURAL ASPECTS OF THE VOLCANIC ROCKS OF THE MATAGAMI MINING CAMP, QUÉBEC ; IMPLICATIONS FOR THE NORITA ORE DEPOSIT : Economic Geology, **88** (6), 1542–1558.
- PILKINGTON, M., 1997, 3-D MAGNETIC IMAGING USING CONJUGATE GRADIENTS : Geophysics, **62** (4), 1132–1142.
- PLOUFF, D., 1976, GRAVITY AND MAGNETIC FIELDS OF POLYGONAL PRISMS AND APPLICATION TO MAGNETIC TERRAIN CORRECTIONS : Geophysics, **41** (4), 727–741.
- PORTNIAGUINE, O., ET ZHDANOV, M. S., 1999, FOCUSING GEOPHYSICAL INVERSION IMAGES : Geophysics, **64** (3), 874–887.
- PORTNIAGUINE, O., ET ZHDANOV, M. S., 2002, 3-D MAGNETIC INVERSION WITH DATA COMPRESSION AND IMAGE FOCUSING : Geophysics, **67** (5), 1532–1541.
- PORWAL, A., CARRANZA, E. J. M., ET HALE, M., 2003, ARTIFICIAL NEURAL NETWORKS FOR MINERAL-POTENTIAL MAPPING : A CASE STUDY FROM ARAVALLI PROVINCE, WESTERN INDIA : Natural Resources Research, **12**, 155–171.
- POULTON, M., STERNBERG, K., ET GLASS, C., 1992, NEURAL NETWORK PATTERN RECORDING OF THE SUBSURFACE EM IMAGES : Journal of Applied Geophysics, **29**, 21–36.
- PRESS, F., 1968, EARTH MODELS OBTAINED BY MONTE CARLO INVERSION : J. Geophys. Res., **73** (16), 5223–5234.
- RABEAU, O., 2010, DISTRIBUTION DE L'OR DE TYPE OROGÉNIQUE LE LONG DE GRANDS COULOIRS DE DÉFORMATION ARCHÉENS : MODÉLISATION NUMÉRIQUE SUR L'EXEMPLE DE LA CEINTURE DE L'ABITIBI : PhD. thesis, Institut National Polytechnique de Lorraine, Université du Québec - UQAM.
- REMY, N., SHTUKA, A., LEVY, B., ET CAERS, J., 2002, GSTL : THE GEOSTATISTICAL TEMPLATE LIBRARY IN C++ : Computers & Geosciences, **28** (8), 971 – 979.

- RHÉAUME, P., GÉOLOGIE DU FEUILLET LAC WATSON (32F12-200-0201), ET DES PORTIONS 611 ATTENANTES DES FEUILLETS RIVIÈRE SUBERCASE (32E09-200-0202), LAC DE LA GAUCHETIÈRE (32E16- 612 200-0102) ET LAC MCIVOR (32F13-200-0101), RÉGION DE MATAGAMI :; Technical report, Ministère des Ressources naturelles et de la Faune du Québec, GM 64950 (in French), 2010.
- RICHARD, V., BAYER, R., ET CUER, M., 1984, AN ATTEMPT TO FORMULATE WELL-POSED QUESTIONS IN GRAVITY : APPLICATION OF LINEAR INVERSE TECHNIQUES TO MINING EXPLORATION : *Geophysics*, **49** (10), 1781–1793.
- RÖTH, G., ET TARANTOLA, A., 1994, NEURAL NETWORKS AND INVERSION OF SEISMIC DATA. : *Journal of Geophysical Research*, **99**, 811–822.
- ROTHMAN, D. H., 1985, NONLINEAR INVERSION, STATISTICAL MECHANICS, AND RESIDUAL STATICCS ESTIMATION : *Geophysics*, **50** (12), 2784–2796.
- ROY, L., SEN, M. K., BLANKENSHIP, D. D., STOFFA, P. L., ET RICHTER, T. G., 2005, INVERSION AND UNCERTAINTY ESTIMATION OF GRAVITY DATA USING SIMULATED ANNEALING : AN APPLICATION OVER LAKE VOSTOK, EAST ANTARCTICA : *Geophysics*, **70** (1), J1–J12.
- RUMMELHART, D. E., HINTON, G. E., ET WILLIAMS, R., 1986, LEARNING INTERNAL REPRESENTATION BY BACKPROPAGATING ERRORS : *Nature*, **332**, 533–536.
- SAMBIDGE, M., ET MOSEGAARD, K., 2002, MONTE CARLO METHODS IN GEOPHYSICAL INVERSE PROBLEMS : *Reviews of Geophysics*, **40** (3), 1–29.
- SAUNDERS, J. H., HERWANGER, J. V., PAIN, C. C., WORTHINGTON, M. H., ET DE OLIVEIRA, C. R. E., 2005, CONSTRAINED RESISTIVITY INVERSION USING SEISMIC DATA : *Geophysical Journal International*, **160** (3), 785–796.
- SCOTT, C. R., MUELLER, W. U., ET PILOTE, P., 2002, PHYSICAL VOLCANOLOGY, STRATIGRAPHY, AND LITHOGEOCHEMISTRY OF AN ARCHEAN VOLCANIC ARC : EVOLUTION FROM PLUME-RELATED VOLCANISM TO ARC RIFTING OF SE ABITIBI GREENSTONE BELT, VAL D'OR, CANADA : *Precambrian Research*, **115**, 223 – 260.
- SHAMSIPOUR, P., CHOUTEAU, M., KEATING, P., ET MARCOTTE, D., 2010A, THREE-DIMENSIONAL STOCHASTIC INVERSION OF GRAVITY DATA : APPLICATION TO GRAVITY DATA FROM THE MATAGAMI REGION, QÉBEC : Geological Survey of Canada, **Current Research 2010-12**, 10 p.

- 2010b, 3D STOCHASTIC INVERSION OF GRAVITY DATA USING COKRIGING AND COSIMULATION : *Geophysics*, **75** (1), I1–I10.
- SILVA, J. B. C., MEDEIROS, W. E., ET BARBOSA, V. C. F., 2002, PRACTICAL APPLICATIONS OF UNIQUENESS THEOREMS IN GRAVIMETRY : PART 1—CONSTRUCTING SOUND INTERPRETATION METHODS : *Geophysics*, **67** (3), 788–794.
- SINGER, D., ET KOUDA, R., 1996, APPLICATION OF A FEEDFORWARD NEURAL NETWORK IN THE SEARCH FOR KUROKO DEPOSITS IN THE HOKUROKU DISTRICT, JAPAN : *Mathematical Geology*, **28**, 1017–1023.
- STEFANO, M. D., ANDREASI, F. G., RE, S., VIRGILIO, M., ET SNYDER, F. F., 2011, MULTIPLE-DOMAIN, SIMULTANEOUS JOINT INVERSION OF GEOPHYSICAL DATA WITH APPLICATION TO SUBSALT IMAGING : *Geophysics*, **76** (3), R69–R80.
- STREBELLE, S., ET A., J., 2001, RESERVOIR MODELING USING MULTIPLE-POINT STATISTICS : SPE 71324 presented at the 2001 Society of Petroleum Engineers Annual Technical Conference and Exhibition, **New Orleans, Louisiana**, 30 September–3 October.
- STREBELLE, S., 2002, CONDITIONAL SIMULATION OF COMPLEX GEOLOGICAL STRUCTURES USING MULTIPLE-POINT STATISTICS : *Mathematical Geology*, **34**, 1–21.
- SWANSON, D., 1988, A NEW GEOLOGICAL VOLUME COMPUTER MODELING SYSTEM FOR RESERVOIR DESCRIPTION : SPE Annual Conference and Technical Exhibition, pages 293–302.
- TALWANI, M., WORZEL, J. L., ET LANDISMAN, M., 1959, RAPID GRAVITY COMPUTATIONS FOR TWO-DIMENSIONAL BODIES WITH APPLICATION TO THE MENDOCINO SUBMARINE FRACTURE ZONE : *Journal of Geophysical Research*, **64** (1), 49–59.
- TALWANI, C. T., 1976, THEORETICAL MODELING OF THE MAGNETIC AND GRAVITATIONAL FIELDS OF AN ARBITRARILY SHAPED THREE-DIMENSIONAL BODY : *Geophysics*, **41** (6), 1353–1364.
- TARANTOLA, A., ET VALETTE, B., MAY 1982, GENERALIZED NONLINEAR INVERSE PROBLEMS SOLVED USING THE LEAST SQUARES CRITERION : *Reviews of Geophysics and Space Physics*, **20**, 219–232.
- TARANTOLA, A., 2005, INVERSE PROBLEM THEORY AND METHODS FOR MODEL PARAMETER ESTIMATION : Society for Industrial and Applied Mathematics.

- TARANTOLA, A., 2006, POPPER, BAYES AND THE INVERSE PROBLEM : Nature Physics, **2** (8), 492–494.
- TAYLOR, J. R., 1997, AN INTRODUCTION TO ERROR ANALYSIS : THE STUDY OF UNCERTAINTIES IN PHYSICAL MEASUREMENTS : 2<sup>nd</sup> Edition, University Science Books.
- TERTOIS, A.-L., ET MALLET, J.-L., 2007, EDITING FAULTS WITHIN TETRAHEDRAL VOLUMES IN REAL TIME, Geological Society, London, Special Publications : Structurally Complex Reservoirs, **292**, 89–101.
- TERTOIS, A.-L., 2007, CRÉATION ET MODIFICATION DE MODÈLES EN GÉOLOGIE PAR CHAMPS DE POTENTIELLE APPLICATION AU MODÈLE GEOCHRON : PhD. thesis, Institut National Polytechnique de Lorraine. Nancy, France.
- TONDI, R., DE FRANCO, R., ET BARZAGHI, R., 2000, SEQUENTIAL INTEGRATED INVERSION OF REFRACTION AND WIDE-ANGLE REFLECTION TRAVELTIMES AND GRAVITY DATA FOR TWO-DIMENSIONAL VELOCITY STRUCTURES : Geophysical Journal International, **141** (3), 679–698.
- TRAN, T. T., AUGUST 1994, IMPROVING VARIOGRAM REPRODUCTION ON DENSE SIMULATION GRIDS : Computers and Geosciences, **20**, 1161–1168.
- TRYGGVASON, A., ET LINDE, N., APR 2006, LOCAL EARTHQUAKE (LE) TOMOGRAPHY WITH JOINT INVERSION FOR P- AND S-WAVE VELOCITIES USING STRUCTURAL CONSTRAINTS : Geophysical Research Letters, **33** (7), L07303.
- VALLABH SHARMA, P., 1966, RAPID COMPUTATION OF MAGNETIC ANOMALIES AND DEMAGNETIZATION EFFECTS CAUSED BY BODIES OF ARBITRARY SHAPE : Pure and Applied Geophysics, **64**, 89–109.
- VAN DE MEULEBROUCK, J., BAYER, R., ET BURG, J., 1988, DENSITY AND MAGNETIC TOMOGRAPHY OF THE UPPER CONTINENTAL CRUST : APPLICATION TO A THRUST AREA OF THE FRENCH MASSIF CENTRAL : Annales Geophysics, **2** (5), 579 – 592.
- WERBOS, E., 1994, THE ROOTS OF BACK-PROPAGATION : John Wiley Sons, Inc.
- WONG, L., DAVIS, D., KROGH, T., ET ROBERT, F., 1991, U-Pb ZIRCON AND RUTILE CHRONOLOGY OF ARCHEAN GREENSTONE FORMATION AND GOLD MINERALIZATION IN THE VAL D'OR REGION, QUÉBEC : Earth and Planetary Science Letters, **104**, 325 – 336.

- WONG, P., ET SHIBLI, S., 2001, MODELLING A FLUVIAL RESERVOIR WITH MULTI-POINT STATISTICS AND PRINCIPAL COMPONENTS : Journal of Petroleum Science and Engineering, **31**, 157 – 163.
- XUWENLONG, T. T. S. R. J. A., 1992, INTEGRATING SEISMIC DATA IN RESERVOIR MODELING : THE COLLOCATED COKRIGING ALTERNATIVE : Proceedings - SPE Annual Technical Conference and Exhibition, **Omega**, 833–842.
- YAM, J. Y. F., ET CHOW, T. W. S., 2000, A WEIGHT INITIALIZATION METHOD FOR IMPROVING TRAINING SPEED IN FEEDFORWARD NEURAL NETWORK : Neurocomputing, **30**, 219–232.
- ZEYEN, H., ET POUS, J., 1993, 3-D JOINT INVERSION OF MAGNETIC AND GRAVIMETRIC DATA WITH A PRIORI INFORMATION : Geophysical Journal International, **112** (2), 244–256.
- ZHOU, X., 2009, GENERAL LINE INTEGRALS FOR GRAVITY ANOMALIES OF IRREGULAR 2D MASSES WITH HORIZONTALLY AND VERTICALLY DEPENDENT DENSITY CONTRAST : Geophysics, **74** (2), I1–I7.
- ZURADA, J., 1992, INTRODUCTION TO ARTIFICIAL NEURAL SYSTEMS : Boston : PWS Publishing Company.

## **ANNEXE A**

### **Gtetra Class**

**Gtetra** est un module d'extension sous le logiciel gOcad, ce plugin a été programmé en langage C++, il est dédié à la modélisation gravimétrique et magnétique dont les principales classes et fonctions sont documentées ci-après :

## A.1 Gtetra :: \_Gtetra\_gapi\_decl Protocol Reference

### Static Public Member Functions

- static bool **gravicompute** (TSolid \*tetra\_model, const CString &density\_name, AtomicGroup \*acquisition, const CString &bouguer\_name, const float ratio)
- static bool **gravi\_gauss\_compute** (TSolid \*tetra\_model, const CString &density\_name, AtomicGroup \*acquisition, const CString &bouguer\_name, const float ratio)
- static bool **gravi** (TSolid \*tsolid, const CString &density, AtomicGroup \*data\_acquisition, const CString &bouguer\_anom)
- static bool **calculate\_gravimetric\_response** (GridObj \*grObj, const CString &density, AtomicGroup \*acquisition, const CString &model\_anom, float min\_dim)
- static bool **calculate\_magnetic\_response** (GridObj \*grObj, const CString &density, AtomicGroup \*observations, const CString &field\_name, float inclination, float declination, float field)
- static bool **magcompute** (TSolid \*tsolid, const CString &susceptibility\_name, AtomicGroup \*data\_acquisition, const CString &xmag, const CString &ymag, const CString &zmag, float ratio, float inclination, float declination, float region\_field, const CString total\_field, bool field\_projection, bool remanent\_magnetization, const float magnetisation, const float azimut, const float plongement)
- static bool **mag\_clos\_sfr** (TSurf \*model, const CString &susceptibility, AtomicGroup \*data\_acquisition, const CString total\_field, float inclination, float declination, float region\_field)
- static bool **calculate\_electromagnetic\_response** (TSolid \*tsolid, const CString &conductivity, VSet \*data\_acquisition, float intensity, const CString &bz, const CString &bx)
- static bool **gravity\_inversion** (TSolid \*tetra\_model, const CString &density\_name, VSet \*acquisition, const CString &observed\_field, const CString &calculated\_field, const CString &diff\_field, const float ratio, const int itteration, bool constraint\_inversion, const float density\_min, const float density\_max)
- static bool **gravity\_mt** (TSolid \*tsolid, VSet \*data\_acquisition, const CString &density\_name, const CString &observed\_field, int points\_number, const CString &density\_properties, int itteration, float density\_min, float density\_max, float misfit, int Roughness\_factor, bool weighted, bool smooth\_dsi, bool information, VSet \*prior\_information, const CString &prior\_property)
- static bool **magnetic\_mt** (TSolid \*tsolid, VSet \*data\_acquisition, const CString &density\_name, const CString &observed\_field, int points\_number, const CString

```

&density_properties, int itteration, float density_min, float density_max, float misfit,
int Roughness_factor, bool weighted, bool smooth_dsi)
- static bool gravity_mpolis (TSolid *tsolid, const CString &density_name,
VSet *data_acquisition, const CString &observed_field, const CString &density_
properties, int itteration, float density_min, float density_max, float perturbation,
float liklihood, float sigma_x, float sigma_y, float sigma_z, int heterogen_factor, int
rug_factor)
- static bool gravity_inversion_step (TSolid *tetra_model, const CString
&density_name, AtomicGroup *acquisition, const CString &observed_field, const
CString &calculated_field, const CString &diff_field, const float ratio, const int itter-
ation, bool constraint_inversion, const float density_min, const float density_max)

- static bool check_sgs (GObj *model, const CString density_name, SGrid *grd_-
model, PtrList<char> : iterator properties, AtomicGroup *data_acquisition, const
CString bouguer_name, float likelihoode)
- static bool paint_property (TSolid *tsolid, const CString &density_name, VSet
*data_acquisition, const CString &observed_field)
- static bool gravity_inversion_region (TSolid *tetra_model, PtrList<char> : iterator
region, const CString &density_name, VSet *acquisition, const CString
&observed_field, const CString &calculated_field, const CString &diff_field, const
float ratio, const int itteration, bool constraint_inversion, const float density_min,
const float density_max)
- static bool calculate_density_probability (GObj *model, PtrList<char> : iterator
properties, const CString &density_probability, float density_value, float tolerance)
- static bool error (AtomicGroup *data_acquisition, const CString &observed_field,
const CString &calculated_field)
- static bool liklihood (AtomicGroup *data_acquisition, const CString &observed_-
field, const CString &calculated_field, float sigma)
- static bool mean (AtomicGroup *data, PtrList<char> : iterator properties, const
CString &mean_property)
- static bool Upward_continuation (GSurf *potential_field_data, const CString
&potentiel_field_name, const CString &potentiel_filter, const float elevation)
- static bool Derivate_potentiel_field (GSurf *potential_field_data, const CString
&field_name, const CString &potentiel_filter, const int order)
- static bool Gradient_potentiel_field (GSurf *potential_field_data, const CString
&field_name, const CString &xfilter, const CString &yfilter, const CString &zfilter)
- static bool Grid_partition (GSurf *gridded_data, const CString &surface, const
CString &transferred_property, const int region_number)

```

```

- static bool anomaly (PtrList< GSurf > gsurf, VSet *acquisition, const CString
  &bouguer_name, const float density, GSurf *surface, const float reference)
- static bool Anomaly_profil (PtrList< GSurf > gsurf, VSet *vset, const CString
  &bouguer_anom, const int density_number, const float density, const float step)
- static bool Anomaly_profil (PtrList< GSurf > gsurf, VSet *vset, const CString
  &bouguer_anom, const int density_number, const float density, const float step)
- static bool Upward_continuation (TSurf *potential_field_data, const CString
  &potentiel_field_name, const CString &potentiel_filter, float elevation, float reso-
  lution)
- static bool Fourier_specter (TSurf *potential_field_data, const CString
  &property_name, const CString &surface_name, const CString &specter, const
  CString &phase, int resolution)
- static bool Derivate_field (TSurf *potential_field_data, const CString
  &property_name, const CString &filtred_name, int orde, int resolution)
- static bool Low_pass_filter (TSurf *potential_field_data, const CString
  &property_name, float frequency, int order, float resolution)
- static bool Hi_pass_filter (TSurf *potential_field_data, const CString
  &property_name, float frequency)
- static bool Surface_deform (TSurf *potential_field_data, const CString
  &property_name, float *deromation_factor)
- static bool Frequency_2_spatial (GSurf *fourier_transformed, const CString
  &amplitude_name, const CString &phase_name, TSurf *spatial_surface)
- static bool Surfaces_response (TSurf *bottom_surface, const CString &density_-
  name, TSurf *top_surface, VSet *observed_field_)
- static bool Surface_median (TSurf *int_surface, const CString &int_property,
  TSurf *last_surface, const CString &final_property, float factor, const CString
  &result_surface)
- static bool Anomaly_residual (TSurf *potential_field_data, const CString
  &potentiel_field_name, const CString &residual, const CString &regional, float r,
  int u_resolution, int v_resolution)
- static bool AnomalyRegional (TSurf *potential_field_data, const CString
  &potentiel_field_name, const CString &residual, const CString &regional, int u_-
  resolution, int v_resolution, int iterations, bool smooth, bool conjugate, int fitting_-
  factor)
- static bool Closed_surface_deform (TSurf *model)

```

### A.1.1 Detailed Description

Definition at line 28 of file Gtetra\_api.h.

### A.1.2 Member Function Documentation

**A.1.2.1 static bool Gtetra ::\_Gtetra\_gapi\_decl ::anomaly (PtrList< GSurf > *gsurf*, VSet \* *acquisition*, const CString & *bouguer\_name*, const float *density*, GSurf \* *surface*, const float *reference*) [static]**

a revoir Computes the gravity anomaly induced by a tetrahedral model on a point set.

#### Parameters

*tetra\_model* The 3D model perturbin the Earth Gravity Field  
*density\_name* The density property on tsolid  
*acquisition* The observation points  
*observed\_field* The name of the Bouguer gravity anomaly mesured  
*calculated\_field* The name of the Bouguer gravity anomaly calculated after each itterations on vset. If the property already exists, it will be overwritten ; otherwise, it is created.

**A.1.2.2 static bool Gtetra ::\_Gtetra\_gapi\_decl ::calculate\_density\_-  
 propability (GObj \* *model*, PtrList< char > : :iterator *properties*,  
 const CString & *density\_probability*, float *density\_value*, float  
*tolerance*) [static]**

Compute the root mean square error between tow property on the Vset

#### Parameters

*data\_acquisition* The observation points  
*observed\_field* The reference property on the vset  
*calculated\_field* The property on the vset

**A.1.2.3 static bool Gtetra ::\_Gtetra\_gapi\_decl ::calculate\_-  
 gravimetric\_response (GridObj \* *grObj*, const CString & *density*,  
 AtomicGroup \* *acquisition*, const CString & *model\_anom*, float  
*min\_dim*) [static]**

API function linking the user interface to the simple gravimetric response computation.

**A.1.2.4 static bool Gtetra ::\_Gtetra\_gapi\_decl ::check\_sgs (GObj \* model, const CString density\_name, SGrid \* grd\_model, PtrList< char > : :iterator properties, AtomicGroup \* data\_acquisition, const CString bouguer\_name, float likelihoode) [static]**

Select good properties form Sequential Gaussian simulation

**A.1.2.5 static bool Gtetra ::\_Gtetra\_gapi\_decl ::Derivate\_potentiel\_field (GSurf \* potential\_field\_data, const CString & field\_name, const CString & potentiel\_filter, const int order) [static]**

Calculates vartical derivate of potential-field. The vertical derivate is used to amplify a short wavelenght caused by the shalow sources. A field values are specified on a rectangular grid, each GridSize (nu, nv) must be power of tow. (constraint to calculate a Fast Fourier Transform.

#### Parameters

***potential\_field\_data*** The rectangulr grid surface with field potential-field prop-  
erty.

***field\_name*** The name of The potential field data existed.

***potentiel\_filter*** The name of the filtrng potential field.

***order*** the order of the vertical derivate (if order = 1 -> first derivate else second  
derivate).

**A.1.2.6 static bool Gtetra ::\_Gtetra\_gapi\_decl ::Gradient\_potentiel\_field (GSurf \* potential\_field\_data, const CString & field\_name, const CString & xfilter, const CString & yfilter, const CString & zfilter) [static]**

Calculates the gradient of potential-field The horizontal gradient is used to locate the  
abrut lateral variation of the density A field values are specified on a rectangular grid,  
each GridSize (nu, nv) must be power of tow. (constraint to calculate a Fast Fourier  
Transform).

**Parameters**

***potential\_field\_data*** The rectangular grid surface with field potential-field property

***field\_name*** The name of the potential field data existed

***xfilter*** the name of the horizontal gradient potential field in the u direction

***yfilter*** the name of the horizontal gradient potential field in the v direction

***zfilter*** the name of the maximum horizontal gradient ( $z^2 = x^2 + y^2$ )

**A.1.2.7 static bool Gtetra :: \_Gtetra\_gapi\_decl :: gravicompute (TSolid \* *tetra\_model*, const CString & *density\_name*, AtomicGroup \* *acquisition*, const CString & *bouguer\_name*, const float *ratio*) [static]**

Computes the gravity anomaly induced by a tetrahedral model on a point set.

**Parameters**

***tetra\_model*** The 3D model perturb in the Earth Gravity Field.

***density\_name*** The density property on tsolid.

***acquisition*** The observation points.

***bouguer\_name*** The name of the Bouguer gravity anomaly created. on vset. If the property already exists, it will be overwritten ; otherwise, it is created.

***ratio*** The float value which checks the subdivided condition if the condition is to check, the elementary tetrahedral cells are refined into smaller tetrahedral cells.

**A.1.2.8 static bool Gtetra :: \_Gtetra\_gapi\_decl :: gravity\_inversion (TSolid \* *tetra\_model*, const CString & *density\_name*, VSet \* *acquisition*, const CString & *observed\_field*, const CString & *calculated\_field*, const CString & *diff\_field*, const float *ratio*, const int *iteration*, bool *constraint\_inversion*, const float *density\_min*, const float *density\_max*) [static]**

Inverse gravity modeling To determine the density distribution in the model starting from the observed data and 3D model with initail density value.

**Parameters**

***tetra\_model*** The 3D model perturb in the Earth Gravity Field

***density\_name*** The density property on tsolid with initial property value whose the property will be to determine after inversion.

***acquisition*** The observation points.

***observed\_field*** The name of the Bouguer gravity anomaly mesured

***calculated\_field*** The name of the Bouguer gravity anomaly calculated from numerical model on vset. If the property already exists, it will be overwritten ; otherwise, it is created.

***diff\_field*** The name of the difference between the observed gravity field and calculated gravity field on vset. If the property already exists, it will be overwritten ; otherwise, it is created.

***ratio*** The float value which checks the subdivided condition if the condition is to check, the elementary tetrahedral cells are refined into smaller tetrahedral cells.

***constraint\_inversion*** boolean parameter to limit the density value

***density\_min*** (if constraint\_inversion is true) The minimal value that cannot the density exceed

***density\_max*** (if constraint\_inversion is true) The maximal value that cannot the density exceed

```
A.1.2.9 static bool Gtetra ::_Gtetra_gapi_decl ::gravity_inversion_-  
region (TSolid * tetra_model, PtrList< char > ::iterator region,  
const CString & density_name, VSet * acquisition, const  
CString & observed_field, const CString & calculated_field,  
const CString & diff_field, const float ratio, const int itтерation,  
bool constraint_inversion, const float density_min, const float  
density_max) [static]
```

Inverse gravity modeling in the fixed region(s) To determine the density distribution in the select region starting from the observed data and 3D model with initail density value.

Computes the gravity anomaly induced by a tetrahedral model on a point set.

**Parameters**

***tetra\_model*** The 3D model perturbin the Earth Gravity Field

***density\_name*** The density property on tsolid

***acquisition*** The observation points

***observed\_field*** The name of the Bouguer gravity anomaly measured

***calculated\_field*** The name of the Bouguer gravity anomaly calculated from numerical model on vset. If the property already exists, it will be overwritten; otherwise, it is created.

***diff\_field*** The name of the difference between the observed gravity field and calculated gravity field on vset. If the property already exists, it will be overwritten; otherwise, it is created.

***ratio*** The float value which checks the subdivided condition if the condition is to check, the elementary tetrahedral cells are refined into smaller tetrahedral cells.

***constraint\_inversion*** boolean parameter to limit the density value

***density\_min*** (if constraint\_inversion is true) The minimal value that cannot the density exceed

***density\_max*** (if constraint\_inversion is true) The maximal value that cannot the density exceed

**A.1.2.10** static bool Gtetra :: \_Gtetra\_gapi\_decl :: gravity\_mt (TSolid \* *tsolid*, VSet \* *data\_acquisition*, const CString & *density\_name*, const CString & *observed\_field*, int *points\_number*, const CString & *density\_properties*, int *itтерation*, float *density\_min*, float *density\_max*, float *misfit*, int *Roughness\_factor*, bool *weighted*, bool *smooth\_dsi*, bool *information*, VSet \* *prior\_information*, const CString & *prior\_property*) [static]

Monte-Carlo sampling

**A.1.2.11** static bool Gtetra :: \_Gtetra\_gapi\_decl :: Grid\_partition (*GSurf* \* *gridded\_data*, const CString & *surface*, const CString & *transferred\_property*, const int *region\_number*) [static]

Break up the initial grid into several concentric grids (number of the new grids = 2\*number of the region -2) the mesh

### Parameters

***gridded\_data*** The rectangular grid surface with the elevation data property "Z"

*surface* The name of the new rectangulare grids

*transferred\_property* The property to be transferred form the initial Grid to the new Grids

*region\_number* the number of the region

```
A.1.2.12 static bool Gtetra ::_Gtetra_gapi_decl ::magcompute (TSolid
* tsolid, const CString & susceptibility_name, AtomicGroup
* data_acquisition, const CString & xmag, const CString &
ymag, const CString & zmag, float ratio, float inclination, float
declination, float region_field, const CString total_field, bool
field_projection, bool remanent_magnetization, const float
magnetisation, const float azimut, const float plongement)
[static]
```

Computes the Magnetic anomaly induced by a tetrahedral model on a point set.

#### Parameters

*tetra\_model* The 3D model perturb in the Earth Magnetic Field.

*susceptibility\_name* The Magnetic susceptibility property on *tsolid*.

*acquisition* The observation points.

*xmag* The name of the Magnetic field anomaly created on X direction on vset. If the property already exists, it will be overwritten ; otherwise, it is created.

*ymag* The name of the Magnetic field anomaly created on Y direction on vset. If the property already exists, it will be overwritten ; otherwise, it is created.

*zmag* The name of the Magnetic field anomaly created on Z direction on vset. If the property already exists, it will be overwritten ; otherwise, it is created.

*ratio* The float value which checks the subdivided condition if the condition is to check, the elementary tetrahedral cells are refined into smaller tetrahedral cells.

*inclination* of Magnetic field.

*declination* of Magnetic field.

```
A.1.2.13 static bool Gtetra ::_Gtetra_gapi_decl ::Upward_continuation
    (GSurf * potential_field_data, const CString &
     potentiel_field_name, const CString & potentiel_filter, const
     float elevation) [static]
```

Upward continuation stransforms the potential-field measured on one surface to the field that would be measured. This transformation(Passe low filter) attenuates anomalies with the short-wavelength due to near-sruface. A field values are specified on a rectangular grid, each GridSize (nu, nv) must be power of tow. (constraint to calculate a Fast Fourier Transform).

#### Parameters

***potential\_field\_data*** the rectangulr grid surface with potential field property  
***potentiel\_field\_name*** the name of the potential field data existed  
***potentiel\_filter*** the name of the potential field upward continues  
***elevation*** the continuation distance float (meter), in same units as u and v length  
of the 2dGrid

The documentation for this protocol was generated from the following files :

- /home/foudilbey/Plugins/Gtetra/include/Gtetra/gapi/Gtetra\_api.h
- /home/foudilbey/Plugins/Gtetra/include/Gtetra/gapi/map\_processing\_api.h

## A.2 Gtetra :: \_Gtetra\_gravicompute\_decl Protocol Reference

```
#include <gravity_voxet.h>
```

### Classes

- class [Point\\_cell](#)
- class [Point\\_tetra3d](#)
- class [PointProperty](#)

### Public Member Functions

- **PotentielField** (TSolid \*model, const CString &model\_property, AtomicGroup \*acquisition)
- **PotentielField** (TSurf \*model, const CString &model\_property, AtomicGroup \*acquisition)
- **PotentielField** (TSurf \*model)
- void [subdivide\\_tsolid](#) (const float ratio, bool region\_part=false)
- void [cal\\_mag\\_closurf](#) (const CString &field\_name, float inclination, float declination, float region\_field)
- void [evaluate\\_mag](#) (const CString &xmag\_field, const CString &ymag\_field, const CString &zmag\_field, const float inclination, const float declination, const float region\_field, const CString total\_field, bool field\_projection, bool remanent\_magnetization, const float magnetisation, float azimut, float plongement)
- void [evaluate\\_gravity](#) (const CString &bouguer\_anom)
- void [evaluate\\_gravity\\_exact](#) (const CString &bouguer\_anom)
- void [evaluate\\_em](#) (const CString &bz\_field, const CString &bx\_field, const float intensity)
- void [gauss\\_value](#) (const CString &name, float ratio)
- void [gravity\\_inversion\\_mt](#) (const CString &observed\_field, int points\_number, const CString &density\_properties, int itteration, float density\_min, float density\_max, float misfit, int Roughness\_factor, bool weighted, bool smooth\_dsi, bool information, VSet \*prior\_information, const CString &prior\_property)
- void [magnetic\\_inversion\\_mt](#) (const CString &observed\_field, int points\_number, const CString &density\_properties, int itteration, float density\_min, float density\_max, float misfit, int Roughness\_factor, bool weighted, bool smooth\_dsi)
- void [gravity\\_inversion\\_mpolis](#) (const CString &observed\_field, const CString &density\_properties, int itteration, float density\_min, float density\_max, float perturbation, float liklihood, float sigma\_x, float sigma\_y, float sigma\_z, int het\_factor, int rug\_factor)

- void **select\_sqs\_model** (SGrid \*grd\_model, PtrList<char> : iterator properties, AtomicGroup \*data\_acquisition, const CString bouguer\_name, float likelihoode)
- void **inversion\_region** (AtomicGroupRegion \*group\_region, float ratio, const CString &observed\_field, const CString &diff\_field, const CString &calculated\_field, const int itteration, bool constraint\_inversion, const float density\_min, const float density\_max)
- void **gravity\_inversion** (const CString &observed\_field, const CString &diff\_field, const CString &calculated\_field, const int itteration)
- void **gravity\_inversion\_step** (const CString &observed\_field, const CString &diff\_field, const CString &calculated\_field, const int itteration, bool constraint\_inversion, const float density\_min, const float density\_max)
- void **gravity\_inversion\_stp** (const CString &observed\_field, const CString &diff\_field, const CString &calculated\_field, const int itteration, bool constraint\_inversion, const float density\_min, const float density\_max)
- void **density\_distribution\_Tsolid** (PtrList<Point\_tetra3d> near\_tetra3d)
- void **paint\_density\_in\_region** (AtomicGroupRegion \*region, PtrList<Point\_tetra3d> near\_tetra3d)
- const PtrList<Point\_tetra3d> & **tetra3d\_list** ()
- PtrList<Point\_tetra3d> **tatra\_list** ()
- PtrList<Point\_tetra3d> **tatra\_list\_region** ()
- PtrList<PtrList<Point\_tetra3d>> **list\_part\_tetra** ()
- **GravityResponse** (GridObj \*grObj, const CString &density, AtomicGroup \*acquisition, const CString &model\_anom)

*Class constructor used by the API functions.*

- ~**GravityResponse** ()

*Class destructor.*

- void **geometric\_coef** (float min\_dim)
- void **add\_cell\_list** (const Cell3d &cell, float density, float min\_dim, Point3d p\_obs=Point3d(-99999.99,-99999.99,-99999.99))
- void **compute\_gravity** (const CString &boug\_name)

*Computes the gravimetric response of the model (GridObject) using exact formula.*

- void **evaluate\_gravity** (const CString &boug\_name)

*Computes the Gravimetric response of the model (GridObject) using approximation.*

- void **compute\_magnetic** (float inclination, float declination, float region\_field)

*Computes the total Magnetic field of the model (GridObject) using exact formula.*

```

-- void accepted_simulation (const CString &boug_name, float likelihood)
-- MagResponse (TSolid *model, const CString &density_name, VSet *acquisition)
-- void evaluate_mag (const CString &xmag_field, const CString &ymag_field, const
  CString &zmag_field, const float inclination, const float declination__)
-- void density_distribution_Tsolid (PtrList< Point_tetra3d > near_tetra3d)
-- void subdivide_tsolid (const float ratio)
-- const PtrList< Point_tetra3d > & tetra3d_list ()
-- PtrList< Point_tetra3d > tatra_list ()
-- PtrList< Point_tetra3d > tatra_list_region ()

```

### A.2.1 Detailed Description

Basic class for the gravimetric response computation. It uses downcasting to use its derived classes' functions.

Definition at line 31 of file gravicompute.h.

### A.2.2 Member Function Documentation

#### A.2.2.1 void Gtetra :: \_Gtetra\_gravicompute\_decl :: subdivide\_tsolid (const float ratio, bool region\_part = false)

check subdivded condition and add all tetraedra (new ans old) on the list

##### Parameters

*ratio* dist(bary, acquisition\_point) / dist (bary, tetra\_vertex)

The documentation for this protocol was generated from the following files :

- gravicompute.h
- gravity\_voxet.h
- magcompute.h